Aalborg Universitet

AALBORG UNIVERSITY
DENMARK

Compressed Sensing Methods in Radio Receivers Exposed to Noise and Interference

Pierzchlewski, Jacek

Publication date:
2013

Document Version
Accepted author manuscript, peer reviewed version

[Link to publication from Aalborg University](#)

Citation for published version (APA):
Pierzchlewski, J. (2013). *Compressed Sensing Methods in Radio Receivers Exposed to Noise and Interference.* Department of Electronic Systems, Aalborg University.

Compressed Sensing Methods in Radio Receivers Exposed to Noise and Interference

Ph.D. Thesis

Jacek Pierzchlewski

Aalborg, 28 February 2013

Compressed Sensing Methods in Radio Receivers Exposed to Noise and Interference

by Jacek Pierzchlewski

Supervisors:
Prof., Dr. Techn. Torben Larsen
Assist. Prof. Thomas Arildsen

List of papers:

> Paper 1**:** Jacek Pierzchlewski, Torben Larsen, "LTE Downlink Transmitter Simulation Using MATLAB", *Microwave Journal*, vol. 55(10), pp. 136-143, Oct. 2012

> Paper 2: Jacek Pierzchlewski, Thomas Arildsen, Torben Larsen, "Compressed Sensing-Based Direct Conversion Receiver", *Proc. International Symposium on Communication and Information Technologies ISCIT 2012*, 2-5 October 2012, Gold Coast, Australia

> Paper 3: Jacek Pierzchlewski, Thomas Arildsen, Torben Larsen, "Sampling Patterns for Frequency-Selective Compressed Sensing", Submitted to: *IEEE Transactions on Wireless Communications*

This thesis has been submitted for assessment in partial fulfillment of the PhD degree. The thesis is based on the submitted or published scientific papers, which are listed above. Parts of the papers are used directly or indirectly in the extended summary of the thesis. As part of the assessment, co-author statements have been made available to the assessment committee and are also available at the Faculty. The thesis is not in its present form acceptable for open publication but only in limited and closed circulation as copyright may not be ensured.

Acknowledgements

I would like to express my sincerest gratitude to my supervisor, Professor Torben Larsen for his enthusiastic encouragement, professional guidance and patient support during the whole PhD project, as well for his useful critiques of my work, which have been essential not only to the thesis itself, but also to my personal development as a researcher.

I wish also to extend special thanks to Assistant Professor Thomas Arildsen for his constant, excellent assistance and many valuable contributions. Furthermore, I would like to show a great appreciation to my colleagues from Technology Platforms Section, especially Hao Shen, Pawel Pankiewicz, Karsten Fyhn, and Ruben Grigoryan for their help in different aspects of my thesis as well as for their friendship and support.

Besides, I am particularly grateful for all administrative assistance given by Eva Hansen and Allan Sloth Faber. Their willingness to help me so generously has been very much appreciated.

Last but not least, I thank my parents, who have supported my education and development throughout my whole life. Thanks are also due to my wife Malgorzata, together with my soon-to-be-born daughter Victoria, who motivated me to work on the project till its very end.

English abstract

Currently we observe a dramatical increase of wireless data traffic and a rising number of mobile radio transceivers like Bluetooth, WiFi or LTE. Wireless networks become more robust and deliver data rates many times higher than rates available a couple of years ago. LTE, which is the currently implemented standard for mobile communication, implements performance parameters which not so long ago were available only for cable networks.

There is also observed a trend to implement many radio receivers in a single integrated circuit. Radio receivers become more software-based, due to significant increase of computational power avaialible in integrated circuits. Nevertheless, some necessary analog-domain processing is still a must. Analog elements are an obstacle in integrated implementation of radio receivers, digitization of radio receivers is desirable. Unfortunatelly, due to the constantly increasing traffic, there is a problem of interference, which makes digitization of radio receivers even more difficult. High-order low-pass filters are needed to remove interfering signals and secure a high-quality reception.

In the mid-2000s a new method of signal acquisition, called compressed sensing, emerged. Compressed sensing is a mathematical tool which allows for sub-Nyquist signal sampling. In this thesis the author opens a new possibility of relaxing requirements for analog signal filtering in a direct conversion receiver by applying compressed sensing. In the proposed solution,high-order low-pass filters which separate the downconverted baseband signal and interference, may be replaced by low-order filters. Additional digital signal processing is a price to pay for this feature. Hence, the signal processing is moved from the analog to the digital domain.

Filtering compressed sensing, which is a new application of compressed sensing, is proposed. The author shows that by applying appropriate signal acquisition it is possible to filter out the wanted signal with a reduced signal sampling frequency and reduced filter order. A compressed-sensing based direct conversion receiver is proposed. An LTE signal generator, which is a side accomplishment of the project is also presented.

Dansk abstrakt

I tiden ser vi en dramatisk stigning i trådløs data trafik og et stigende antal mobile radiotranscievere, såsom Bluetooth, WiFi og LTE. Trådløse netværk bliver mere robuste og overfører datarater mange gange højere end det var muligt for nogle få år siden. LTE, som er den nuvæ rende, implementerede standard til mobilkommunikation, implementerer ydelses parametre, som for ikke så lang tid siden kun var mulige i kablede netværk.

Der ses også en tendens til at implementere mange radiomodtagere i et enkelt integreret kredsløb. Radiomodtagere bliver mere softwarebaserede, på grund af en signifikant stigning i tilgængelig beregningskraft i integrerede kredsløb. Dog må en del af signalbehandlingen stadig foregå i det analoge domæne. Analoge komponenter er en hindring i implementationen af integrerede kredsløb i radiomodtagere, digitalisering af radiomodtagere er at foretrække. Uheldigvis, på grund af konstant stigende trafik, er interferens et problem, som komplicerer digitalisering af radiomodtagere yderligere. Lavpasfiltre af høj orden er nødvendige for at fjerne interfererende signaler og sikre signalmodtagelse af høj kvalitet.

I midten af 2000'erne opstod en ny metode til signal må linger, kaldet compressive sensing. Compressive sensing er et matematisk værktj, som tillader at tage målinger af signalet under Nyquistraten. I denne afhandling åbner forfatteren for muligheden for at sænke kravene til den analoge signal filtrering i en direct conversion modtager, ved at anvende compressive sensing. I den foreslåede løsning kan lavpassfiltre af høj orden, som separerer the nedkonverterede baseband signal og det interfererende signal, erstattes af lavpassfiltre af lav orden. En ulempe ved denne teknik er en stigning i digital signal processering. Dermed flyttes signal processeringen fra det analoge til det digitale domæne.

Ydermere foreslås filtering compressive sensing, som er en ny anvendelse af compressive sensing. Forfatteren viser at ved at anvende passende signal målinger er det muligt at filtrere det ønskede signal ud med en sænket signalmålingsfrekvens og reduceret filter orden. En compressive sensing-baseret

direct conversion modtager foreslås. En LTE signal generator, som er et biprodukt af projektet, præsenteres også.

Contents

Chapter 1

Introduction

1.1 Problem overview

1.1.1 Demand for integration and digitization

In 1956 an integrated circuit was invented in AT&T labs. Integrated circuit implements electronic circuits on a chip of silicon material, hence its colloquial name "chip". It is impossible to overestimate influence of this invention on electronics engineering. Nowadays, finding an electronic device which does not contain at least one integrated circuit would be a difficult task, if not impossible. For the last couple of decades there is a trend to integrate more and more electronic circuits into silicone chips. There are both technological and economical reasons behind this tendency. Using integrated circuits significantly simplifies electronic circuits design. Electronic devices built with integrated circuits are also cheaper and far more reliable. There is observed a constant progress in integrated circuits fabrication technology, thus the process of increasing integration is practically possible. In the year 2000 180 nm fabrication process was the best technology available - now (2013) 14 nm fabrication process is available. It is probable that the recent invention in material technology (graphen etc.) will allow fabrication of even more miniaturized integrated circuits.

Together with integration of electronic circuits comes a strong demand for digitization. Digital electronic circuits process data which is quantized in values and discrete in time. There are few strong arguments for digitization. Firstly, digital systems are significantly easier in practical implementation. As it was mentioned, a huge part of today's electronic devices is build using integrated circuits. Field effect transistors, which construct modern digital electronic circuits, are relatively easy in integrated circuits implementation.

On the other hand passive analog elements, like resistors, capacitors or coils are difficult and problematic in implementation. Furthermore, digitization is a desired process from an electronics designer perspective. Currently, virtually all electronic circuits are designed with use of systems for computer-aided design (CAD systems). Automatization of digital circuits design is relatively easy when compared to automatization of analog circuits design. Finally, digital data can be stored without signal quality loss. It must be mentioned however, that digital data storage requires more memory than analog data storage. Fortunately, in the last 2 decades technology of digital memory devices made a resplendent progress, hence it's no longer a practical problem. Therefore, currently in electronics engineering there is an unstoppable trend to digitlize as many parts of the devices as possible, which in signal processing circuits means moving signal processing from the analog to the digital domain.

This tendency to digitization is also present in radio receivers. It is expected that future radio receivers will be more software-based than hardware-based. It can be already observed that heterodyne receivers, which consist of many analog blocks, are displaced by direct conversion receivers [23]. Additionally to already mentioned adventages for digitization, software-based receivers will allow for more flexible implementation of new radio communication standards - a receiver can be updated by uploading new software instead of changing the whole hardware. This paradigm is known as software defined radio [19, 23, 21]. Furthemore, digitization of radio receivers is a promising process due to implementation of electronic filters and mixers which are commonly used in radio receivers. Analog filters occupy large space on a chip and cause many dificulties in integrated circuit implementation. Ditial filters do not have this disadvantages, hence are far more implementable [24, 11, 10, 13, 14]. Unfortunatelly, due to noise and interference [34, 35, 36] there are sginificant obstacles in digitization of analog filters. Removing analog filtering completely would force enourmous sampling frequency of analog-to-digital converters, and huge data flow from an analog-to-digital converter to a digital signal processing circuit [9, 2, 11, 23]. In this thesis the author tries to open a path to obey the interference obstacle in receiver digitization by applying a relatively new mathematical technique called compressed sensing [37, 38, 39, 40, 42, 41] to acquire signals. Strictly speaking, the author put the following hypothesis: *It is possible to relax analog filtering in a direct conversion receiver and move more signal processing into the digital domain by applying compressed sensing to the acquisition of downconverted signals.*

1.1.2 Organization of the thesis

The thesis is organized as follows. Chapter 1 (current) brings necessary entry knowledge. To put this thesis in some historical context, run-down of radio receivers and computational machines is briefly recalled in Section 1.1.3. Basics of analog-to-digital conversion are recalled in Section 1.2. Background of compressed sensing theory is recollected in Section 1.3. Motivation for the conducted research is presented in Section 1.4. Some radio receivers theory is recalled in this Section. The current thesis is written as a collection of papers. Three scientific papers are included as appendices. Scientific contribution of these papers is discussed in Section 1.5 of the introductory Chapter.

1.1.3 Historical context

In the last century radio communication systems made a stunning career. We are surrounded by radio receivers, even though usually we do not even notice this fact. Most of the radio receivers are not AM/FM receivers, which are colloquially called "radios", but data receivers present in mobile phones and computers, like GSM/3G/LTE or Bluetooth peripherials. Due to popularization of mobile systems, in developed countries there are multiple radio receivers per household and this number is constantly increasing.

Inventions in radio transmission date as back as late 19th century, when german inventor Heinrich Hertz transmitted and received electromagnetic waves for the first time. After Hertz, famous italian inventor Guglielmo Marconi and american Nicola Tesla independently continued work on radio. Marconi in 1901 firstly transmitted radio signal over the Atlantic Ocean, from Cornwall, Great Britain to Newfoundland in Canada. At its beginning radio communication used Morse code to transmit information, even though canadian scientist Reginald Fessenden firstly transmitted voice over the radio waves as early as 1901. The breakthrough in speach transmission came after invention of a superhetrodyne receiver in 1918 by american Edwin Armstrong. Just a decade after, first radio receivers became enough small and portable to be installed in cars and soon become a standard equipment in personal vehicles. After the Second World War the market of radio receivers started to develop quickly and new higher-frequency bands were utilized. License-free ISM (Industry, Scientific, Medicine) band was established in 1985, which launched new applications of short-distance radio transmission. First cellular network system, yet still analog, was Nordic Mobile Telephony (NMT) established in early 1980s in the Nordic countries.

Similarly to radio receivers, computational circuits are present today in so

many devices, that usually we do not even notice them. Counter intuitively, most of these computers are not personal computers, but embedded systems which are present in consumer electronics, vehicles and industrial machines. In the last couple of decades, computers were implemented into a large number of business and industrial processes, which raised automatization of industry into a new level and tremendously increased economic efficiency of services and production. Hence to computer systems today's transportation facilites, like cars, aircrafts or trains, are less dangerous. It is because in many time-critical, complex control tasks computer systms are far more reliable than humans and can predict potential faults in these transport facilites faster and more reliable. Last but not least, we can not forget computer systems embedded into medical devices, which very literally save lifes of millions of humans.

All the above is well-known as digital revolution, and its origins date back to the Second World War. Let us recall some important milestones of this process. Nearly a century ago not only computing machines were extremely expensive, heavy and huge in size, but also very unrealiable. At that time computers were purely analog systems of a very limited practical application. Second World War brought a breakthrough, since computing machines were found very successful for military code-breaking tasks. Soon it apeared that in application to computing, digital systems are far better solution than analog technology. After the war, british mathmatician Allan Turing proposed an idea of Turing's machine which is an important foundation for today's computing. At the same time american hungarian-born scientist John von Neuman developed Von Neumann computer architecture, in which program and data share the same memory. Most of the modern computers implement this architecture. In 1947 Shockley, Brattain and Bardeen during their research in AT&T Labs invented a transitor. Transistors substituted big, cumbersome and unreliable electron tubes as basic elements for building computers. In 1958 Jack Kilby invented an integrated circuit, which enabled miniaturization and mass-production of computer elements. On the physical, implementation level transitors implemented into integrated circuits are the nuts-and-bolts of absolutely every modern computer. For their invention, Shockley, Brattain and Bardeen got the Nobel Prize in Physics in 1956, while Kilby need to wait until 2000 for being honored by Royal Swedish Academy of Sciences for his invention. In the late 1970s Intel brought the first x86 architecture microprocessor into the market. Few years after IBM introduced their first IBM-PC computer, which is based on x86 microporcessor, and made IBM-PC standard open and publicily available. The IBM-PC soon became a world standard, and now is an ordinary household appliance in developed countries.

History of development of radio systems and history of computers were

year	radio	computer	radio data transmission / software defined radio
2010			- First LTE is deployed
			- GNU radio is started
2000	- Nordic Mobile Telephone established in Nordic Countries		- Bluetooth
			- Software Defined Radio
1990		- Linux operating system	- GSM is launched
		- ARM microprocessor	- Digital Audio Broadcasting
1980	- Industrial, Scientific, Medicine (ISM) band is created	- IBM PC Computer	- First WI-FI standard is set
		- x86 microprocessor by Intel	
1970		- First integrated circuit	
1960			
	- First satelite radio contact (Sputnik)	- Transistor is invented	
1950	- First VHF radio station opened in Germany	- Turing machine is proposed	
		- Von Neumann computer architecture is proposed	
1940		- Mark 1 computer	
		- ENIAC computer	
1930			
	- British Broadcast Corporation (BBC) is established		
1920			
	- Superhetrodyne receiver is invetned		
1910	- First voice transmission by Fessenden.		
	- Marconi transmitts data over the Atlantic Ocean		
1900			
1890			
	- Hert's experiments with electromagnetic waves		
1880			

Figure 1.1: Timeline with milestones in history of radio, computer and radio data transmission/software defined radio

recalled separatelly, because unitl 1980's radio transceivers technology and computer systems technology were separate areas of the electrical engineering. Standard IEEE 802.11, also known as WI-FI, implemented an idea of wireless local area network. This standard brought possibility of radio data communication between computer systems and significantly increased mobility of personal computers. Few years later, wireless Bluetooth standard enabled short-distance communication between many types of different electronics de-

vices, like phones, computers or tablets. The second, already digital genera-
tion of cellular networks, Global System for Mobile Communication (GSM),
started in Europe in early 1990s. Currently, fourth generation of digital cellu-
lar networks, called Long Term Evolution is being deployed in many countries
around the globe. Currently, most of the state-of-the-art consumer electronics
is equipped with a multistandard data radio transceiver.

Not only radio transmitters became present in computer systems, but also
computational circuits became a part of radio transmitters and receivers. For
many decades radio receivers were designed as purely analog circuits. Super-
heterodyne was the most widely used receiver architecture due to its superior
performance quality, and remained the most popular receiver architecture un-
til late 1990s. In 1991 Joe Mitola coined a term "Software Defined Radio",
in which antenna signal is directly sampled by an analog-to-digital converter
and further processed by a digital signal processing circuit. Unfortunatelly,
this idea is impossible to be implemented with today's technology and turned
out to stay fully conceptual - among practical engineers it is often an object of
derision. It is due to huge sampling frequency needed to acquire antenna sig-
nals which induces enormous energy dissipation and massive data flow, which
in practice cannot be handled. Nevertheless, computational power available
to be implemented in integrated circuits increases, and the digitization of ra-
dio receivers is an ongoing process. Around the year 1990 very most of all
the receivers were heterodyne, but already in the late 1990s direct conversion
receivers outnumberred superheterodyne receivers due to implementation is-
sues - a direct conversion receivers consist of significantly less analog elements.
Analog elements occupy large space on chip and cause far more difficulties in
design. Currently, engineers aim to reduce the analog part of the receiver by
moving signal processing into the digital part of a receiver. Antenna signal
is preprocessed in the analog domain and than sampled by analog-to-digital
converters. The sampled signal is processed by digital signal processing sys-
tem. Soon it came into sight that digitized radio receivers are faster, more
stable and more universal than analog architectures.
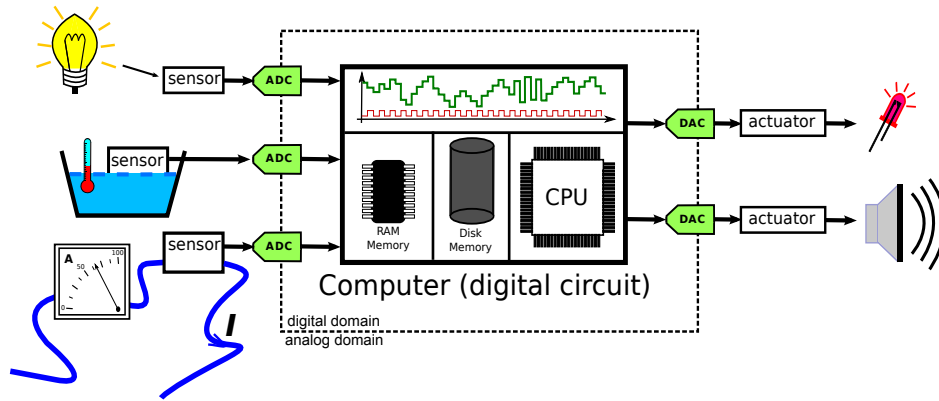
Figure 1.2: The analog-to-digital converters constitute a boudnary between digital circuits and the real analog world. Sensors changes phyiscal values into voltage, which is then translated into digital values. Computer system may interact with a real world by digital-to-analog converters.

1.2   Analog-to-digital conversion

As it was mentioned above, absolutely all today's computers are digital machines. The real world, however, is analogue, because in reality we treat the time and any other signal value as continuous. Maybe it is not entirely true - physicist introduced Planck length and Planck time, because it is possible that in micro-scale the real world is discrete. Nevertheless, this dicretization is so small, that in macro-scale the time and any real value are virtually continuous. This difference between computers and the real world enforces using devices which transforms continuous, real values into discrete values. These devices are analog-to-digital converters (ADCs). As Figure 1.2 shows, analog-to-digital converters [1, 2, 3, 4, 5, 9] connect the real, analog domain with the digital domain, while digital-to-analog converters perform the vice-versa translataion. Information theory states that it is easier to build a digital-to-analog converter than an analog-to-digital converter, which is beyond question confirmed in practice. In modern radio receivers analog-to-digital converters are used to acquire a preprocessed radio signal and transform it into the digital domain [3, 10, 11, 12, 13, 14]. Theory of analog-to-digital conversion is recalled in the following subsection.

1.2.1 Sampling rate

Analog to digital conversion is a process of transforming an analog signal into a sequence of numbers (Figure 1.3). Let us analyze an analog, continuos signal $s(t)$:

$$s(t) = \cos(2\pi f t), \quad -\infty < t < +\infty \tag{1.1}$$

where f is a signal frequency, t is time. Uniform sampling [1, 15, 16, 17] is the most widely used sampling scheme. In this scheme a given signal is sampled in regular time moments, which are uniformly distributed (hence the name). Uniform sampling transforms a signal $s(t)$ into a discrete series of samples $s[k]$, $k \in \mathbb{Z}$ according to:

$$s[k] = \cos(2\pi f k T_\mathrm{s}), \quad k \in \mathbb{Z} \tag{1.2}$$

where T_s is a uniform sampling period. The signal sampling frequency is $f_\mathrm{s} = T_\mathrm{s}^{-1}$. Very important in the theory of sampling is Dirac's delta function $\delta(t)$. Generalized function $\delta(t)$ [18] can be approximated as:

$$\delta(t) = \frac{1}{x\sqrt{\pi}} e^{\frac{-t^2}{x^2}} \quad x \to \infty \tag{1.3}$$

This function has the follwing characteristic:

$$\int_{-\infty}^{+\infty} \delta(t) = 1 \tag{1.4}$$

Function $\sigma(t)$ consists of $N \to \infty$ Dirac's delta functions $\delta(t)$ shifted in time. These shifts are multiples of the sampling period T_s:

$$\sigma(t) = \sum_{k \in \mathbb{Z}} \delta(t - k T_\mathrm{s}) \tag{1.5}$$

From strictly mathmatical point of view, sampling of a given signal $s(t)$ is a convolution between $\sigma(t)$ and the given signal $s(t)$:

$$s[k] = s(t) * \sigma(t) \tag{1.6}$$

It can be observed that sampling gives a very limited information about the sampled signal, since it is unknown how does the signal look like in between the moments of sampling. It is easy to prove, that a series of samples $s[k]$ is identical for the signal $s(t) = \cos(2\pi f t)$ and any other signal $f(t) = \cos(2\pi f t + n T_\mathrm{s})$, $n \in \mathbb{Z}$, if the uniform sampling period is T_s [15, 16, 17]. Therefore, for a given T_s, many different signals corresponds to the same series of samples
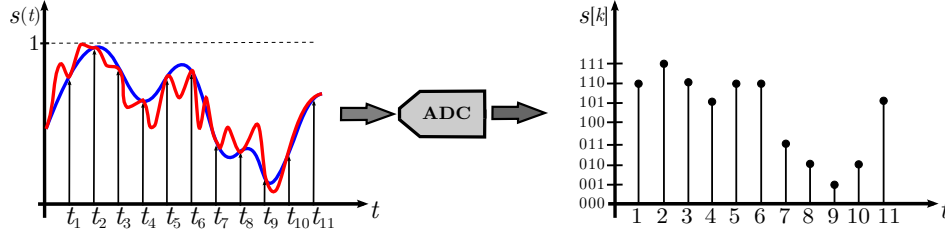
Figure 1.3: Analog to digital conversion. Two different signals are represented with the same series of samples. Sampled signal on the right is discrete in time and quantized in values. The signal in red is clearly sampled with too low sampling frequency

$s[k]$. This principle is presented in Figure 1.3. The famous Shannon-Nyquist sampling theorem [15, 16, 17] addresses this problem. The theorem states that a finite energy signal of the highest signal frequency component B can be unambigously represented by a sequence of uniform samples $s[k]$, if the samples are taken with a sampling frequency f_s, which is at least twice higher than the highest frequency component present in the signal:

$$f_s > 2B \tag{1.7}$$

The above is a crucial theorem for digital signal processing. The Nyquist frequency of a signal $s(t)$ is equal to twice the highest frequency component present in the signal:

$$f_N = 2B \tag{1.8}$$

Ratio of a signal sampling frequency to the Nyquist frequency of this signal is known as the oversampling ratio (OSR):

$$\beta = \frac{f_s}{f_N} \tag{1.9}$$

If the oversampling ratio β is lower than 1, then, according to Nyquist-Shannon sampling theorem, signal is not represented correctly and can not be reconstructed. In the last decade, a new sampling theorem known as compressed sensing arised, which enables sub-Nyquist sampling if certain conditions are fulfilled.

1.2.2 Analog-to-digital converter model

Conceptual model of an ADC converter is presented in Figure 1.4. Sample-and-hold is a central element of an ADC. The sample-and-hold consists of a
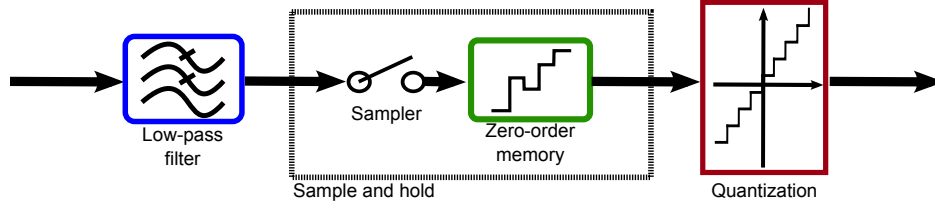
Figure 1.4: Conceptual model of an ADC converter

sampler, which samples signal in a given moments of time and a zero-order memory which holds the sampled values. The sampler is externally controlled by a clock signal. An analog-to-digital converter has its certain maximum frequency of an input signal. This maximum frequency, called Full-Power Bandwidth (FPBW), comes from technological constraints. If the highest frequency component of an input signal is higher than FPBW, then the signal is distorted by input circuitry of the ADC before the signal is sampled. After the signal is sampled, the sampled values are quantized [7, 6]. Quantization function $Q(s[n])$ transforms the sampled signal values $s[n] \in \mathbb{R}$ into an N-bit discrete-valued signal $y[n] \in \mathbb{Q}$, where $\mathbb{Q}$ is the quantized domain:

$$y[n] = Q(s[n]) \tag{1.10}$$

The number of output bits N, usually called resolution, is one of the basic parameters of an analog-to-digital converter. Currently, there are ADCs with resolution from 8 to 24 bits available on the market [2, 9]. Quantization interval $\triangle_N$ is the largest possible difference between two different values of the sampled signal which gives the same quantized value. If a uniform quantization is used, then $\triangle_N$ is:

$$\triangle_N = \frac{L_{\mathrm{r}ef}^{+}}{2^N + 1} \tag{1.11}$$

where $L_{\mathrm{r}ef}^{+}$ is the higer reference level. The above assumes that zero is treated as the lower reference level. There are many different formulas for quantization function. An example of quantization function is:

$$y[n] = \left\lfloor \frac{s[n] + 0.5\triangle_N}{\triangle_N} \right\rfloor \tag{1.12}$$

where $\lfloor \rfloor$ is a floor rounding function. In this case limitations for the sampled signal are as follows:

$$-0.5\triangle_N \leq s[n] < L_{\mathrm{r}ef}^{+} + 0.5\triangle_N \tag{1.13}$$

It can be observed that two different values of $s[n]$ may give the same quantized value $y[n]$. Due to the above, quantization introduce an information loss. Error between the real sampled value $s[n]$ and the sampled value which corresponds to the quantized value $y[n]$ is known as quantization noise $e[n]$ [8]:

$$e[n] = \triangle_N \cdot y[n] - s[n] \tag{1.14}$$

If the uniform quantization is used, signal-to-noise ratio of a quantized signal is:

$$SNR_{\text{ideal}} \, [db] = 6.02N - 1.76 + 10\log(\beta) \tag{1.15}$$

where β (1.9) is the signal oversampling ratio . The above SNR_{ideal} is a theoretical ideal value of an SNR, valid only if an analog-to-digital converter is modeled as ideal. Noise and other hardware imperfections made that the signal-to-noise ratio is lower in practical implementations. Nevertheless, SNR_{ideal} sets the limit of the signal-to-nosie ratio and gives an overview about the possible performance of signal conversion. It is clear from 1.15, that the higher ADC resolution, the better quality of signal sampling.

1.2.3 Implementation issues of analog-to-digital conversion

Currently, there are several types of practical realizations of analog-to-digital converters [1, 2, 4, 5, 7, 9], of which the most important are: sigma-delta, flash (direct conversion), half-flash, pipelined, and succesful approximation (SAR). In all of these realizations of analog-to-digital converters there is always a tradeoff between available maximum sampling frequency, available quantization, power dissipation and a price of a converter. In his famous paper [1] Walden gives two figures-of-merit which combine performance parameters of analog-to-digital converters:

$$P = 2^N \cdot f_{\text{s}} \tag{1.16}$$

$$F = \frac{2^N \cdot f_{\text{s}}}{P_{\text{diss}}} \tag{1.17}$$

where P_{diss} is the power dissipated by an ADC. According to [1] the F parameter increases in time, while P stays more or less constant. However, Le et. al. [2] observed that the P parameter also increases with a development of ADC technology and updated Walden's findings. Fig. 1.5 shows the availiable analog-to-digital converters produced by one of the largest manufacturers [9]. Red line shows the highest possible sampling frequency available for different quantization. Prices for the high-end converters are also given. Blue line shows the highest possible sampling frequency availiable for different quantization,
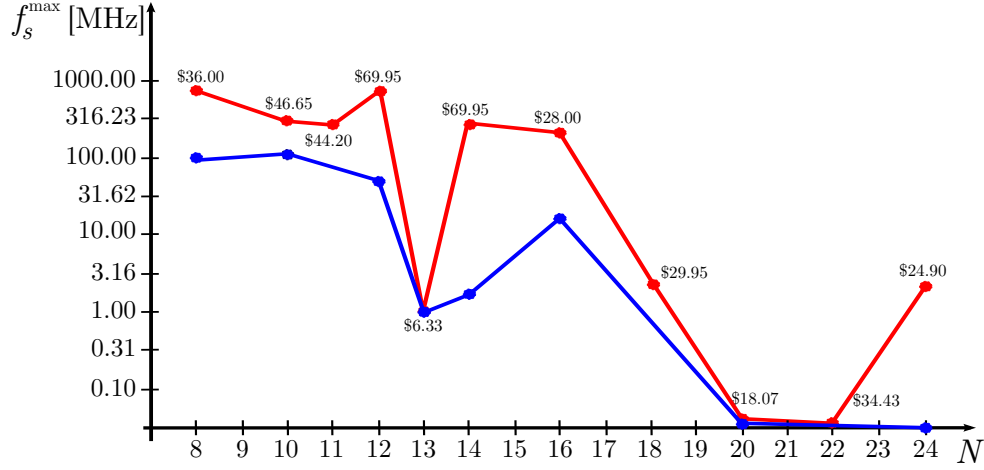
Figure 1.5: The highest available sampling frequency f_s vs. the quantization N (red plot). Prices for the high-end converters are given. The highest available sampling frequency f_s vs. the quantization N if the price limit is \$10 p. unit. (blue plot).

with an additional requirement that the price p. unit does not exceed \$10. It can be observed, that sampling frequency available for $N = 24$ is few hundreds lower than the sampling frequency available for $N = 8$. It is also clear that the high-end converters are significantly more expensive. Obviously, it is only an example of a manufacturer, nevertheless the general rule is similiar for all manufacturers. The data rate f_d of information given by a converter and the disspated power P_{diss} increase if the average sampling frequency f_s or the resolution N increase [1, 2]:

$$f_d \propto f_s N \qquad (1.18)$$

$$P_{\text{diss}} \propto f_s N \qquad (1.19)$$

When combining the above with (1.15) it can be stated, that to increase the quality of a signal acquisition, it is reasonable to apply these solutions which require low sampling frequency.

1.3 Background on compressed sensing

1.3.1 Mathmatical model of compressed sensing

Nyquist-Shannon sampling theorem [15, 17] assumes that the only knowledge about the sampled signal is its bandwidth B, which is the highest frequency component present in the signal spectrum. It is a very limited knowledge and as its consequence the minimum signal sampling frequency according to this theorem is set up high - as twice the signal bandwidth B. Compressed sensing [39, 41, 38, 37, 40, 42] emerged in the mid 2000s as a mathmatical theory which enables below-Nyquist signal sampling. With this theory it is possible to acquire significantly fewer signal samples than in the Nyquist sampling and still reconstruct the sampled signal perfectly. Applying compressed sensing into a direct conversion receiver is the core solution proposed to support the main hypothesis of this work.

A concept of signal compressibility is strongly connected to the theory of compressed sensing. Let us define a zero norm $\|\mathbf{v}\|_0^0$ as:

$$\|\mathbf{v}\|_0^0 = \mathrm{card}\{v_i : |v_i| > 0\}, \quad i \in \{1, ..., L\} \tag{1.20}$$

where v_i are coefficients of a given vector $\mathbf{v} \in \mathbb{C}^{L \times 1}$. In english, zero norm defines the number of non-zero coefficients in a vector. A vector is sparse if most of its coefficients are zeros. Strictly speaking, a vector $\mathbf{v}$ is S-sparse, if S of its coefficients are non-zero:

$$\|\mathbf{v}\|_0^0 = S \tag{1.21}$$

Let us define a signal vector $\mathbf{x} \in \mathbb{R}^{N \times 1}$. The given signal $\mathbf{x}$ is compressible if it can be well-approximated by a sparse vector $\mathbf{v} \in \mathbb{R}^{L \times 1}$ in some dictionary matrix $\mathbf{\Psi} \in \mathbb{R}^{N \times L}$

$$\mathbf{x} \approx \mathbf{\Psi} \mathbf{v} \tag{1.22}$$

During an acquisition process the signal vector $\mathbf{x}$ is acquired and translated into an observation vector $\mathbf{y} \in \mathbb{R}^{M \times 1}$:

$$\mathbf{y} = \mathbf{\Phi} \mathbf{x}, \quad \mathbf{\Phi} \in \mathbb{R}^{N \times M} \tag{1.23}$$

where $\mathbf{\Phi} \in \mathbb{R}^{N \times M}$ is an observation matrix. The number of rows M in the matrix $\mathbf{\Phi}$ is lower than the number of columns N. Therefore, the observed signal $\mathbf{y}$ is shorter than the original signal $\mathbf{x}$. Compressed sensing theory states, that it is possible to reconstruct the original signal $\mathbf{x}$ from the observed shorter signal $\mathbf{y}$, if the original signal $\mathbf{x}$ is compressible as defined above (1.22).
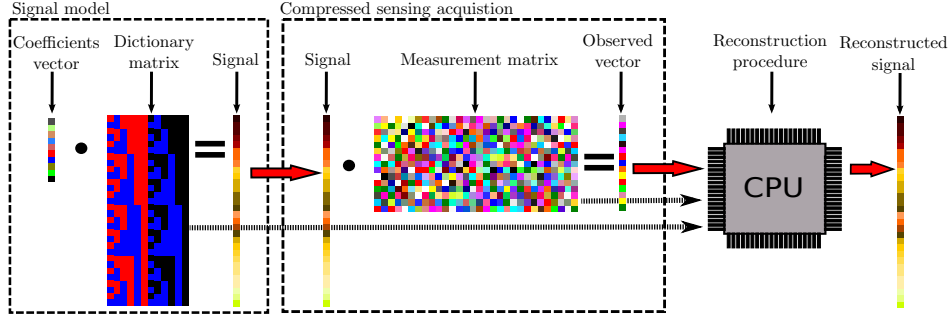
Figure 1.6: Canonical model of a compressed sensing system

A reconstruction algorithm $\mathcal{R}$ generates a reconstructed vector with signal coefficients $\hat{\mathbf{v}}$ based on the observed signal $\mathbf{y}$, the signal dictionary $\boldsymbol{\Psi}$ and the measurement matrix $\boldsymbol{\Phi}$:

$$\mathcal{R}(\mathbf{y}, \boldsymbol{\Psi}, \boldsymbol{\Phi}) \rightsquigarrow \hat{\mathbf{v}} \tag{1.24}$$

Then, the reconstruted signal $\hat{\mathbf{x}}$ is:

$$\hat{\mathbf{x}} = \boldsymbol{\Psi}\hat{\mathbf{v}} \tag{1.25}$$

Figure C.8 shows the canonical model of a compressed sensing system. Signal $\mathbf{x}$, which is modeled as in (1.22), is acquired by the measurement matrix $\boldsymbol{\Phi}$, hence the observed vector $\mathbf{y}$ is created. The orignal signal is reconstructed computationally.

It is easy to show a connection between compressed sensing and sub-Nyquist spectrum sensing when a generalized inverse Fourier transform dictionary $\boldsymbol{\Psi}_{\mathrm{I}} \in \mathbb{R}^{N \times Q}$ is used. This dictionary is a matrix $\boldsymbol{\Psi}_{\mathrm{I}}$:

$$\boldsymbol{\Psi}_{\mathrm{I}} = \begin{bmatrix} \psi_{1,-K} & \cdots & \psi_{1,0} & \cdots & \psi_{1,K} \\ \vdots & \ddots & \ddots & \ddots & \vdots \\ \psi_{N,-K} & \cdots & \psi_{N,0} & \cdots & \psi_{N,K} \end{bmatrix} \tag{1.26}$$

where:

$$\psi_{n,k} = \exp[j2\pi t_n f_k] \tag{1.27}$$

The number of columns in the matrix $\boldsymbol{\Psi}_{\mathrm{I}}$ is $Q = 2K + 1$, where K is the number of posititve frequencies represented by the dictionary. Frequency separation between columns of the matrix $\boldsymbol{\Psi}_{\mathrm{I}}$ is γ. A k-th column of the matrix $\boldsymbol{\Psi}_{\mathrm{I}}$ corresponds to a tone of a frequency f_k:

$$f_k = k\gamma \quad k \in \{-K, ..., 0, ..., K\} \tag{1.28}$$

Time period represented by the dictionary $\boldsymbol{\Psi}_\mathrm{I}$ is t_d. Signal representation sampling frequency f_r of the dictionary columns is:

$$f_\mathrm{r} = \frac{N}{t_\mathrm{d}} \tag{1.29}$$

Bandwidth reflected by the dictionary is $B = K\gamma$. Dictionary oversampling ratio $\beta_{\boldsymbol{\Psi}}$ is:

$$\beta_{\boldsymbol{\Psi}} = \frac{f_\mathrm{r}}{2K\gamma} \tag{1.30}$$

In practical applications if the acquistion as in (1.23) holds the inequality:

$$M < \frac{N}{\beta_{\boldsymbol{\Psi}}} \tag{1.31}$$

than the acquistion reflects the sub-Nyquist spectrum sampling if the original signal $\mathbf{x}$ is modeled with a given dictionary $\boldsymbol{\Psi}_\mathrm{I}$.

1.3.2 Signal reconstruction

If a signal is sampled according to the Nyquist principle, then its reconstruction is straightforward. On the contrary, signal reconstruction in compressed sensing requires usage of extensive computational algorithms. As a tradeoff, rate of a signal acquisition is relaxed. Since computational circuits are implemented in the digital domain, it can be stated that with compressed sensing it is possible to move some part of a signal acquisition from the analog to the digital domain.

Reconstruction of a vector with frequency coefficients $\mathbf{v}$ as in (1.24) is a non-trivial task. Currently, there are extensive research tasks performed in many institutions on methods of compressed sensing reconstruction, and already many algorithms were elaborated [41, 38, 44, 45, 40, 46]. These methods differ in reconstruction performance, execution time and memory consumption. Hence, in practical application a reconstruction method must be matched to a given problem.

To make the compressed sensing possible, the original signal $\mathbf{x}$ must be compressible. If this signal is compressible, the correctly reconstructed vector with dictionary coefficients is sparse. The naive reconstruction is based on a search for the most sparse signal:

$$\hat{\mathbf{v}} = \underset{\mathbf{v}}{\mathrm{argmin}} \|\mathbf{v}\|_0 \quad \mathrm{subj.\,to:}\ \|\boldsymbol{\Theta}\mathbf{v} - \mathbf{y}\|_2 = 0 \tag{1.32}$$

where matrix $\boldsymbol{\Theta} \in \mathbb{C}^{M \times Q}$ is:

$$\boldsymbol{\Theta} = \boldsymbol{\Phi}\boldsymbol{\Psi} \tag{1.33}$$

The reconstruction as in (1.32) gurantees the best possible reconstruction performance [41]. Unofortunatelly, in virtually all practical applications this reconstruction is impossible to be performed. It is because the problem of looking for the most sparse signal is an NP-hard computational problem and size of this problem is so huge, that the reconstrucion as in (1.32) is impractical. To make the problem feasible, it is possible to replace the reconstruction which is based on ℓ_0 minimization with a reconstrucion based on ℓ_1 minimization. Such a reconstruction it is:

$$\hat{\mathbf{v}} = \underset{\mathbf{v}}{\operatorname{argmin}} \|\mathbf{v}\|_1 \quad \text{subj. to:} \ \|\mathbf{\Theta}\mathbf{v} - \mathbf{y}\|_2 = 0 \qquad (1.34)$$

In the theory of compressed sensing the above is known as basis pursuit. Solving the above optimization problem is feasible because, if certain conditions are met, this problem is convex. In practice, reconstrucion performance of ℓ_1 minimization as in (1.34) is insignificantly lower than ℓ_0 minimization as in (1.32).

In real world, the sampled signal is polluted with noise. In this case reconstruction as in (1.34) is incorrectly stated becasue its feasible region is defined too strictly. Therefore, the feasible region of the ℓ_1 minimization must be relaxed:

$$\hat{\mathbf{v}} = \underset{\mathbf{v}}{\operatorname{argmin}} \|\mathbf{v}\|_1 \quad \text{subj. to:} \ \|\mathbf{\Theta}\mathbf{v} - \mathbf{y}\|_2 < \epsilon \qquad (1.35)$$

Optimization defined as in the the above is known as basis pursuit denoising. The higher the signal noise level, the higher ϵ value should be used. Reconstruction performance of basis pursuit denoising depends significantly on accuracy of adjusting value of the ϵ parameter. Too low ϵ makes the optimization problem infasible. Too high epsilon compromise the quality of reconstruction, since the feasibly region is too large. In practice, adjusting the ϵ cause problems since the level of noise may be difficult to predict. Basis pursuit denoising regularization is another version of a reconstruction based on ℓ_1 optimization:

$$\hat{\mathbf{v}} = \underset{\mathbf{v}}{\operatorname{argmin}} \lambda \|\mathbf{v}\|_1 + 0.5\|\mathbf{y} - \mathbf{\Theta}\mathbf{v}\|_2^2 \qquad (1.36)$$

Similarly to the ϵ parameter in basis pursuit denoising, in the above optimization the λ parameter must be adjusted to the noise level.

In compressed sensing columns of the $\mathbf{\Theta}$ matrix are non-orthogonal. Possibility of successful reconstruction of the sampled signal depends on level of this non-orthogonality. Restricted isometry property (RIP) [41, 38, 43] quantifies how much non-orthogonal are the columns of the matrix $\mathbf{\Theta}$, if only S columns from the matrix are considered at a time.
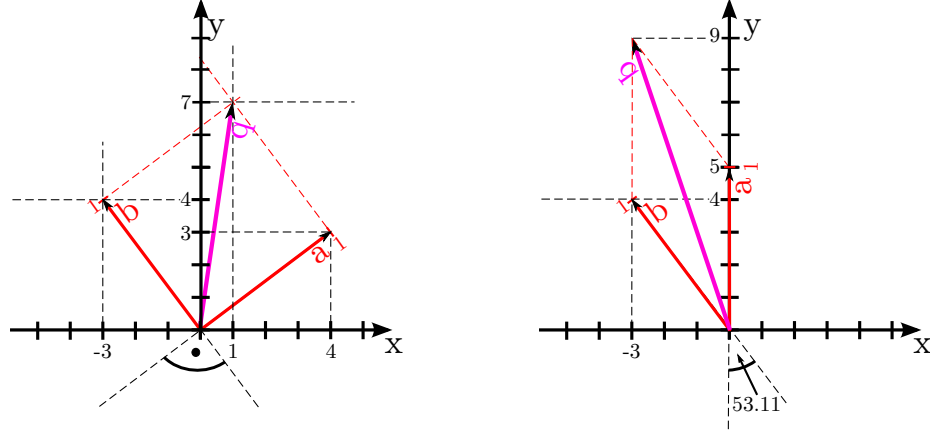
Figure 1.7: Example of an orthogonal (left) and a non-orthogonal (right) system of vectors.

The RIP constant ζ_S of the matrix $\mathbf{\Theta}$ is the smallest number which fulfills the inequality:

$$(1 - \zeta_S)||\mathbf{q}||_2^2 \leq ||\mathbf{Aq}||_2^2 \leq (1 + \zeta_S)||\mathbf{q}||_2^2 \tag{1.37}$$

for all vectors $\mathbf{q}$, for all the possible matrices $\mathbf{A}$ which consits of S columns from a given matrix $\mathbf{\Theta}$. The lower ζ_S, the more orthogonal are columns of a matrix $\mathbf{A}$. The restricted isometry property is based on an observation that the more non-orthogonal are columns of a given matrix $\mathbf{A}$, the less preserved is length of a vector mutliplied by this matrix. Definition as in (C.31) is correct if columns of the matrix $\mathbf{A}$ are orthonormal. If columns of the matrix $\mathbf{A}$ are not normalized, but still have identical length, then correct is the inequality:

$$\sqrt{\lambda}(1 - \zeta_S)||\mathbf{q}||_2^2 \leq ||\mathbf{Aq}||_2^2 \leq \sqrt{\lambda}(1 + \zeta_S)||\mathbf{q}||_2^2 \tag{1.38}$$

where the rescaling parameter λ is equal to the length of columns the matrix $\mathbf{A}$:

$$\lambda = ||\mathbf{a}_s||_2^2 \quad \mathbf{a}_s = \{1, ..., S\} \tag{1.39}$$

Let us consider the following example of systems of vectors, which are showed in Figure 1.7. On the left hand side of the Figure 1.7 there is a coordinate system $\mathbf{A}$ defined as

$$\mathbf{A} = \begin{bmatrix} 4 & 3 \\ -3 & 4 \end{bmatrix} = [\mathbf{a} \ \mathbf{b}] \tag{1.40}$$

This system consists of two vectors **a** and **b** which are clearly orthogonal to each other. Length of these two vectors is $\|\mathbf{a}\|_2 = \|\mathbf{b}\|_2 = 5$, hence the rescaling parameter $\lambda = 5$. Let us define in the system **A** a vector $\mathbf{q_A} = [\; 1 \;\; 1 \;]^\mathrm{T}$, length of the vector defined in the system **A** is $\|\mathbf{q_A}\|_2 = \sqrt{2}$. The canonical system **B** is:

$$\mathbf{B} = \begin{bmatrix} 0 & 1 \\ 1 & 0 \end{bmatrix} \tag{1.41}$$

Vector $\mathbf{q_A}$ defined in the canonical system **B** is:

$$\mathbf{q_B} = \mathbf{A}\mathbf{q_A}. \tag{1.42}$$

hence in the presented example it is $\mathbf{q_B} = [\; 1 \;\; 7 \;]^\mathrm{T}$. It ieasy to check that the inequality (1.38) holds for $\zeta_\mathrm{S} = 0$. If the system **A** is as given, inequality (1.38) holds for any vector **q**. In the second example, on the right hand side of the Figure 1.7 vectors which constitute the system **A** are non-orthogonal to each other. When a vector $\mathbf{q_A} = [\; 1 \;\; 1 \;]^\mathrm{T}$ defined in the system **A** is represented in the canonical system **B** length of the vector is changed, so in general, the inequality (1.38) holds for $\zeta_\mathrm{S} > 0$.

The second class of reconstruction algorithms, are greedy algorithms [45, 46]. These algorithms are not based on a convex optimization. Although the computational complexity of these algorithms is signifcantly lower if compared to the convex-based reconstruction algorithms, usuall reconstruction performance of greedy algorithms is substantially poorer. Therefore, in this thesis the author concentrates on ℓ_1-based reconstruction algorithms.

1.3.3 Signal acquistion

Quality of signal reconstruction depends to a high degree on the resticted isometry property of a given matrix $\boldsymbol{\Theta}$. The matrix $\boldsymbol{\Theta}$ (1.33), depends on a measurement matrix $\boldsymbol{\Phi}$ and a dictionary matrix $\boldsymbol{\Psi}$. Hence, for a given dictionary matrix $\boldsymbol{\Psi}$ performance of a signal reconstruction depends to a high degree on a compressed sensing acquisition, which is reflected by the measurement matrix $\boldsymbol{\Phi}$. Quite some work has been done in the area of Compressed Sensing acquisition. Kirolos et al. [47] proposed a Random Demodulator framework, further developed in [49]. The Random Demodulator uses modulation and filtering before signal sampling. This acquisition system provides good performance and high durability against clock jitter effect, however it requires massive analog preprocessing applied to the input signal. Furthermore, Random Demodulator is also sensitive to the filter imperfections [48]. Mishali and Eldar [51, 52] presented their work on sub-Nyquist sampling of
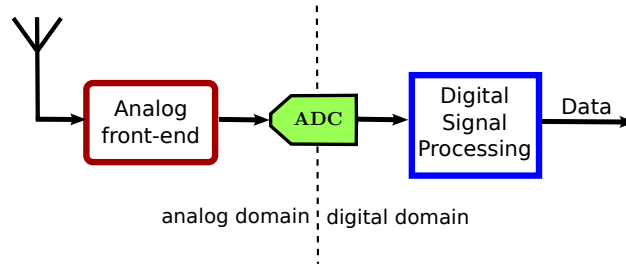
Figure 1.8: General structure of a data receiver

sparse wideband analog signals. They developed a Modulated Wideband Converter (MWC) which is a multi-sampler, analog system dedicated to sample wideband signals. This work combine a Random Demodulator approach with Multi Coset Sampling [54] strategy. Albeit the MWC guarantees good performance, expanded analog preprocessing is an unavoidable part of the MWC. Furthermore, multi-sampler architecture makes this system useless in many mobile and power-constraint applications.

In the thesis, compressed sensing is applied to a radio receiver. hence, a multi-sampler compressed sensing acquisition system is not suitable for this thesis. Furthermore, an acquisition system should not impose additional signal preprocessing in the analog domain. Therefore, a single-ADC sampling acquisition system, which implements random sampling is considered in the thesis.

1.4 Motivation - digitization and silicon integration of data receivers

General structure of a data receiver is shown in Figure 1.8. Signal from the antenna is firstly preprocessed in the analog domain by an analog front-end of a receiver. The preprocessed signal is then sampled by an analog-to-digital converter and further processed in the digital domain by a digital signal processing system. The analog-to-digital converter is a border between the two domains, therefore it is desired to place the analog-to-digital converter as close to the antenna as possible, to minimize signal processing in the analog domain. There superheterodyne receiver and a direct conversion receiver are recalled in this Section. Furthermore, an idea of software defined radio is recalled and discussed. Finally, motivation and main hypothesis of this work is discussed.

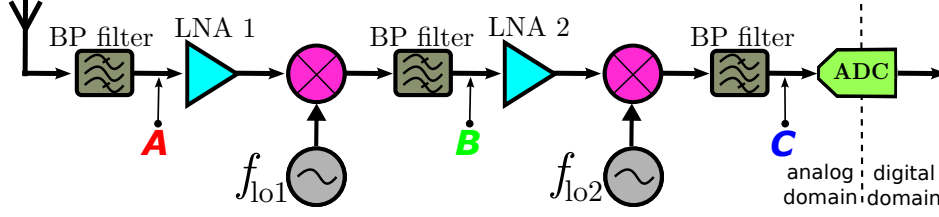Figure 1.9: Architecture of a 2-stage superheterodyne receiver

1.4.1 Superheterodyne receiver

The architecture of a 2-stage superheterodyne receiver is shown in Fig. 1.9. Frequency mixer is the core of a stage of the receiver. Ideal frequency mixer is an electronic circuit which output signal is a product of its two input signals. In superheterodyne receivers one of a mixer input is driven by a local frequency oscilator, a remaing input is treated as a signal input. The mixer output signal $s_{\text{out}}(t)$ it is:

$$s_{\text{out}}(t) = s_{\text{in}}(t) \cdot s_{\text{lo}}(t) \tag{1.43}$$

where $s_{\text{in}}(t)$ is a mixer input signal, $s_{\text{lo}}(t)$ is a local oscilator signal. If the mixer input signal $s_{\text{in}}(t)$ is a modulated signal $s_{\text{in}}(t) = a(t) \cos(2\pi f_{\text{in}} t)$ and the frequency oscilator signal $s_{\text{lo}}(t)$ is a wave with constant frequency and amplitude $s_{\text{lo}}(t) = \cos(2\pi f_{\text{lo}} t)$ than the mixer output signal is:

$$s_{\text{out}}(t) = \underbrace{\frac{1}{2}a(t) \cos(2\pi(f_{\text{in}} - f_{\text{lo}})t)}_{\text{downconverted signal}} + \underbrace{\frac{1}{2}a(t) \cos(2\pi(f_{\text{in}} + f_{\text{lo}})t)}_{\text{upconverted signal}} \tag{1.44}$$

The above is a fundamental equation which describes a frequency mixer. The mixer output signal consists of two separate signals with two different frequencies. The first signal component (downconverted) is the input signal $s_{\text{in}}(t)$ moved down in the frequency domain from fequency f_{in} to $f_{\text{in}} - f_{\text{lo}}$. For contradiction, the second signal component is the input modulated signal $s_{\text{in}}(t)$ shifted up in the frequency domain from fequency f_{in} to $f_{\text{in}} + f_{\text{lo}}$. For simplicity, it is convenient to use the frequency notation to describe the mixer input/output:

$$f_{\text{out}} = \underbrace{f_{\text{in}} - f_{\text{lo}}}_{\text{downconversion}} + \underbrace{f_{\text{in}} + f_{\text{lo}}}_{\text{upconversion}} \tag{1.45}$$

A superheterodyne receiver consists of multiple stages. Before the wanted antenna signal of a frequency f_{r} is downconverted to the desired low frequency
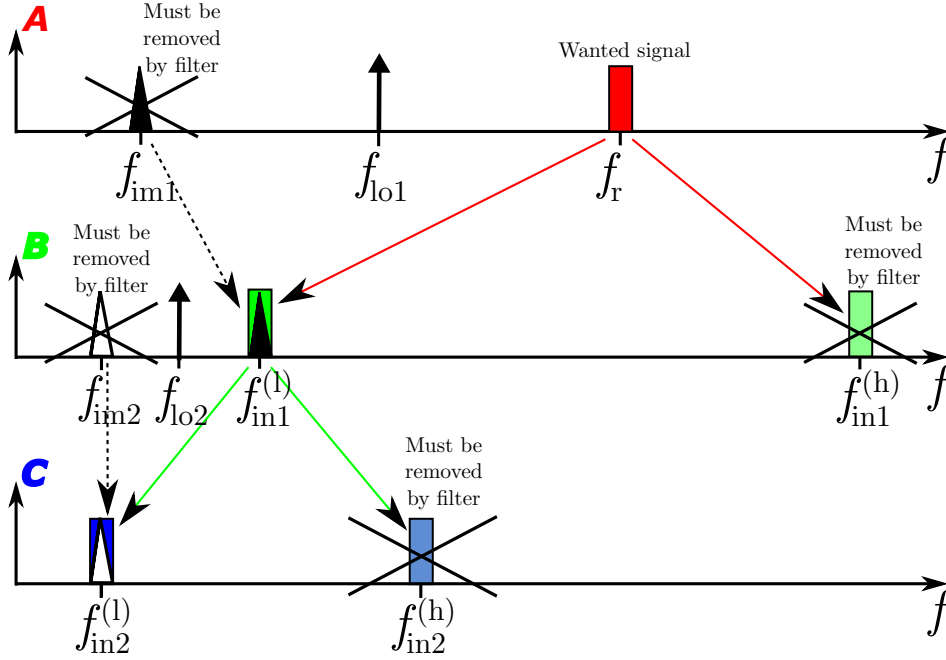
Figure 1.10: Conversion of signals in a superheterodyne receiver

f_{low}, the antenna signal is downconverted in the stages to intermediate frequencies. Frequency oscilator in a k-stage, generates a signal of a frequency $f_{\text{lo}k}$. This signal is mixed with a stage input signal. Hence, in every k-stage the input signal is downconverted in the frequncy domain to a lower intermediate frequency $f_{\text{in}k}$. According to (1.45), the intermediate frequency signal $f_{\text{in}k}$ consists of the wanted downconverted component $f_{\text{in}k}^{(1)}$ and the unwanted upconverted component $f_{\text{in}k}^{(\text{h})}$:

$$f_{\text{in}k} = f_{\text{in}k}^{(1)} + f_{\text{in}k}^{(\text{h})} \tag{1.46}$$

The upconverted component $f_{\text{in}k}^{(\text{h})}$ must be filtered out, therefore in every stage there is a band-pass filter applied after the mixer. Furthemore, in a superheterodyne receiver there is a problem of an image signal. Let us consider the first stage of the superheterodyne architecture. The wanted antenna signal f_{r} is downconverted to a lower intermediate frequency $f_{\text{in}1}^{(1)}$. It is easy to show that there may exists an image signal of a frequency $f_{\text{im}1} \neq f_{\text{r}}$ which is moved by a frequency mixer to the same intermediate frequency:

$$f_{\text{in}1}^{(1)} = f_{\text{lo}1} - f_{\text{im}1} \tag{1.47}$$

Frequency of the wanted antenna signal is $f_{\mathrm{r}} = f_{\mathrm{lo1}} + f_{\mathrm{in1}}^{(\mathrm{l})}$, frequency of the image signal is $f_{\mathrm{im1}} = f_{\mathrm{lo1}} - f_{\mathrm{in1}}^{(\mathrm{l})}$. This image signal overlaps the wanted signal in the intermediate frequency and therefore causes severe signal corruption. Similiar problem occurs in every next stage of a superheterodyne receiver. Therefore, an additional filter which rejects the unwanted image signal is often used in superheterodyne receivers. In Figure 1.9 architecture of a 2-stage superheterodne receiver is presented. Conversion of signals in a receiver is shown in Figure 1.10.

The superheterodyne receiver was invented in 1918 and for many years this architecture was the most widely used receiver architecture. The most important reason for adopting the superheterodyne architecture as the world standard was its superior performance. In 1995 more than 98% of all the receivers were heterodyne [22]. Nevertheless, currently superheterodyne is considered as a declining technology. Due to multiple frequency mixers and local signal generators, which are fully-analog elements, the superheterodyne architecture is difficult in integrated circuit implementation. Furthermore, band-pass filters are implemented off-chip, which generates additional implementation problems, especially in signal routing. Therefore, in the current implementations, a direct conversion architecture takes place of the superheterodyne architecture.

1.4.2 Software defined radio

Software defined radio (SDR) architecture is shown in Figure 1.11. Software defined radio, which was firstly proposed by Mitola in [19] is a receiver architecture which goes in a completely diffent direction than superheterodyne receiver. In this architecture signal from an antenna is directly sampled by an analog-to-digital converter. Althought there is no analog preprocessing, the idea of software defined radio is unrealizable for typical radio frequencies used for data transmission ($f_{\mathrm{r}} > 100\mathrm{MHz}$). As for now, the full software defined radio stays only conceptual. It is due to extremely high sampling frequency
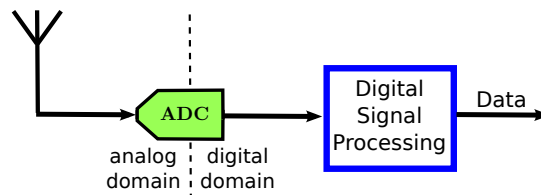
Figure 1.11: Concept of full software defined radio
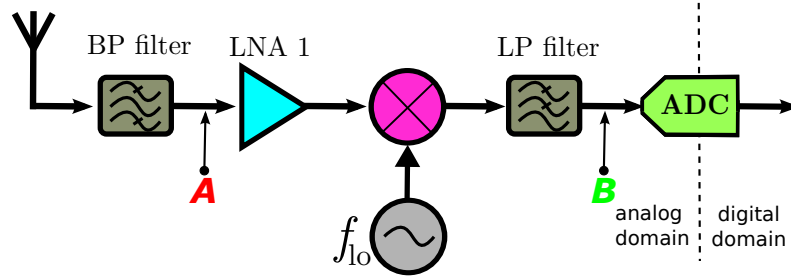
Figure 1.12: Architecture of a direct conversion receiver

needed to acquire the antenna signal, which would cause huge energy dissipation and very high data rate infeasible to be processed by a digital signal processing circuit. According to the Nyquist theory [15, 17] the antenna signal must be sampled with a frequency f_s higer than twice the antenna signal bandwidth:

$$f_s > 2B \qquad (1.48)$$

The analog-to-digital converter has a resolution of N bits, hence the rate of data flow from the converter is:

$$f_d[\text{bps}] > 2BN \qquad (1.49)$$

For instance, if bandwidth of an antenna signal is $B = 4\text{GHz}$, and the resolution is $N = 10$ bits, than the sampling frequency f_s must be higher than 8GHz and the data flow f_d is higher than 80bps, which is infeasible in realization. Furthermore, due to the noise present in the antenna signal there is a need for high signal oversampling, and accoridng to Abidi [22] $N = 10$ bits of resolution is not enough.

But even though the idea of software defined radio is impractical, it points a direction of an evolution of radio receivers. Instead of a revolutionary transformation into software defined radio, an evolutionary change in radio receiver architectures can be observed in the last two decades [22, 23, 21, 24, 14, 12]. The costdriven evolution has been proceeding towards implementation in integrated circuits and moving more signal processing from the analog to the digital domain.

1.4.3 Direct conversion receiver

In Figure 1.12 an architecture of a direct conversion receiver is presented. In this architecture the input antenna signal is filtered with a band-pass filter,
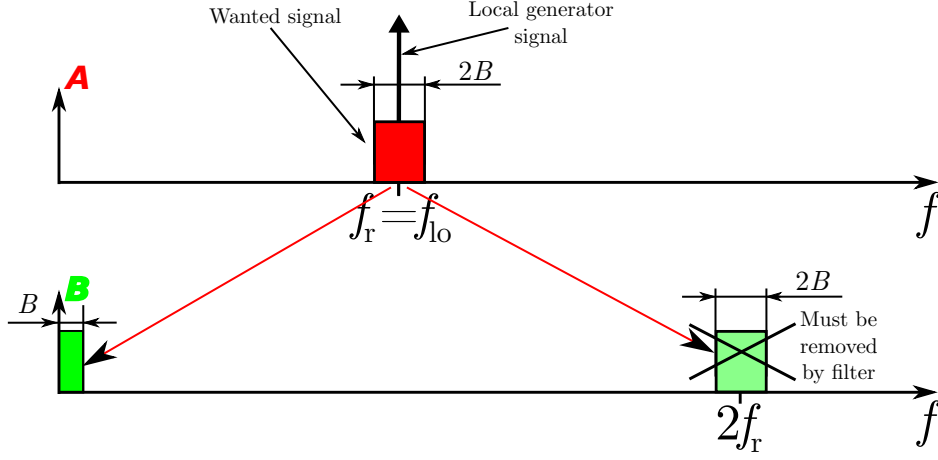
Figure 1.13: Conversion of signals in a direct conversion receiver

amplified and downconverted by a mixer directly to a baseband signal. The mathmatical description of this operation is as follows. The mixer input signal is the antenna signal $s_r(t) = a(t)\cos(2\pi f_{in}t)$. In the described architecture, frequency of a signal s_{lo} generated by a local oscilator is equal to the frequency of the received antenna signal:

$$s_{lo}(t) = \cos(2\pi f_{in}t) \tag{1.50}$$

The converted signal $s_c(t) = s_r(t) \cdot s_{lo}(t)$ is then:

$$s_c(t) = a(t)\cos(2\pi f_{in}t) \cdot \cos(2\pi f_{in}t) \tag{1.51}$$

The above can be transformed to:

$$s_c(t) = s_c^{(l)} + s_c^{(h)} = \underbrace{\frac{1}{2}a(t)}_{\text{baseband signal}} + \underbrace{\frac{1}{2}\cos(4\pi f_r t)}_{\text{high frequency signal}} \tag{1.52}$$

The transformed signal consists of the low frequency component $s_c^{(l)}$ and the high frequency component $s_c^{(h)}$. The low frequency component is the wanted baseband signal, the high frequency component must be removed by a low-pass filter. The baseband signal is then sampled by an analog-to digital converter. Conversion of signals in a direct conversion receiver is presented in Figure 1.13. The direct conversion architecture have serious drawbacks, if compared to the superheterodyne architecture. Firstly, due to only one stage of signal processing this architecture is more vulnerable to distortion. The signal s_{lo} generated
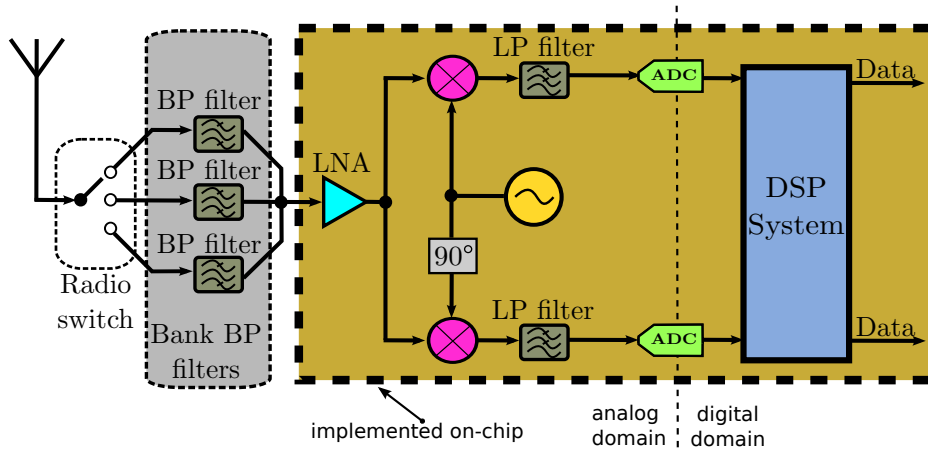
Figure 1.14: Architecture of a quadrature direct conversion receiver

by the local oscilator has the high frequency f_{lo} equal to the frequency of the received radio signal f_r, which may cause problems in implementation of the local oscilator. Furthermore, together with imperfections in mixer implementation, the high frequency generated by the local generator causes spurious leackage and DC-offset present in the baseband signal. Nevertheless, direct conversion receivers consist of significantly fewer analog elements than superheterodyne receivers. Hence, the direct conversion receivers are more convenient in integrated circuit implementation. Therefore, in the last two decades implementations of direct conversion architecture outnumbered implementations of superheterodyne architecture, even though performance of the latter is visibly better.

1.4.4   Motivation and the main hypothesis

A block diagram of a quadrature direct conversion receiver is shown in Figure 1.14. After the antenna there is a bank of band-pass filters, which choose the wanted radio channel. Then the filtered radio signal is amplified and downconverted by a quadrature downconverter. In the quadrature downconverter there are two separated paths for I and Q signals. Frequency mixers are used to downconvert the I and Q signals, low-pass filters are used to separate wanted baseband signals with unwanted high-frequency components. When the high frequency components are removed by the low-pass filters, analog-to-digital converters acquire the baseband signal, which is transformed to the digital domain.

The band-pass filters are implemented off-chip. The amplifier, the mixers and the low-pass filters are on-chip analog elements. Low-pass filters used in practical realizations of the direct conversion architecture must be high-order filters. It is due to interference signals which are present in the radio antenna signal and were not removed by the band-pass filters. In currently implemented stanards (LTE, WiMAX) there are many possible radio channels with a different frequency width. In receivers which are dedicated for many standards it is virtually impossible to implement all the needed band-pass filters and efficiently remove all interference signals. Let us assume that there is an interfering signal s_b in the radio spectrum:

$$s_b(t) = b(t) \cos(2\pi f_b t), \quad f_b = f_r + f_x \tag{1.53}$$

where f_r is the frequency of the wanted radio signal, f_x is the frequency separation between the interfering signal and the wanted radio signal. The signal after the mixer s_c consists of a low frequency component $s_c^{(l)}$ and a high frequency component $s_c^{(h)}$. If there is an interfering signal, then $s_c^{(l)}$ and $s_c^{(h)}$ in the in-phase path are as follows:

$$s_c^{(l)} = \underbrace{\frac{1}{2}a(t)}_{\text{baseband}} + \underbrace{\frac{1}{2}b(t)\cos(2\pi f_x t)}_{\text{interference}} \tag{1.54}$$

$$s_c^{(h)} = \underbrace{\frac{1}{2}a(t)\cos 4\pi f_r t}_{\text{baseband}} + \underbrace{\frac{1}{2}b(t)\cos(2\pi(2f_r + f_x)t)}_{\text{interference}} \tag{1.55}$$

It is easy to show that the interfering signal is present in the signal after the mixer. The same problem occurs in quadrature-phase path. Now, let as assume that the interfering signal s_b is close to the wanted radio signal, such that

$$f_x \ll f_r \tag{1.56}$$

Impact of the interfering signal on the conversion of radio signal in a direct conversion receiver is presented in Figure 1.15. Removing the whole high-frequency component $s_c^{(h)}$ (together with the interference) can be easily done with a low-order filter. However, after the mixers, there is an unwanted low-frequency interfering signal which also must be removed. If the interfering signal is close to the radio signal as in (1.56), than characteristics of the low-pass filters after the mixers must be very sharp to separate the wanted baseband signal from the interference (blue line in Figure 1.15). Furthermore, there must be many low-pass high-order filters implemented, for different sizes

of the bandwidth of the wanted signal. These low-pass filters cause severe implementation problems. According to Nyquist principle, avoiding these high-order filters would require a very high signal sampling frequency, which would also casue implementation problems and extreme energy dissipation, In many cases such a high sampling frequency is impossible to being implemented in practice.

In this thesis the author tries to answer the following problem: is it possible to avoid high-order low-pass filters and apply a first-order filter on a baseband signal after the mixer without increasing the analog-to-digital sampling frequency to the Nyquist frequency of the interfered signal?

New possibilities for solving this problem appear with increasing computational power available in receivers. In 2000 a high performance semi-SDR limited to high frequency signals was proposed [21]. A new receiver architecture which was supposed to be feasible for Software Defined Radio for GSM (Global System for Mobile Communications) frequencies was proposed in [23]. Recently, Ben-Romdhane et al. [24, 25, 26] proposed a direct conversion circuit in which uniform sampling is replaced with a pseudorandom sampling technique, then the sampled signal is reconstructed in a DSP (Digital Signal Processing) system. Hence, a minor reduction of the order of the quadrature downconverter filters was possible.

Compressed sensing opens new areas in the theory of signal acquistion, however, there is still a shortage of practical applications of compressed sensing. In this thesis the author puts the following hypothesis: *By applying compressed sensing to the acquisition of downconverted signals it is possible to relax analog filtering in a direct conversion receiver and move more signal processing into the digital domain without increasing the analog-to-digital sampling frequency to the Nyquist frequency of the interfered signal.*

1.5 Research contribution

This section summarizes the main research contributions in Publications A to C.

1.5.1 Publication A

The first paper published, it is a paper about LTE system simulations in Matlab. The paper was published in Microwave Journal. During work on modern communication systems it was found that there is a shortage of publicly-availalbe software dedicated to LTE simulations. The LTE standard introduces significant performance increase when compared to the previous stan-
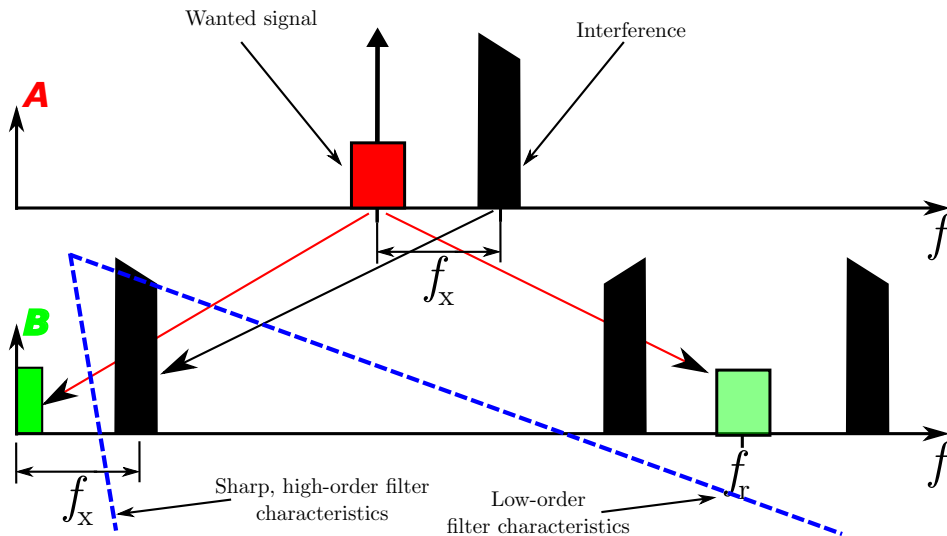
Figure 1.15: Conversion of signals in a direct conversion receiver if an interference signal is present

dards, but as a tradeoff, there is a high level of system complexity. Therefore, simulation of LTE systems is a non-trivial task.

Methodology of simulating LTE systems was proposed. A relevant software was developed and published on a website. Additionally, some visualization software, called "LTE Professor", was developed. The paper comments physical layer of the LTE standard (downlink) and presents the proposed methodology. The developed software and some simulations are demonstrated.

1.5.2 Publication B

The second paper was published in Proceedings of the International Symposium on Communication and Information Technologies ISCIT 2012. The paper presents the problem of high-order low-pass filters in a direct conversion receiver, which are needed to filter out the interference.

A method which relaxes requirements for low-pass signal filtering in a receiver is presented. In this method compressed sensing is proposed to mitigate the problem of interference. Idea of the relaxed compressed sensing reconstruction problem, in which only a part of a sampled spectrum is to be reconstructed is presented. Random single-ADC sampling device is proposed as a sampler. Both the theoretical and experimental results show that with the proposed method it is possible to apply first-order filters after the mixers

in a direct conversion receiver and still filter out interfering signals without a huge increase of the sampling rate.

1.5.3   Publication C

The third paper is submitted to the IEEE Transactions on Wireless Communications. In this paper the method of compressed sensing filtering, firstly presented in the paper B, is developed. Filtering restricted isometry property is introduced. With this parameter it is possible to assess sampling patterns in respect of compressed sensing filtering. Additionally, an idea of interference scenario generator, which significantly decreseas the amount of computations needed to calculate the restricted isometry parameter, is presented.

An algorithm which generates random sampling patterns with additional constraints is presented in the paper, together with a method and a system which chooses the best sampling pattern. It is shown that sampling grid has a huge impact on the compressed sensing filtering.

The above allow for finding a sampling pattern which enables a compressed sensing filtering. An experiment which proves that method works well in practice is presented.

1.5.4   Conclusion

A method of compressed sensing-based interference mitigation, and its application to a direct conversion receiver is a results of the research conducted in this work. Based on the proposed compressed sensing-based method of relaxing the low-pass filtering it can be concluded that *By applying compressed sensing to the acquisition of downconverted signals it is possible to relax analog filtering in a direct conversion receiver and move more signal processing into the digital domain without increasing the analog-to-digital sampling frequency to the Nyquist frequency of the interfered signal.*

Bibliography

[1] R. H. Walden, "Analog-to-Digital Converter Survey and Analysis.", *IEEE J. Sel. Areas Commun.*, vol. 17(4), Apr. 1999.

[2] B. Le, T. W. Rondeau, J. H. Reed, W. Bostian, "Analog-to-Digital Converters. A review of the past, present, and future.", *IEEE Sig. Proc. Mag.*, vol. 22(6), Nov. 2005.

[3] Z. Razak, T. Arslan, "Analog to Digital Converter Specification for UMTS/FDD Receiver Applications", *Proc. 4th IEEE International Symposium on Electronic Design, Test and Applications, DELTA 2008*, pp. 446–449, Paris, France, 2008.

[4] S. Park, M. P. Flynn, "Design techniques for high performance CMOS flash analog-to-digital converters", *Proc. 2005 European Conference on Circuit Theory and Design.*, Cork, Ireland, pp. 131–134, 2005

[5] D.G. Nairn, "Time-interleaved analog-to-digital converters", *Proc. IEEE Custom Integrated Circuits Conference (CICC), 2008*, San Jose, CA, pp. 289–296, 2008.

[6] R. M. Gray, D. L. Neuhoff "Quantization", *IEEE Trans. Inf. Theory*, vol. 44(6), pp. 2325–2383, Oct. 1998.

[7] R. M. Gray, "Oversampled Sigma-Delta Modulation ", *IEEE Trans. Commun.*, vol. 35(5), pp. 481–489, May 1987.

[8] G. A. Gray, G. W. Zeoli, "Quantization and Saturation Noise Due to Analog-to-Digital Conversion", *IEEE Trans. Aerosp. Electron. Syst.*, vol. AES7(1), pp. 222-223, Jan. 1971.

[9] Analog Devices (2009). "A/D Converters. Analog Devices.",[Online] Available: `http://www.analog.com/en/analog-to-digital -converters/ad-converters/products/index.h tml`

[10] H. Baher, "Signal Processing and Integrated Circuits.", Hoboken, USA, *Wiley-Blackwell*, 2012, ISBN: 978-0-470-71026-5.

[11] B. Razavi, "Architectures and Circuits for RF CMOS Receivers.", *Proc. of IEEE 1998 Custom Integrated Circuits Conference*, pp. 393400, Santa Clara, USA, May 1998.

[12] Besser, L. and Gilmore, R., "Practical RF Circuit Design for Modern Wireless Systems.", Norwood, USA, *Artech House*, 2003, ISBN: 978-1-580-53521-2.

[13] M. Pathak, S. K. Lim, "Fast Layout Generation of RF Embedded Passive Circuits Using Mathematical Programming.", *IEEE Trans. Compon. Packag. Manuf. Technol.*, vol. 2(1), pp. 32–45, Jan. 2012.

[14] S. H. Yeung, W. S. Chan, K. T. Ng, K. F. Man, "Computational Optimization Algorithms for Antennas and RF/Microwave Circuit Designs: An Overview.", *IEEE Trans. Ind. Inf.*, vol. 8(2), pp. 216–227, May 2012.

[15] H. Nyquist, "Certain topics in telegraph transmission theory", *Trans. AIEE*, vol. 47, pp. 617-644, Apr. 1928.

[16] R.G Lyons, "Understanding Digital Signal processing, 2nd edition, Prentice-Hall.", Upper Saddle River, USA, *Prentice Hall*, 2010, ISBN: 978-0-137-02731-5.

[17] C.E. Shannon, "Communication in the presence of noise," *Proc. Inst. Radio Eng.*, vol. 37(1), pp. 10–21, Jan. 1949.

[18] M.J Lighthill, "Introduction to Fourier Analysis and Generalised Functions", London, UK, *Cambridge University Press*, 1964,

[19] J. Mitola, "The software radio architecture", *IEEE Commun. Mag.*, vol. 33(5), pp. 26–38, May 1995.

[20] Y. Zhou, Z. Pan, "Impact of LPF Mismatch on I/Q Imbalance in Direct Conversion Receivers", *IEEE Trans. Wireless Commun*, vol. 10(4), pp. 1702–1708, Jun. 2011.

[21] N. C. Davies, "A high performance HF software radio", *Proc. 8th Int. Conf. HF Radio Systems and Techniques*, Guildford, UK, pp. 249-256, 2000.

[22] A. A. Abidi, "Direct-Conversion Radio Transceivers for Digital Communications", *IEEE J. Solid-State Circuits*, vol. 30(12), pp. 1399–1410, Dec. 1995.

[23] A. A. Abidi, "The Path to the Software-Defined Radio Receiver", *IEEE J. Solid-State Circuits*, vol. 42(5), pp. 954–996, Dec 2007.

[24] M. Ben-Romdhane, C. Rebai, P. Desgreys, A. Ghazeli, P. Loumeau, "Flexible Baseband Analog Front-end for NUS based Multistandard Receiver", *Proc. Joint IEEE North-East Workshop on Circuits and Systems and TAISA Conference*, Toulouse, France, pp. 1–4, Jun. 2009.

[25] M. Ben-Romdhane, C. Rebai, P. Desgreys, A. Ghazeli, P. Loumeau, "Pseudorandom Clock Signal Generation for Data Conversion in a Multistandard Receiver", *Proc. IEEE Int. Conference on Design and Technology of Integrated Systems in Nanoscale Era*, pp. 1-4, Tozeur, Tunisia, Mar. 2008.

[26] M. Ben-Romdhane, C. Rebai, K. Grati, A. Ghazel, G. Hechmi, P. Desgreys and P. Loumeau, "Non-Uniform Sampled Signal Reconstruction for Multistandard WiMax/WiFi Receiver", *IEEE International Conference on Signal Processing and Communication*, pp. 181-184, Dubai, Nov. 2007.

[27] 3GPP TS 36.211 v10.0.0 Technical Specification, "3rd Generation Partnership Project; Technical Specification Group Radio Access Network; Evolved Universal Terrestrial Radio Access (E-UTRA); Physical Channels and Modulation.", *3GPP Project 2010*, available on the 3GPP website: http://www.3gpp.org.

[28] 3GPP TS 36.212 v10.0.0 Technical Specification, "3rd Generation Partnership Project; Technical Specification Group Radio Access Network; Evolved Universal Terrestrial Radio Access (E-UTRA); Multiplexing and channel coding.", *3GPP Project 2010*, available on the 3GPP website: http://www.3gpp.org.

[29] S. Sesia, I. Toufik, M. Baker, "LTE - The UMTS Long Term Evolution: From Theory to Practice.", *John Wiley & Sons*, 2009, ISBN: 978-0-470-69-716.

[30] V. Tarokh, "New Directions in wireless Communications Research.", *Springer Science+Business Media LLC* 2009, ISBN: 978-1-4419-0674-4.

[31] E. Dahlman, S. Parkvall, J. Skold, P. Beming, "3G Evolution: HSPA and LTE for Mobile Broadband.", *Elsevier Ltd.* 2007, ISBN: 978-0-5218-8221-7.

[32] F. Khan, "LTE for 4G Mobile Broadband.", *Cambridge University Press* 2009, ISBN: 978-0-5218-8221-7.

[33] H. Holma, A. Toskala, "LTE for UMTS - OFDMA and SC-FDMA Based Radio Access.", *John Wiley & Sons Ltd.* 2009, ISBN: 978-0-470-99401-6.

[34] K. Yang, "Interference management in LTE wireless networks [Industry Perspectives]", *IEEE Wireless Commun. Mag.*, vol. 19(3), pp. 8-9, Jun. 2012.

[35] G. Boudreau, J. Panicker, R. Chang, N. Wang, S. Vrzic, "Interference Coordination and Cancellation for 4G Networks", *IEEE Commun. Mag.*, vol. 47(4), pp. 74-81, Apr. 2009.

[36] M. Huang, W. Xu, "Macro-femto inter-cell interference mitigation for 3GPP LTE-A downlink", *Proc. 2012 IEEE Wireless Communications and Networking Conference Workshops (WCNCW)*, pp. 75–80, Paris, France, Apr. 2012.

[37] R.G. Baraniuk, "Compressive Sampling," *IEEE Signal Process. Mag.*, vol. 24(4), pp. 118–120,124 Jul. 2007.

[38] E.J. Candès, J. Romberg and T. Tao, "Robust Uncertainty Principles: Exact Signal Reconstruction From Highly Incomplete Frequency Information.", *IEEE Trans. Inf. Theory*, vol. 52(2), pp. 489–509, Feb. 2006.

[39] E.J. Candès and M. B. Wakin, "An Introduction To Compressive Sampling.", *IEEE Signal Process. Mag.*, vol. 25(2), pp. 21–30, Mar. 2008.

[40] M. Elad, "Sparse and Redundant Representations. From Theory to Applications in Signal and Image Processing.", Berlin, Germany, *Springer*, 2010, ISBN 978-1-441-97011-4.

[41] E.J. Candès and T. Tao, "Decoding by Linear Programming.", *IEEE Trans. Inf. Theory*, vol. 51(12), pp. 4203–4215, Nov. 2005.

[42] D.L. Donoho, "Compressed Sensing", *IEEE Trans. Inf. Theory*, vol. 52(4), pp. 1289–1306, Apr. 2006.

[43] R.G. Baraniuk, M. Davenport, R. Devore, M. Wakin, "A Simple Proof of the Restricted Isometry Property for Random Matrices", *Constructive Approximation*, vol. 28(3), pp. 253–236, Dec. 2008.

[44] J.A. Tropp, "Just Relax: Convex Programming Methods for Identifying Sparse Signals in Noise", *IEEE Trans. Inf. Theory*, vol. 52(3), pp. 1030–1051, Mar. 2006.

[45] J.A. Tropp and A.C. Gilbert, "Signal Recovery From Random Measurements Via Orthogonal Matching Pursuit", *IEEE Trans. Inf. Theory*, vol. 53(12), pp. 4655–4666, Dec. 2007.

[46] T. Blumensath, M. Davies, "Gradient Pursuits", *IEEE Trans. Sig. Process.* , vol. 56(6), pp. 2370-2382, Jun. 2008.

[47] S. Kirolos, J. Laska, M. Wakin, M. Duarte, D. Baron, T. Ragheb, Y. Massoud, R. Baraniuk, "Analog-to-Information Conversion via Random Demodulation", *Proc. IEEE Dallas/CAS Workshop on Design Applications Integration and Software (DCAS)*, Dallas, USA, pp. 71–74, 2006.

[48] P. J. Pankiewicz, T. Arildsen, T. Larsen, "Sensitivity of the random demodulation framework to filter tolerances", *Proc. 19th European Signal Processing Conference (EUSIPCO)*, Barcelona, Spain, pp. 534–538, 2011.

[49] J. Tropp, J. Laska, M. Duarte, J. Romberg, and R. Baraniuk, "Beyond Nyquist: Efficient Sampling of Sparse Bandlimited Signals", *IEEE Trans. Inf. Theory*, vol. 56(1), pp. 520–540, Jan. 2010.

[50] J. Laska, S. Kirolos, Y. Massoud, R. Baraniuk, A. Gilbert, M. Iwen and M. Strauss, "Random Sampling for Analog-to-Information Conversion of Wideband Signals", *Proc. IEEE Dallas Circuits and Systems Workshop (DCAS)*, pp. 119–122, Dallas, USA, 2006.

[51] M. Mishali, Y. C. Eldar, "From Theory to Practice: Sub-Nyquist Sampling of Sparse Wideband Analog Signals", *IEEE J. Sel. Topics Signal Process.*, vol. 4(2), pp. 375-391, Apr. 2010.

[52] M. Mishali, Y. C. Eldar, A. Elron, "Xampling: Signal Acquisition and Processing in Union of Subspaces", *IEEE Trans. Sig. Proc.*, vol. 59(16), pp. 4719-4734, Oct. 2011.

[53] P. Feng, and Y. Bresler, "Spectrum-Blind Minimum-Rate Sampling and Reconstruction of Multiband Signals", *Proc. 1996 IEEE Intl. Conf. Acoustics, Speech, and Signal Processing (ICASSP)*, Atlanta, USA, pp. 1688-1691, 1996.

[54] H. S. Shapiro, R. A. Silverman, "Alias free sampling of Random Noise", *IEEE Trans. Info. Theory*, vol. 16, pp. 147–152, Jun. 1960.

[55] J.J. Wojtiuk, "Randomized Sampling for Radio Design", *PhD Thesis*, University of Southern Australia, 2000.

[56] I. Bilinskis, A. Mikelsons, "Randomized Signal Processing.", Cambridge, UK, *Prentice Hall*, 1992, ISBN: 978-0-137-51074-0.

[57] F. Papenfuß, Y.Artyukh, E. Boole, D. Timmermann, "Nonuniform Sampling Driver Design For Optimal ADC Utilization", *Proc. Internal Symposium on Circuits and Systems, 2003 (ISCAS'03)*, Bangkok, Thailand, vol. 4, pp. 516–519, 2003.

[58] A. C. Gilbert, M. J. Strauss, and J. A. Tropp, "A Tutorial on Fast Fourier Sampling", *IEEE Signal Process. Mag.*, vol. 25(2), pp. 57–66, Mar. 2008.

[59] Y. P. Lin, and P.P. Vaidyanathan, "Periodically Nonuniform Sampling of Bandpass Signals", *IEEE Trans. Circuits Syst. II*, vol. 45(3), pp. 340-351, Mar. 1998.

[60] I. Homjakovs, M. Greitans, R. Shavelis, "Real-Time Acquisitions of Wideband Signals Data Using Non-Uniform Sampling", *Proc. IEEE Eurocon 2009*, Saint-Petersburg, Russia, pp. 1158-1163, 2009.

[61] J. Bang-Jensen, G. Gutin, "Digraphs, Theory, Algorithms and Applications.", *Springer-Verlag*, 2006, ISBN 978-1-85233-611-0.

[62] P. Vandewalle, J. Kovacevic, and M. Vetterli, "Reproducible Research in Signal Processing [What, why and how]", *IEEE Signal Process. Mag.*, vol. 26(3), pp. 37-47, May 2009.

Appendix A

LTE Downlink Transmitter Simulation Using MATLAB

Jacek Pierzchlewski and Torben Larsen

A.1   Introduction

Long Term Evolution (LTE) is a state-of-the-art standard for wireless communication, currently in technical implementation [3, 4, 5]. The standard has been defined by the 3GPP organization and it is publicly available – every engineer, researcher or student can download the official specification from the www.3gpp.org website. The 3GPP organization manages an international project called EPS (Evolved Packet System), which is widely known as the 4th generation of mobile telecommunication systems (4G). The Evolved Packet System includes the entire architecture of the 4G mobile systems, both packet network and radio interface. LTE is a part of the EPS project, which refers to a 4G air interface standard. Currently many companies in the world, as well as many universities, conduct research and development on this technology. The authors of this paper are in volved in research on signal processing for LTE systems, and they found that there is a lack of free software able to generate LTE signals. Although open source advanced LTE system simulators exist, no easy-to-use, public domain signal generators exist to be used in signal processing research and development. This article presents a toolbox to fill this gap. Functions able to generate the downlink LTE signals are the main part of the toolbox. Together with the functions, a module named LTE Professor is presented. LTE Professor is a GUI (Graphical User Interface) which is able to generate LTE signals, analyze these signals and visualize LTE time/frequency resources utilization. The whole source code is GPL licensed and is publicly available at the authors website [8].

The presented article is divided into two main parts. The first part is an introduction to the LTE downlink Physical Layer. Here we discuss basics of the LTE downlink time/frequency resources and signal generation. The second part of the article presents usage and architecture of the software, together with some examples of generated LTE signals.

A.2   LTE downlink introduction

The 4th generation of mobile telecommunication systems has, at least in theory, very good performance parameters in comparison to the previous generations [5]. Unfortunately, this gain came at a price of significant complication of the whole system. The LTE protocol stack is divided into several layers. Additionally, there is a distinction between the downlink and uplink protocol stacks, since there are significant asymmetries between the different directions of data transmission. Description of the entire LTE system would
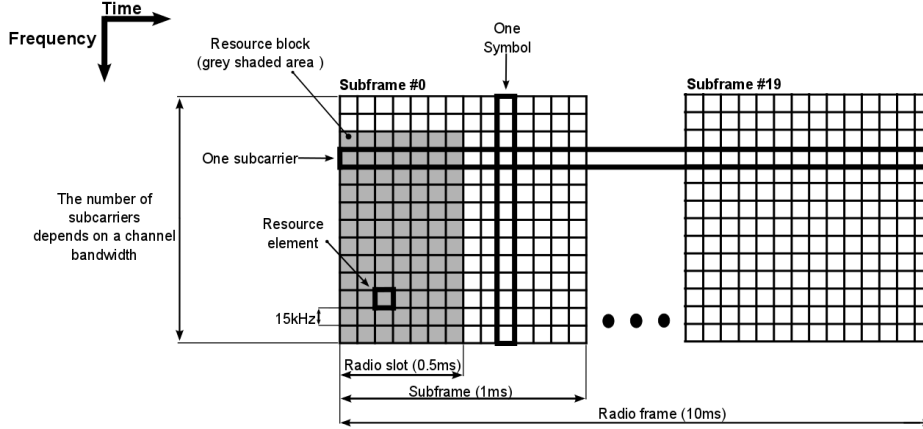
Figure A.1: Time/frequency resources organization

exceed the limitations of a single article. Therefore, this work is focused on a MATLAB toolbox which emulates the LTE downlink transmitter. This transmitter translates codewords, which are the input to the transmitter, into the LTE radio signal. The software is dedicated to engineers and scientists who are involved in research on modern communication signals and systems. In particular, this toolbox is useful in research on the LTE BTS transmission circuits, antenna systems and User Equipment (UE) receiver front ends. It can also be practical in investigation of the LTE and OFDM channel models. In addition, this software can cooperate with models of higher LTE downlink layers.

During the downlink data is passed from a base station (BTS) to a number of user equipment (UE) which is currently within a range of the BTS. To provide downlink data transmission service for multiple users, LTE systems use Orthogonal Frequency Division Multiple Access (OFDMA). The baseband signal is created using Orthogonal Frequency Division Modulation (OFDM). In OFDMA resources are represented in a time/frequency plane (Figure 2) - one Resource Element (RE) is an atomic unit in the plane. The LTE standard fully supports multi antenna technology, so there may be up to 8 time/frequency planes.

The accessible bandwidth is divided into a number of subcarriers [1]. In the LTE standard the separation between subcarriers is 15kHz during regular transmission. Subcarriers are gathered in Resource Blocks (RB), where one RB consists of 12 subcarriers. The number of subcarriers depends on the size of
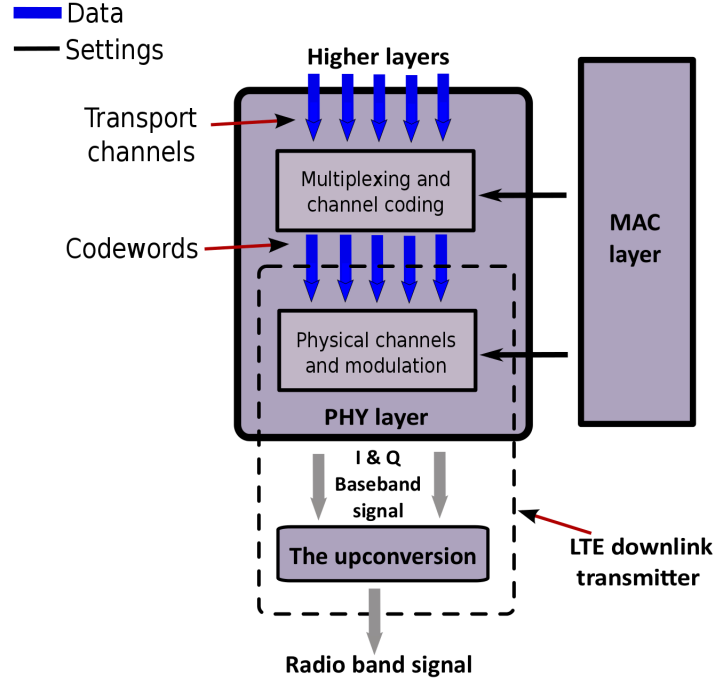
Figure A.2: The LTE downlink transmitter in the LTE stack

the baseband. However, there is always an integer number of resource blocks in the baseband. There are six possible bandwidths in the LTE standard: 1.4MHz, 3MHz, 5MHz, 10MHz, 15MHz, and 20MHz.

The time organization is a bit more complicated [1, 3, 5]. One symbol is an atomic unit of the time/frequency plane. The base length of a symbol (t_s) is equal to a multiplicative inverse of the subcarriers separation, so $t_s = (15\text{kHz})^{-1} = 66.7\mu s$. The Inverse Fast Fourier Transform (IFFT) operation is used to generate a downlink signal. To ensure reliable transmission, a copy of the last part of a symbol is copied to the beginning of every symbol, this copy is called 'Cyclic Prefix' (CP). Cyclic Prefix has a length t_{CP}, and this length may differ depending on the current CP settings. There are two basic CP settings: normal CP and extended CP.

The symbols are grouped in Radio Slots (RS). The duration of a single RS is always $500\mu s$. The number of symbols in one RS depends on the cyclic prefix type currently in use. There are six symbols in one RS in case of the extended cyclic prefix. In case of the normal cyclic prefix there are seven symbols in one RS. Additionally, in the latter case every first symbol in a
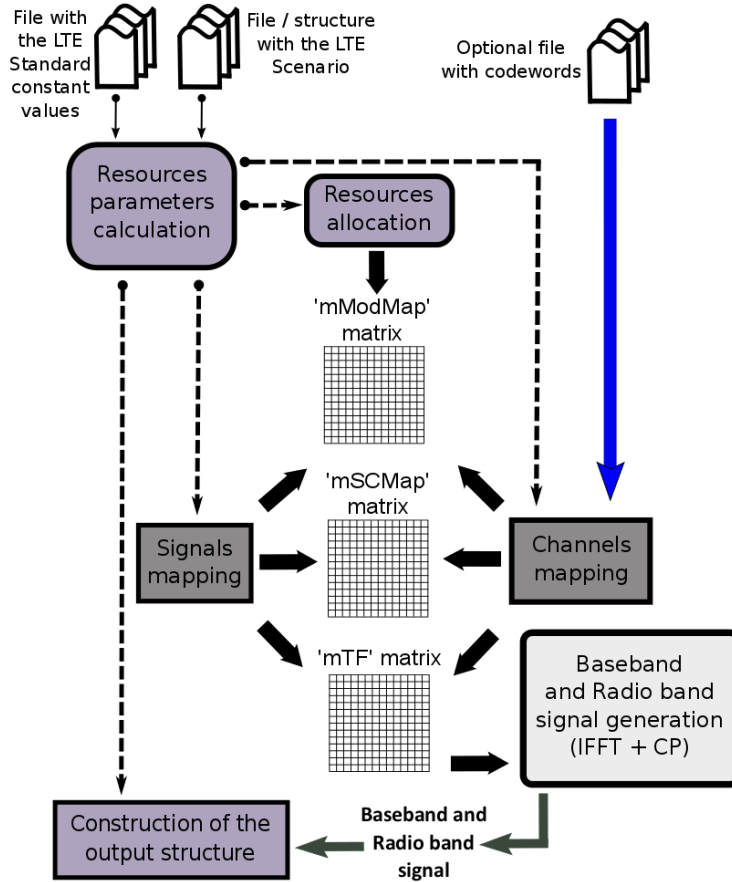
Figure A.3: The LTE trassmitter model architecture

RS has a longer cyclic prefix. A longer LTE time unit is a Subframe (SF).
The subframe has a time length of 1 ms and it consists of two Radio Slots.
A group of consecutive ten Subframes constructs a Radio Frame (RF). The
RF is the longest time unit in the LTE standard. The duration of one RF is
10ms (Figure 2). In the LTE downlink bandwidth resources are granted to a
specific UE as a group of resource blocks. The resource assignment is renewed
in every SF and cannot be changed until the end of a SF.

A.3 The MATLAB models of the LTE transmitter

A.3.1 LTE downlink transmitter

Figure 1 shows the position of the LTE downlink transmitter in the LTE protocol stack. There are two main parts of the LTE Physical Layer responsible for processing data from the higher layers. The upper part is responsible for multiplexing and channel coding [2]. The bottom part is responsible for physical channels modulation and mapping to the resource elements [1]. The MAC layer controls the entire physical layer [1, 2, 3, 5]. The presented MATLAB model emulates the bottom part of the Physical Layer.

The resource planes, in which signals and channels are mapped, are given to the OFDM modulator. The modulator generates the baseband signal. The baseband signal is then up-converted to the LTE radio signal. The presented software emulates both the baseband signal generator and the radio frequency generator. The baseband in-phase and quadrature signals (I and Q signals), as well as the radio frequency signal are the output from the presented model. Additionally, users have access to the resource planes and modulation symbols mapped to all physical signals and channels. Downlink data comes to the transmitter in the form of codewords. Codewords are mapped to physical channels. Different physical channels can be in use depending on the current type of transmission. In the LTE standard different types of transmission are used on different Antenna Ports (AP). The implemented MATLAB model supports the most common type, the transmission with Cell Specific Reference (CRS) signals [1]. The multi antenna transmission is supported. In the current software version the first and the second transmission modes are implemented.

A.3.2 The LTE transmitter model and supplementary software

The presented MATLAB model is available in the form of a toolbox. The detailed description of the toolbox can be found in [8]. The 'LTE scenario' structure must be passed as an argument to the main generator function. This structure is necessary to run the generator. It groups user settings and settings coming from the MAC layer. The toolbox contains examples of LTE scenario files to be used by users as a base for their own LTE scenario

The second data structure passed to the generator is a structure with codewords data. In general this structure is not required since in the case of no input data the LTE generator sends random bits. Additionally, it is possible to include codewords only for a few physical channels the missing
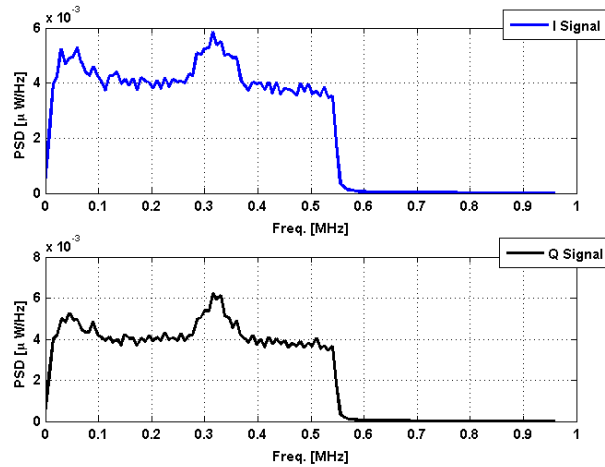
Figure A.4: Power spectral density of the baseband signals (1.4 MHz bandwidth).
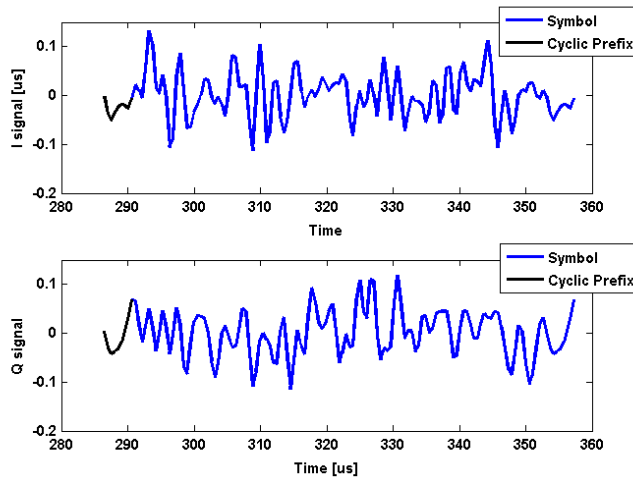
Figure A.5: Baseband signals in the time domain (1.4 MHz bandwidth).

data will be randomly generated.

The generator returns one structure. Obviously this structure contains the baseband and radio band signals. Beside of these signals there are resource matrices that indicate signals/channels mapping and modulation mapping, matrices with symbols mapped to particular channels and structures with LTE

Physical Layer specific parameters. The detailed description of this structure can be found in [8].

The next essential part of the presented toolbox is the 'LTE Professor' module. This module consists of two main parts. The first part is dedicated to be a graphical interface for the developed MATLAB LTE model functions. With this part users are able to set all parameters of the LTE scenario used by the LTE transmitter function. It is possible to get information about time and frequency parameters of the signal which corresponds to the adjusted scenario settings. Finally the user is able to generate the LTE downlink signal and store in the chosen file.

The second part of the LTE Professor is able to analyze and visualize generated signals. Users can observe the detailed view of the signals and channels mapping. This view gives information about modulation schemes and values mapped to all Resource Elements used in the analyzed LTE signal (Figure 6). It is possible to generate the indicative 'helicopter view' of the entire resources plane (Figure 7). Moreover, the entire LTE signal, as well as every particular LTE symbol in the generated transmission, can be viewed and analyzed in the frequency and time domains (Figures 4, 5). The extensive description of the LTE Professor is available at [8].

The validation of the software was performed in a few different ways. The LTE Professor module, which is also a part of the presented toolbox, was originally dedicated to validate the generator. The generated signals were analyzed with the LTE Professor. Mapping of LTE signals into time/frequency resources were compared with the maps that can be found in literature. Additionally, the peak-to-average- power ratio of the generated LTE bandwidth signals was measured to ensure that the generated signals are correct.

A.3.3   The software internals

Figure 3 shows the architecture of the implemented MATLAB models. The main 'LTE_DL1a' script controls the whole process. The LTE Resource Parameters Calculation unit (RPC) is run as the first sub module. This unit generates three structures: 'sP','sF' and 'sT', which contain LTE system parameters, LTE bandwidth parameters and LTE time parameters respectively. These three structures are used in all later steps of the LTE signal generation. After running the RPC unit, three identical matrices are allocated in the Resources Allocation (RA) unit. These matrices reflect the time/frequency resources. The number of rows in the matrices is equal to the number of subcarriers and the number of columns is equal to the number of symbols in the entire LTE transmission. The reference and synchronization signals are
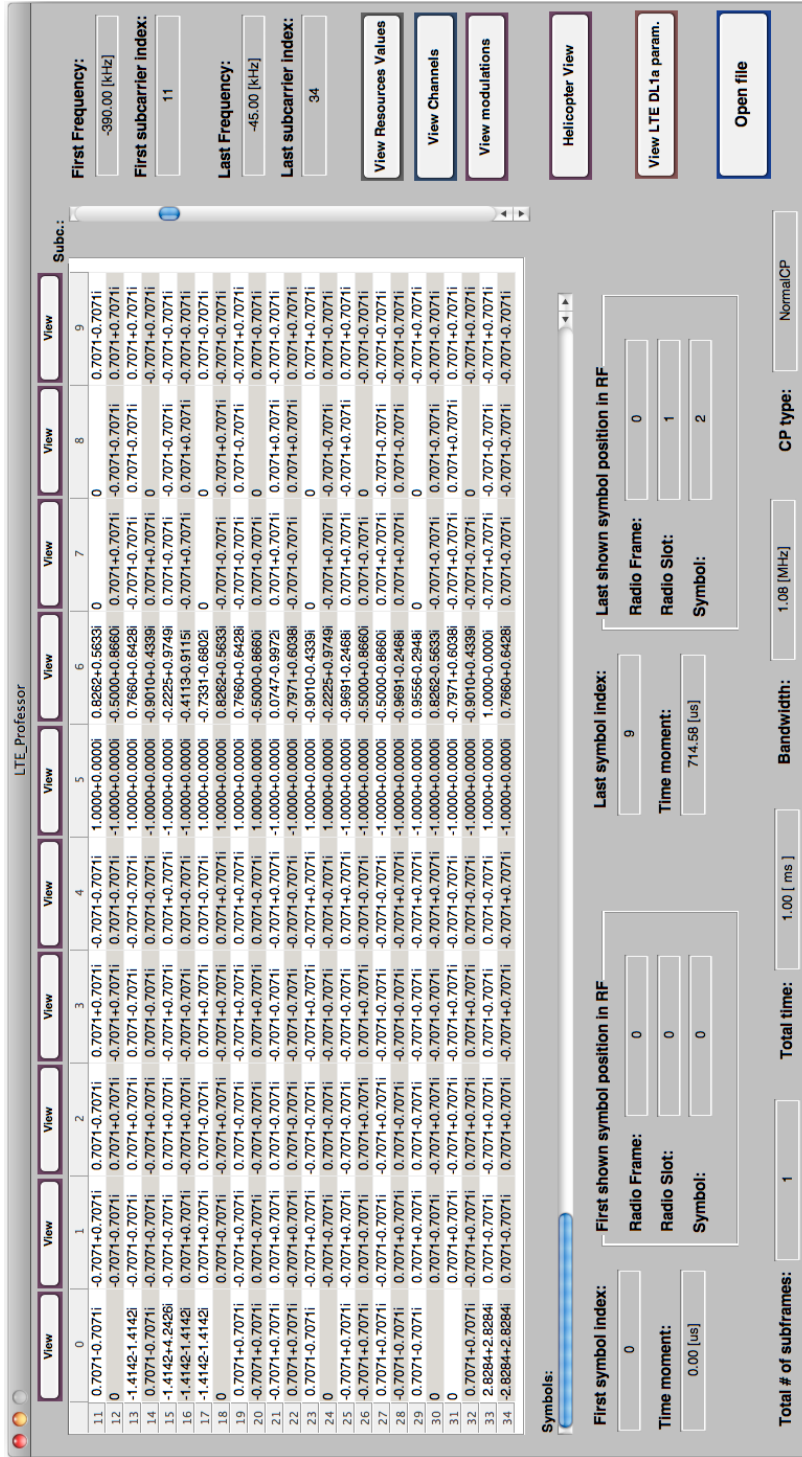
Figure A.6: Screen shot of the LTE Professor.

added in the Signals Mapping (SM) unit. The channels are mapped to the time/frequency resources in the Channel Mapping (CM) unit.

When all signals and channels are mapped to the LTE resources, the IFFT module generates the pure OFDM signal (without CPs). Adding cyclic prefixes to the pure OFDM signal generates the final baseband signal. Afterwards, the signal is up-converted to the radio frequency.

A.3.4   Examples of signals generated by the software

Figure 4 shows the power spectrum density of the example baseband signal generated by the software. The signal on this figure is a 1.4 MHz LTE baseband signal. It appears that the power is not uniformly distributed, which is due to the nonuniform channels and signals mapping. In the LTE standard not all resource elements are in use during transmission. Rules of the channel and signal mapping can vary due to the current bandwidth settings.

In Figure 5 the above LTE baseband signals are shown in the time domain. The time length of the shown signals is equal to the time length of one symbol with a cyclic prefix. The cyclic prefix, marked in black, is exactly the same as the last part of the symbol it is correct according to the LTE standard. The presented plots are generated automatically using the LTE Professor software. A screenshot of this software, with a view on the resource elements with mapped signals and channels is presented in Figure 6. Figure 7 show the LTE signal in the time/frequency domain. The resource elements, in which the LTE signals and channels are mapped, are depicted. This map is generated by the 'helicopter view' option in the LTE Professor. The map presents the first Subframe in the Radio Frame.

The signal presented above is just an example of the LTE signal which can be generated by the software. Hence, due to the GUI interface and predefined scenarios delivered with the software, it is easy to generate signals that correspond to the demands of the user. With relevance to reproducible research the authors prepared MATLAB scripts which can be used to generate the presented signals. The scripts are available on the project website [8].

A.3.5   Summary

The MATLAB toolbox which is able to generate LTE downlink signals has been presented. This program is published under the GPL open source license. The authors have prepared a website where the code is available for users. The website also contains also a blog about the MATLAB LTE signal generator
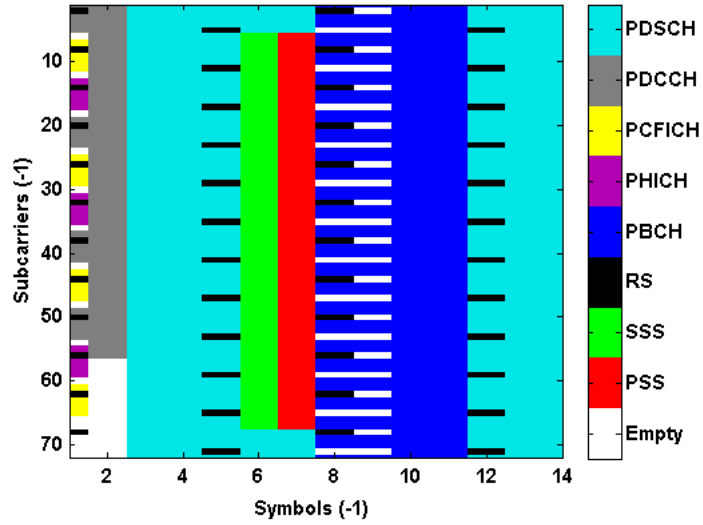
Figure A.7: LTE signals and physical channels map made by the software (1.4
bandwidth).

and a message board for information and comments exchange. The signals
generated by the software are also included.

[1] 3GPP TS 36.211 v10.0.0 Technical Specification, "3rd Generation Partnership Project; Technical Specification Group Radio Access Network; Evolved Universal Terrestrial Radio Access (E-UTRA); Physical Channels and Modulation.", *3GPP Project 2010*, available on the 3GPP website: http://www.3gpp.org

[2] 3GPP TS 36.212 v10.0.0 Technical Specification, "3rd Generation Partnership Project; Technical Specification Group Radio Access Network; Evolved Universal Terrestrial Radio Access (E-UTRA); Multiplexing and channel coding.", *3GPP Project 2010*, available on the 3GPP website: http://www.3gpp.org

[3] S. Sesia, I. Toufik, M. Baker, "LTE - The UMTS Long Term Evolution: From Theory to Practice.", *John Wiley & Sons 2009*, ISBN 978-0-470-69-716

[4] V. Tarokh, "New Directions in wireless Communications Research.", *Springer Science+Business Media LLC 2009*, ISBN 978-1-4419-0674-4

[5] E. Dahlman, S. Parkvall, J. Skold, P. Beming, "3G Evolution: HSPA and LTE for Mobile Broadband.", *Elsevier Ltd. 2007*, ISBN 978-0-5218-8221-7

[6] F. Khan "LTE for 4G Mobile Broadband.", *Cambridge University Press 2009*, ISBN 978-0-5218-8221-7

[7] H. Holma, A. Toskala, "LTE for UMTS - OFDMA and SC-FDMA Based Radio Access.", *John Wiley & Sons Ltd. 2009*, ISBN 978-0-470-99401-6

[8] Authors website with code repository and a blog dedicated for the presented software: http:/sparsesampling.com/lte.htm

Appendix B

Compressed Sensing-Based Direct Conversion Receiver

Jacek Pierzchlewski, Thomas Arildsen and Torben Larsen

The current layout has been revised compared to the published version.

Abstract

Due to the continuously increasing computational power of modern data receivers it is possible to move more and more processing from the analog to the digital domain. This paper presents a compressed sensing approach to relaxing the analog filtering requirements prior to the ADCs in a direct conversion receiver. In the presented solution, the filtered down-converted radio signals are randomly sampled with an average sampling frequency lower than its Nyquist rate, and then reconstructed in a DSP system. To enable compressed sensing, this approach exploits the frequency domain sparsity of the down-converted radio signals.

As shown in an experiment presented in the article, when the proposed method is used, it is possible to relax the requirements for the quadrature down-converter filters. A random sampling device and an additional digital signal processing module is the price to pay for these relaxed filter requirements.

B.1 Introduction

Twenty years ago around 98% of the radio frequency communication receivers were heterodyne [1], but the cost-driven evolution dethroned heterodyne receivers from this position. At present, direct conversion receivers [1, 3, 4] are widely used in mobile devices, though heterodyne receivers are still used in more expensive equipment due to superior performance. There are many disadvantages of the direct conversion receiver architecture [3, 4], of which the most important is sensitivity to distortion produced by strong interfering signals, spurious leakage of local oscillators, DC offset after the mixer, mismatching between in-phase and quadrature-phase signals and generally poor sensitivity. Nevertheless, direct conversion receivers consist of significantly less analog elements than heterodyne receivers, which makes them cheaper and more suitable for integration.

The current challenge is to relax the requirements for the analog parts of a direct conversion receiver, due to design and integration problems which are caused by the analog parts. New possibilities for solving this problem appear with increasing computational power available in receivers. The present paper investigates the problem of relaxing the requirements for the quadrature down-converter filters. In the direct-conversion receivers there are high requirements for the down-conversion filters due to noise, interference, and high frequencies generated by the down-conversion process. These filters cause challenges in integration, mostly due to IC (Integrated Circuit) area required to implement these filters. Recently there was proposed a direct conversion circuit in which

uniform sampling is replaced with a pseudorandom sampling technique [8, 7, 6]. Afterwards, the sampled signal is reconstructed in a DSP (Digital Signal Processing) system. Hence, a minor reduction of the order of the quadrature down-converter filters was possible.

In the presented solution, the frequency domain sparsity of a down-converted signal is exploited. In this paper the authors propose to randomly sample the down-converted signals with an average frequency lower than the Nyquist rate of the signal. Then, a reconstruction of the down-converted signals is performed using compressed sensing reconstruction algorithms. Compressed sensing is a signal processing technique which allows sampling of a signal below its Nyquist rate and, under certain assumptions, recover the signal afterwards using a reconstruction algorithm [9, 10, 11, 12]. To make a compressed sensing process possible, the sampled signal must be compressible. A signal is compressible if it possible to approximate this signal in some domain with a sparse vector. In this paper the authors show that the down-converted radio signal is sparse in the frequency domain and hence, it can be compressively sampled. A random sampler which acquires the signal and a modified reconstruction method is presented. Hence to the proposed solution, the down-converted radio signal can be compressively sampled without a high order post-mixer low-pass filter. A random sampling process and an additional DSP module is the price pay in order to enable the proposed modifications.

The paper is organized as follows. The problem of the down-converter filters and the idea of the compressed sensing-based homodyne receiver is presented in Section B.2. A practical experiment is presented in section B.3. Finally, some conclusions are presented in section B.4.

B.2 Compressed sensing-based direct conversion receiver

B.2.1 Quadrature down-converter filters in a direct conversion receiver

A typical direct conversion receiver dedicated to digital communication is presented in Fig. 1. A radio frequency signal from the antenna is filtered by a bank of RF band-pass filters, which selects the currently received band, and amplified by a low noise amplifier. The filtered radio frequency signal $s_r(t)$ is:

$$s_r(t) = s(t) + s_b(t) + n_r(t) \tag{B.1}$$
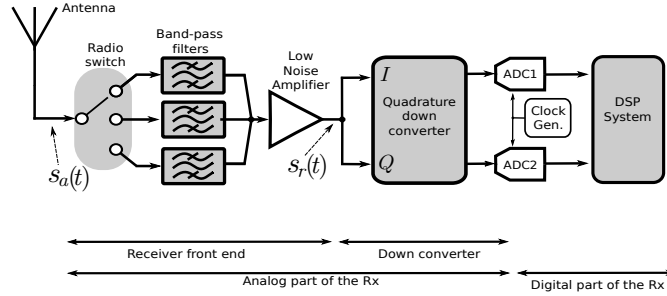
Figure B.1: The analog and the digital part of a direct conversion receiver

where $s(t)$ is the wanted radio signal to be received:

$$s(t) = I(t) \cdot \cos(2\pi f_0 t) - Q(t) \cdot \sin(2\pi f_0 t) \tag{B.2}$$

where f_0 is the carrier frequency, $I(t)$ and $Q(t)$ are transmitted information-carrying band-limited signals. The non-bandlimited noise $n_r(t)$ in (B.1) represents all analog noise (including noise from the entire receiver, the channel and from the transmitter). The $s_b(t)$ component in (B.1) represents adjacent channel interference signals (blockers) present in the filtered radio signals due to the size of frequency spectrum allowed by the band-pass radio filters (Fig. B.2):

$$s_b(t) = s_{b1}(t) + s_{b2}(t) + \cdots + s_{bN}(t) \tag{B.3}$$

where N is the current number of blockers. The frequency range of the radio filter pass-band is $[f_0 - f_r, \ f_0 + f_r]$. The blockers are distributed somewhere in this spectrum, neither the number of blockers nor their exact frequency distribution is known.

The filtered radio frequency signal is processed by a quadrature down-converter circuit. In the down-converter (Fig. 3) the radio frequency signal is split into I and Q, and mixed with a signal of a frequency equal to the radio carrier frequency f_0. This process separates the bandpass signal (B.1) into a low-frequency component ($\lambda_I(t)$ in the I-path and $\lambda_Q(t)$ in the Q-path) and high frequency component ($X_I(t)$ in the I-path and $X_Q(t)$ in the Q-path):

$$s_I(t) = \lambda_I(t) + X_I(t) + n_I(t) \tag{B.4}$$
$$s_Q(t) = \lambda_Q(t) + X_Q(t) + n_Q(t) \tag{B.5}$$

where $s_I(t)$ and $s_Q(t)$ are the down-converted signals in the I and Q respectively (Fig. 3a). In the above equation, the $n_I(t)$ and $n_Q(t)$ represent the

non-bandlimited noise. The low-frequency components $\lambda_I(t)$ and $\lambda_Q(t)$ consist of wanted information-carrying band-limited signals $I(t)$ and $Q(t)$, and unwanted low-frequency down-converted blockers:

$$\lambda_I(t) = \frac{1}{2} \cdot I(t) + \underbrace{b_{I1}(t) + \cdots + b_{IN}(t)}_{\text{Blockers in the } I \text{ path}} \tag{B.6}$$

$$\lambda_Q(t) = \frac{1}{2} \cdot Q(t) + \underbrace{b_{Q1}(t) + \cdots + b_{QN}(t)}_{\text{Blockers in the } Q \text{ path}} \tag{B.7}$$

In the current paper, it is assumed that there is no co-channel interference, so the blockers are distributed in the frequency domain from the wanted signal baseband B until the f_r ($[f_0 + B, f_0 + f_r]$) (Fig. 4).

In the conventional direct conversion receivers the down-converted signals $s_I(t)$ and $s_Q(t)$ are filtered by high-order low-pass filters (Fig. 3a) which remove the high frequency components X_I and X_Q, virtually all the noise and the downconverted blockers (Fig. 4). It can be stated that in the above case the filtered signals $s_I^{\star\star}$ and $s_Q^{\star\star}$ consist of only the information carrying band-limited signals $I(t)$ and $Q(t)$:

$$s_I^{\star\star} = \frac{1}{2}I(t), \quad s_Q^{\star\star} = \frac{1}{2}Q(t) \tag{B.8}$$

The filtered signals $s_I^{\star\star}(t)$ and $s_Q^{\star\star}(t)$ are then uniformly sampled by ADCs:

$$\mathbf{s}_I^{\star\star}[n] = s_I^{\star\star}\left(n\frac{1}{f_u}\right), \quad \mathbf{s}_Q^{\star\star}[n] = s_Q^{\star\star}\left(n\frac{1}{f_u}\right), \quad n \in \mathbb{N} \tag{B.9}$$

where f_u is the uniform sampling frequency which must be higher than the Nyquist frequency of the band-limited signals $I(t)$ and $Q(t)$. Eventually, dis-
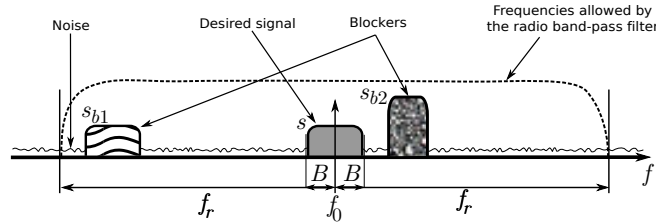
Figure B.2: The filtered radio signal s_r in the frequency domain. Beside of the desired signal there are blockers in the signal spectrum, due to wide frequency range allowed by the radio filter
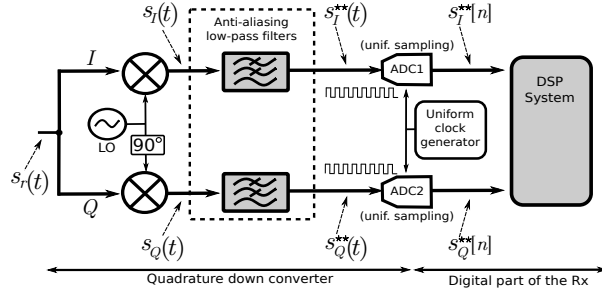
(a) Conventional quadrature down-converter, samplers and a DSP system in a direct conversion receiver
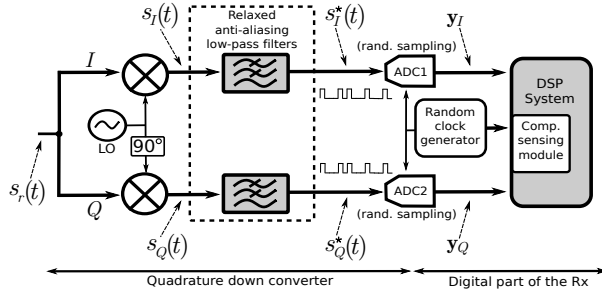
(b) Proposed compressed-sensing based quadrature down-converter with relaxed anti-aliasing filters, random samplers and a DSP system in a direct conversion receiver

Figure B.3: Conventional and proposed down-converter, samplers and DSP System in a direct conversion receiver

crete signals $\mathbf{s}_I^{\star\star}[n]$ and $\mathbf{s}_Q^{\star\star}[n]$ are processed by the DSP hardware. In this paper it is assumed that there is no I/Q imbalance in the receiver [17].

The low-pass anti-aliasing quadrature down-converter filters need to be of a high order, which creates severe problems in IC implementation. This is due to the chip area occupancy and the needed accuracy in filter design. Relaxing requirements for these filters without quality loss in a received signal is a problem which attracts more and more attention in radio communication engineering [8, 7, 6].

B.2.2 Low-order filters in homodyne receivers

In the presented solution the high order low-pass filters are replaced by 1st order low-pass filters (Fig. 3b). With this filter the high-frequency components X_I and X_Q and most of the noise are removed. The downconverted blockers
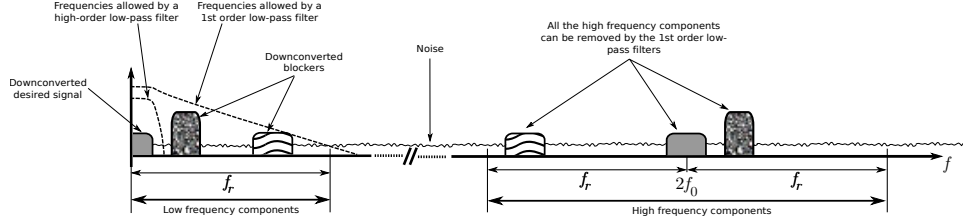
Figure B.4: The downconverted signal in the frequency domain

are still present in the filtered signal (Fig. 4). The signals filtered with a 1st order low-pass filter $s_I^\star$ and $s_Q^\star$ are:

$$s_I^\star(t) = \frac{1}{2} \cdot I(t) + \underbrace{b_{I1}^\star(t) + \cdots + b_{IN}^\star(t)}_{\text{Filtered blockers } (I \text{ path})} + n_I^\star(t) \qquad \text{(B.10)}$$

$$s_Q^\star(t) = \frac{1}{2} \cdot Q(t) + \underbrace{b_{Q1}^\star(t) + \cdots + b_{QN}^\star(t)}_{\text{Filtered blockers } (Q \text{ path})} + n_Q^\star(t) \qquad \text{(B.11)}$$

where $n_I^\star(t)$ and $n_Q^\star(t)$ reflect the noise present in the filtered signal. Due to the fact that blockers present in the signal may be distributed in the frequency domain until the frequency f_r (Fig. 4), the sampling rate needed to acquire the filtered signals $s_I^\star(t)$ and $s_Q^\star(t)$ is significantly higher than the sampling frequency needed to acquire the signals $s_I^{\star\star}(t)$ and $s_Q^{\star\star}(t)$ from (B.9). Implementation of Analog-to-Digital Converters (ADCs) which operate at such a high sampling frequency is impractical due to huge energy dissipation, and is virtually impossible in many applications.

B.2.3   Compressed sensing methodology

Let us consider a continuous analog signal $x(t)$, $0 \leq t \leq t_{\mathrm{x}}$ with the highest frequency component B and the Nyquist frequency $f_{\mathrm{N}} = 2B$. A given signal $x(t)$ is sampled:

$$\mathbf{y} = \phi(x(t)) \qquad \text{(B.12)}$$

where ϕ represents the signal sampling process, $\mathbf{y} \in \mathbb{R}^{M \times 1}$ is a discrete observed signal. Let us assume that the average sampling rate f_{s} of the observed signal $\mathbf{y}$ is lower than the Nyquist frequency f_{N} of the sampled signal $x(t)$:

$$f_{\mathrm{s}} = \frac{M}{t_{\mathrm{x}}}, \quad f_{\mathrm{s}} < f_{\mathrm{N}} \qquad \text{(B.13)}$$

where t_x is the time lenght of the signal $x(t)$. According to the compressed sensing theory [9, 10, 11], under certain conditions it is possible to reconstruct the vector $\mathbf{x} \in \mathbb{C}^{N \times 1}$, from the undersampled observed signal $\mathbf{y}$. The vector $\mathbf{x}$ is a discrete model of the sampled signal $x(t)$:

$$\mathbf{x}[n] = x(nT_{\mathrm{r}}), \quad T_{\mathrm{r}} = \frac{1}{f_{\mathrm{r}}}, \quad f_{\mathrm{r}} > f_{\mathrm{N}} \tag{B.14}$$

The reconstruction is performed with a reconstruction procedure $\mathcal{R} : \mathbf{y} \to \mathbf{x}$. The sampling frequency f_{r} of the discrete reconstructed signal $\mathbf{x}$ is higher than the average sampling frequency f_{s} and higher than the Nyquist rate f_{N} of the signal $x(t)$.

The first condition which must be fulfilled to enable compressed sensing is that the sampled signal $x(t)$ is compressible. The signal $x(t)$ is compressible if its discrete model $\mathbf{x}$ can be approximated in a given domain $\mathbf{\Psi} \in \mathbb{C}^{N \times K}$, $K \leq N$ with a sparse vector $\mathbf{v} \in \mathbb{C}^{K}$:

$$\mathbf{x} \approx \mathbf{\Psi}\mathbf{v}, \quad \|\mathbf{v}\|_0 < K \tag{B.15}$$

where the 'zero norm' [9] describes the number of non-zero elements in the vector. The more sparse the vector $\mathbf{v}$ is, the lower sampling frequency f_{s} is needed to successfully reconstruct the discrete signal $\mathbf{x}$ [9, 10]. Using the vector $\mathbf{x}$ it is possible to represent the acquistion procedure ϕ with a measurement matrix $\mathbf{\Phi} \in \mathbb{R}^{M \times N}$:

$$\mathbf{y} = \mathbf{\Phi}\mathbf{x} \tag{B.16}$$

The relation between the sparse vector and the observed vector may be expressed as:

$$\mathbf{y} = \mathbf{\Theta}\mathbf{v}, \quad \mathbf{\Theta} = \mathbf{\Phi}\mathbf{\Psi}, \quad \mathbf{\Theta} \in \mathbb{C}^{M \times K} \tag{B.17}$$

B.2.4 Sampler

The Restricted Isometry Property (RIP) was introduced in [10]. This property denotes, how close the matrix $\mathbf{\Theta} = \mathbf{\Phi}\mathbf{\Psi}$ behaves like an orthonormal matrix if the vector $\mathbf{v}$ is K-sparse (only K entries of the vector are non-zero). It was showed in [12] that if the measurement matrix $\mathbf{\Phi}$ is a random matrix, then the matrix $\mathbf{\Theta} = \mathbf{\Phi}\mathbf{\Psi}$ fulfills the requirement of Restricted Isometry Property (RIP) for most of the possible sparse vectors. Therefore, the sampling process should be maximally randomized to ensure the correct signal reconstruction. In practical signal sensing circuits it is, however, nontrivial to comply with the demand of randomness. The random demodulator [15] is a well-known single-ADC solution for compressed sensing signal acquisition. Unfortunatelly, the

(a) Uniform sampling measurement matrix

(b) Measurement matrix used in the receiver

(c) Gaussian-random measurement matrix
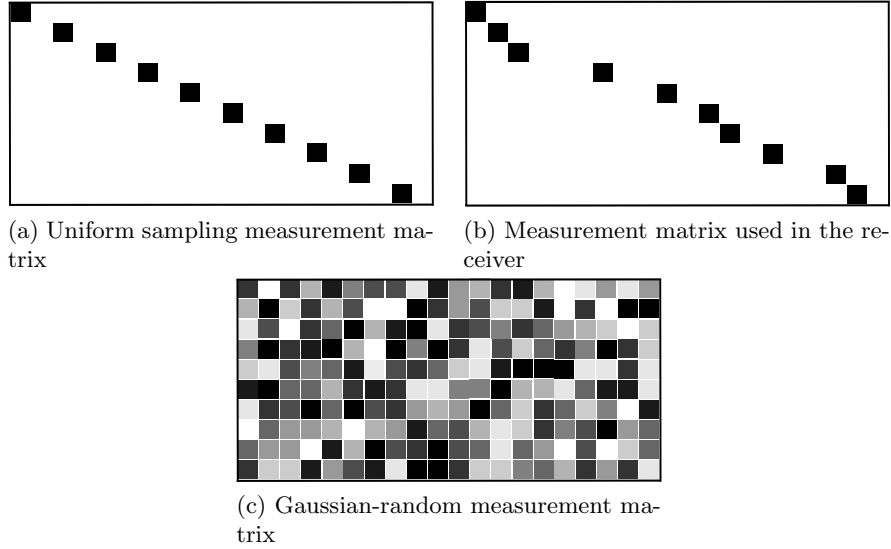
Figure B.5: Comparison of different measurement matrices $\mathbf{\Phi}$. The measurement matrix used in the experiment is a compromise between the randomness in the sampling process and the complexity of the acqusition device

random demodulator contains a multiple-order low-pass filter. Furthermore, imperfections of this filter may severely influence the signal reconstruction [16]. Due to these drawbacks, usage of the Random Demodulator is unacceptable in the considered application.

In the following system we use a random sampler following the post-mixer filters in the quadrature down-converter. The sampler does not include any preconditioning in the derivations to follow. In a practical context it may be necessary with conditioning as always to ensure that the input signals comply with the dynamic range of the sampler and following quantizer. The compressed sensing system processes the sampled signal in blocks of length t_{B}. The moments in which the signal is acquired are gathered in a sampling pattern set $\mathbb{S}$:

$$\mathbb{S} = \{t_1, t_2, ..., t_{\mathrm{M}}\} \quad t_{\mathrm{M}} \leq t_{\mathrm{B}} \tag{B.18}$$

Let us introduce a sampling grid set $\mathbb{G}$:

$$\mathbb{G} = \{\tau_1, \tau_2, ..., \tau_{\mathrm{K}}\}, \quad \tau_k = k\mathrm{T_g} \tag{B.19}$$

where $\mathrm{T_g}$ is a sampling grid period. The sampling pattern is always a subset of the grid set $\mathbb{S} \subset \mathbb{G}$. In other words, the sampling moments can occur only at

multiples of the sampling grid period T_g. Therefore, the sampling grid period describes the resolution of sampling. The average sampling ratio f_s is:

$$f_s = \frac{N_s}{t_B} \tag{B.20}$$

where N_s is the number of samples in a sampling pattern. The sampling grid period T_g is shorter than the shortest time between adjacent signal sampling moments required by the ADC used in the system. It can be stated that $T_g \leq T_{min} \leq T_s$ where T_s is the average sampling period. The sampling patterns are generated such that the minimum time between sampling moments T_{min} is kept. An example of a measurement matrix $\boldsymbol{\Phi}$ is compared to a Gaussian random measurement matrix and a uniform sampling measurement matrix in Fig. 5. The matrix generated by the proposed random sampler contains sufficient level of randomness, as it is shown later in numerical experiments.

B.2.5 Signal reconstruction procedure

The filtered signals $s_I^\star(t)$ and $s_Q^\star(t)$ can be approximated as sparse in the frequency domain (Fig. 4). Therefore, the dictionary $\boldsymbol{\Psi} \in \mathbb{C}^{N \times K}$ used in the experiment is the discrete Fourier transform dictionary:

$$\boldsymbol{\Psi} = [\psi_1, \psi_2, ..., \psi_K] \tag{B.21}$$

where a column ψ_k of the dictionary matrix corresponds to a tone of frequency $k\gamma$, where γ is frequency separation between dictionary tones. A column ψ_k of the dictionary matrix:

$$\psi_k = \cos(2k\pi n T_r) + j \cdot \sin(2k\pi n T_r) \tag{B.22}$$

where $n \in \{1, ..., N\}$, T_r is the sampling period of the reconstructed signal. The frequency separation γ depends on the time length of the processed signal t_B:

$$\gamma < \frac{1}{t_B} \tag{B.23}$$

In the proposed reconstruction γ is set to

$$\gamma = \frac{1}{2t_B} \tag{B.24}$$

The highest tone used in the receiver depends on the maximum frequency component which may be found in the signals filtered with a 1st-order low-pass filter:

$$K = \frac{f_r}{\gamma} \tag{B.25}$$

The signal reconstruction algorithms are based on the ℓ_1 optimization procedure:

$$\mathcal{R}_I : \mathbf{v}_I = \min \|\hat{\mathbf{v}}_I\|_1 \;\; sub.\, to: \;\; \|\mathbf{y}_I - \mathbf{\Phi}_I \mathrm{Re}(\mathbf{\Psi}\hat{\mathbf{v}}_I)\|_2 < \epsilon_I \qquad (\text{B.26})$$

$$\mathcal{R}_Q : \mathbf{v}_Q = \min \|\hat{\mathbf{v}}_Q\|_1 \;\; sub.\, to: \;\; \|\mathbf{y}_Q - \mathbf{\Phi}_Q \mathrm{Re}(\mathbf{\Psi}\hat{\mathbf{v}}_Q)\|_2 < \epsilon_Q \qquad (\text{B.27})$$

where $\mathcal{R}_I$ and $\mathcal{R}_Q$ are the reconstruction procedures for the I- and Q-paths respectively. The matrices $\mathbf{\Phi}_I$ and $\mathbf{\Phi}_Q$ are the measurements matrices which reflect the randomized sampling process in the I- and Q-paths. The parameters ϵ_I and ϵ_Q relax the feasible area of optimization due to noise present in the observed signal. These parameters should be adjusted to the current level of noise. The vectors $\mathbf{y}_I$ and $\mathbf{y}_Q$ are the signals observed in the I- and Q-paths.

The $\mathbf{v}_I$ and $\mathbf{v}_Q$ are the reconstructed vectors of frequency coefficients (Fig. 6). The discrete representation of the wanted information-carrying baseband signals I_r and Q_r is reconstructed as

$$I_r = \mathbf{\Psi}^\dagger \mathbf{v}_I^\dagger, \quad Q_r = \mathbf{\Psi}^\dagger \mathbf{v}_Q^\dagger \qquad (\text{B.28})$$

where $\mathbf{v}_I^\dagger \in \mathbb{C}^{K^\dagger \times 1}$ and $\mathbf{v}_Q^\dagger \in \mathbb{C}^{K^\dagger \times 1}$ are the truncated reconstructed vectors of frequency coefficients. These vectors contain only the frequency coefficients which correspond to the frequencies of the wanted information-carrying signals I and Q:

$$\mathbf{v}_I^\dagger(k) = \mathbf{v}_I(k), \quad \mathbf{v}_Q^\dagger(k) = \mathbf{v}_Q(k) \qquad (\text{B.29})$$

where $k = \{1, .., K^\dagger\}$. The index $K^\dagger$ is:

$$K^\dagger = \frac{B}{\gamma} \qquad (\text{B.30})$$

where B is the bandwidth of the signals I and Q. The dictionary $\mathbf{\Psi}^\dagger \in \mathbb{C}^{N \times K^\dagger}$ is the truncated dictionary used in the reconstruction:

$$\mathbf{\Psi}^\dagger = [\psi_1, \psi_2, ..., \psi_{K^\dagger}] \qquad (\text{B.31})$$

B.3 Numerical Experiment

The numerical experiment was conducted to test the presented concept. The experiment is presented in Fig. 7. The time of the simulation is $t_s = 10\ \mu$s. In the experiment white Gaussian noise signals are transmitted as the I and
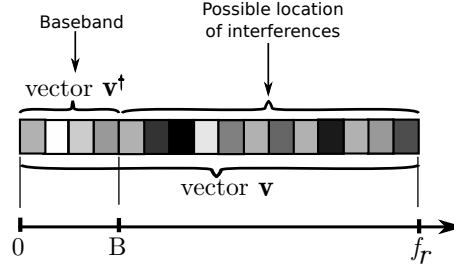
Figure B.6: The vector with frequency coefficients which covers the range $[0, \ f_r]$ is used in the convex optimization procedures (26) and (27). The vector $\mathbf{v}^\dagger$ is used in final reconstruction (28)

Q signals. The baseband of the I and Q signals is $B = 3\,\mathrm{MHz}$, the average power is $P_B = 1\,\mathrm{W}$ each. The I and Q signals are upconverted to a bandpass radio signal s_{tx} with a carrier frequency $f_0 = 800\,\mathrm{MHz}$. The power P_{tx} of the radio signal s_{tx} is 1 W. The signal is summed with interference signal s_{int}. The s_{int} signal consists of 10 continuous wave signals:

$$s_{int} = \sum_{i=1}^{10} a_i \cos(2\pi f_i t) \tag{B.32}$$

where the frequencies f_i of the interfered signals are in the range $(f_0 - f_r \leq f_i \leq f_0 - B)$ or $(f_0 + B \leq f_i \leq f_0 + B)$. There are two possible bandwidths considered, within which the interfering signals are contained: $f_r = 40\,\mathrm{MHz}$ and $f_r = 80\,\mathrm{MHz}$. Two levels of the power P_{int} of the interference signal s_{int} considered in the experiment: $P_{int} = 0.1\,\mathrm{W}$ and $P_{int} = 1\,\mathrm{W}$. The received radio signal s_r is amplified, downconverted and filtered with a 1st order low-pass filter with a cut-off frequency $f_{-3dB} = 20\,\mathrm{MHz}$. The filtered baseband signals are polluted with white Gaussian noise signals. There are 6 levels of noise power considered in the experiment (SNR_n): 10 dB, 15 dB, 20 dB, 25 dB, 30 dB, 35 dB, 40 dB where

$$SNR_n = \frac{P^\star}{P_n} \tag{B.33}$$

where $P^\star$ is the power of the filtered signal, P_n is the power of noise signals n_I and n_Q. The baseband signals are sampled by a random sampler with the average random sampling frequency $f_s = 30\,\mathrm{MHz}$, which corresponds to oversampling $OSR = 0.375$ and $OSR = 0.1875$ for the size of two possible frequency ranges given by $f_r = 40\,\mathrm{MHz}$ and $f_r = 80\,\mathrm{MHz}$ respectively. The baseband signals are reconstructed with the compressed sensing reconstruction
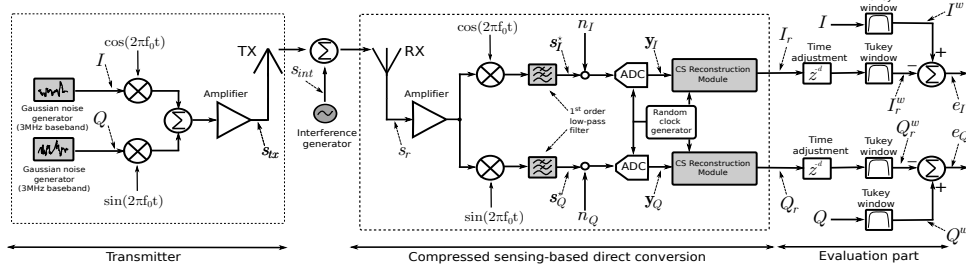
Figure B.7: The conducted numerical experiment

method described in B.2.5. The reconstructed signals I_r and Q_r are compared to the orignal baseband signals I and Q. For evaluation purposes, the average power of each of the reconstructed signals I_r and Q_r is adjusted to P_B (1 W). Before the comparison, the reconstructed signals are shifted in time to compensate delays introduced by the filters. The time shift is set experimentally. Both the reconstructed and the original signals are windowed with the Tukey window to suppress effects of numerical errors at the beginning and at the end of the reconstructed signal. The error vectors e_I and e_Q are computed:

$$e_I = I_r^w - I^w, \quad e_Q = Q_r^w - Q^w \tag{B.34}$$

where I_r^w and Q_r^w are the time-shifted and windowed reconstructed baseband signals, the I^w and Q^w are the windowed original baseband signals. The signal-to-noise ratios of the reconstructed baseband signals are:

$$SNR_I = \frac{P_{I^w}}{P_{e_I}}, \quad SNR_Q = \frac{P_{Q^w}}{P_{e_Q}} \tag{B.35}$$

where P_{I^w} and P_{Q^w} are the power of the windowed orignal signals I^w and Q^w respectively. The P_{e_I} and P_{e_Q} are the power of the error vectors e_I and e_Q signals respectively. The average of the values SNR_I and SNR_Q is treated as the measure of the reconstruction quality:

$$SNR_r = \frac{1}{2}(SNR_I + SNR_Q) \tag{B.36}$$

The results of the experiment are shown in Fig. 8. As it can be seen in Fig. 8 the baseband signal can be reconstructed in adverse conditions even if 1st order low-pass filters are used as the quadrature down-converter filters. As expected, the less polluted with noise, the better reconstruction is achieved. The 10 dB increase of the power of interference causes 5-6 dB loss in the
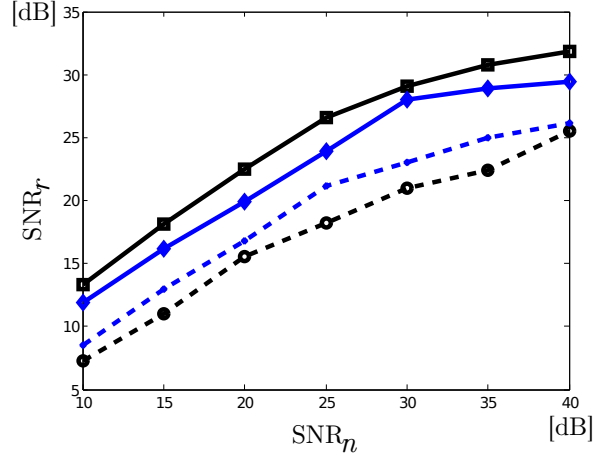
Figure B.8: Results of the experiment. Reconstructed signal SNR_r plotted vs. noise SNR_n. The range of the inteference is $f_r = 40$ MHz and $f_r = 80$ MHz. The power of interference is $P_{in} = 1$ W and $P_{in} = 0.1$ W. ($f_r = 40$ MHz $P_{in} = 1$ W: ·, $f_r = 80$ MHz $P_{in} = 1$ W: ∘, $f_r = 40$ MHz $P_{in} = 0.1$ W: □, $f_r = 80$ MHz $P_{in} = 0.1$ W: ◇)

reconstruction. For the lower value of the size of the possible frequency range which must be checked for interference ($f_r = 40$ MHz) the baseband signal reconstruction quality is 2-3 dB better than in the case of wider frequency range ($f_r = 80$ MHz).

B.4   Conclusions

In this paper, a modified architecture for direct conversion radio receivers is proposed. The architecture is based on compressed sensing principles. It is shown that the proposed solution enables relaxing the requirements for the order of the quadrature filters in a direct conversion receiver. An experiment is presented in which the transmitted quadrature signal is polluted with noise and interference. The experiment demonstrates that the proposed architecture is able to succesfully receive the baseband signal under adverse conditions with the usually high-order quadrature filters reduced to first-order filters.

Acknowledgment

[1] A. A. Abidi, "Direct-Conversion Radio Transceivers for Digital Communications", *IEEE J. Solid-State Circuits*, vol. 30, no 12, pp. 1399-1410, Dec. 1995.

[2] A. A. Abidi, "The Path to the Software-Defined Radio Receiver", *IEEE J. Solid-State Circuits*, vol. 30, no 12, pp. 1399-1410, Dec. 2007.

[3] B. Razavi, "Architectures and Circuits for RF CMOS Receivers.", *Proc. of IEEE 1998 Custom Integrated Circuits Conference*, pp. 393400, Santa Clara, USA, May 1998.

[4] Besser, L. and Gilmore, R., "Practical RF Circuit Design for Modern Wireless Systems.", *Artech House 2003*, ISBN 1-58053-521-6, Norwood, USA

[5] N. C. Davies, "A high performance HF software radio", *Proc. 8th Int. Conf. HF Radio Systems and Techniques*, Guildford, UK, pp. 249-256, 2000

[6] M. Ben-Romdhane, C. Rebai, P. Desgreys, A. Ghazeli, P. Loumeau, "Flexible Baseband Analog Front-end for NUS based Multistandard Receiver", *Proc. Joint IEEE North-East Workshop on Circuits and Systems and TAISA Conference*, Toulouse, France, pp. 1-4, June 2009.

[7] M. Ben-Romdhane, C. Rebai, P. Desgreys, A. Ghazeli, P. Loumeau, "Pseudorandom Clock Signal Generation for Data Conversion in a Multistandard Receiver", *Proc. IEEE Int. Conference on Design and Technology of Integrated Systems in Nanoscale Era*, pp. 14, Tozeur, Tunisia, Mar. 2008.

[8] M. Ben-Romdhane, C. Rebai, K. Grati, A. Ghazel, G. Hechmi, P.Desgreys and P. Loumeau, "Non-Uniform Sampled Signal Reconstruction for Multistandard WiMax/WiFi Receiver", *IEEE International Conference on Signal Processing and Communication*, pp. 181184, Dubai, November 2007.

[9] E.J. Candès and M. B. Wakin, "An Introduction To Compressive Sampling", *IEEE Signal Process. Mag.*, vol. 25(2), pp. 21–30, Mar. 2008.

[10] E.J. Candès and T. Tao, "Decoding by Linear Programming", *IEEE Trans. Inf. Theory*, vol. 51(12), pp. 4203–4215, Nov. 2005.

[11] E.J. Candès, J. Romberg and T. Tao, "Robust Uncertainty Principles: Exact Signal Reconstruction From Highly Incomplete Frequency Information", *IEEE Trans. Inf. Theory*, vol. 52(2), pp. 489–509, Feb. 2006.

[12] R.G. Baraniuk, M. Davenport, R. Devore, M. Wakin, "A Simple Proof of the Restricted Isometry Property for Random Matrices", *Constructive Approximation*, vol. 28(3), pp. 253–236, 2008.

[13] J.A. Tropp, "Just Relax: Convex Programming Methods for Identifying Sparse Signals in Noise", *IEEE Trans. Inf. Theory*, vol. 52(3), pp. 1030–1051, Mar. 2006.

[14] J.A. Tropp and A.C. Gilbert, "Signal Recovery From Random Measurements Via Orthogonal Matching Pursuit", *IEEE Trans. Inf. Theory*, vol. 53(12), pp. 4655–4666, Dec. 2007.

[15] S. Kirolos, J. Laska, M. Wakin, M. Duarte, D. Baron, T. Ragheb, Y. Massoud, R. Baraniuk, "Analog-to-Information Conversion via Random Demodulation", *Proc. IEEE Dallas/CAS Workshop on Design Applications Integration and Software (DCAS)*, pp. 71–74, Dallas, USA, 2006.

[16] P. J. Pankiewicz, T. Arildsen, T. Larsen, "Sensitivity of the random demodulation framework to filter tolerances", *Proc. 19th European Signal Processing Conference (EUSIPCO)*, pp. 534–538, Barcelona, Spain, 2011.

[17] Y. Zhou, Z. Pan, "Impact of LPF Mismatch on I/Q Imbalance in Direct Conversion Receivers", *IEEE Trans. Wireless Commun*, vol. 10(4), pp. 1702–1708, Jun. 2011.

Appendix C

Sampling Patterns for Frequency-Selective Compressed Sensing

Jacek Pierzchlewski, Thomas Arildsen and Torben Larsen

Abstract

In many practical applications of receivers or signal detection systems there is a problem of interference signals. Efficient filtering of interference signals requires either massive analog filtering of the input signal or high sampling frequency applied to the signal. Both of these methods have significant disadventages - chip implementation problems for multiorder low-pass analog filters or high energy dissipation caused by high signal sampling frequency. In this paper, the authors propose a frequency-selective compressed sensing method which allows for digital interference filtering with reduced signal sampling frequency. The authors show that the quality of this frequency-selective compressed sensing depends significantly on a sampling pattern used in the signal acquisition. The authors introduce sampling pattern error parameters and a filtering-RIP parameter, which assess a sampling pattern for a given filtering problem. Finally, a sampling pattern search algorithm is proposed. This system attempts for the best compressed sensing sampling pattern for a given interference filtering problem. A simple experiment is shown to illustrate the method in practice.

C.1   Introduction

The Shannon-Nyquist sampling theorem states that perfect signal reconstruction of any signal requires a sampling frequency higher than twice the maximum frequency component in the signal [1]. In practical situations we thus need analog anti-aliasing fllters prior to the analog-to-digital conversion (ADC) to facilitate the above [2, 4, 5, 6]. Further, in cases where we have prior information on the desired signal with respect to frequency content it may be possible by clever analog filtering to reduce any disturbing or interfering signal at other frequencies to e.g. reduce the risk of saturating the ADC, causing nonlinear distortion [5, 6, 7]. Applying such adaptive analog filtering is, however, design and implementation challenging [8, 9, 10, 11], and a digital solution would be preferred if possible. This is only possible provided the ADC has sufficient dynamic range though [5].

To the authors' best knowledge, there are very few solutions which allow for reduced analog filtering and do not require increasing the sampling frequency above the Nyquist frequency of the unfiltered signal. Subsampling [2, 3], which is a well-know technique, is useless in many practical applications. Ben-Romdhane et. al. [12, 13, 14] proposed a nonuniform sampling scheme to relax requirements for filtering in radio receivers. However, in some communication systems, the achieved filter relaxation is minor [14].

In this paper the authors propose a frequency-selective sampling method based on the compressed sensing technique. In recent years a new idea of signal sensing, known as compressed sensing (CS) has emerged [15, 16, 17, 18, 19]. This technique can be used to successfully reconstruct signals that are sampled at a sub-Nyquist rate, provided the signal is sparse in some domain. In general, compressed sensing can be divided into acquisition and reconstruction. There are two classes of signal reconstruction algorithms: greedy algorithms [22] and convex optimization-based methods [23]. These methods are well elaborated, however, none of them is designed for signal filtering, in which compressed sensing reconstruction selectively favors certain signal spectrum frequencies over others. Quite some work has been done in compressed sensing signal acquisition. The random demodulator framework [24, 25, 26] uses modulation and filtering before signal sampling. The modulated wideband converter (MWC) [27, 28], is a multi-channel analog system dedicated to wideband signal sampling [29]. Albeit the above solutions guarantee good performance, extensive analog preprocessing is a crucial part of all these acquisition systems. Moreover, the modulated wideband converter is a multi-channel architecture. Hence, these solutions may be too costly in terms of power consumption and chip area in many mobile and power-constrained applications. Furthermore, like the reconstruction methods, none of these solutions is designed to exploit the principle of a signal filtering problem.

Frequency-selective compressed sensing proposed in this paper allows for relaxed input signal filtering without increasing the sampling frequency to the Nyquist frequency of the input signal poluted by unwanted high-frequency signals. The method provides a good quality of the reconstructed signal, also for low signal-to-interference ratio. The main idea is to divide the compressed sensing reconstruction procedure into two phases: an optimization phase and a final signal reconstruction phase, and to use a limited dictionary in the final signal reconstruction phase. Furthemore, the authors show that for different sampling patterns, different sampling frequencies are correctly reconstructed. We introduce a new sampling pattern analysis tailored to wanted reconstructed frequencies, which may differ among applications. To facilitate this, a new method of sampling pattern generation and analysis, based on the restricted isometry principle [20, 21], is presented. The paper outlines the idea of frequency-selective compressed sensing, with the main focus on the frequency-selective compressed signal acquisition.

The paper is organized as follows. The problem considered in this paper is discussed in Section C.2. Frequency-selective compressed sensing and the problem of optimal sampling patterns is described in Section C.3. A proposed, modified restricted isometry analysis dedicated to signal filtering is discussed

in the Section C.4. The proposed method of the sampling pattern generation is presented in Section C.5. The performance of the proposed solution is empirically assessed in Section C.6. The paper is concluded in Section C.7.

C.2 Problem formulation

Let us define a bandlimited $(-B_\mathrm{b} \leq f \leq B_\mathrm{b})$ baseband signal $\mathbf{s}_\mathrm{b} \in \mathbb{R}^{N \times 1}$. The signal $\mathbf{s}_\mathrm{b}$ contains information and is received and processed by a given digital processing system. The Nyquist rate of the signal $\mathbf{s}_\mathrm{b}$ is $f_\mathrm{Nb} = 2B_\mathrm{b}$, the power of this signal is P_b. The signal is polluted by a blocking bandpass $\pm(B_\mathrm{b} < f \leq B_\mathrm{x})$ signal $\mathbf{s}_\mathrm{I} \in \mathbb{R}^{N \times 1}$, the power of this signal is P_I. The blocking signal $\mathbf{s}_\mathrm{I}$ consists of N_I blockers:

$$\mathbf{s}_\mathrm{I} = \sum_{i=1}^{N_\mathrm{I}} \mathbf{s}_\mathrm{I}^{(i)} \tag{C.1}$$
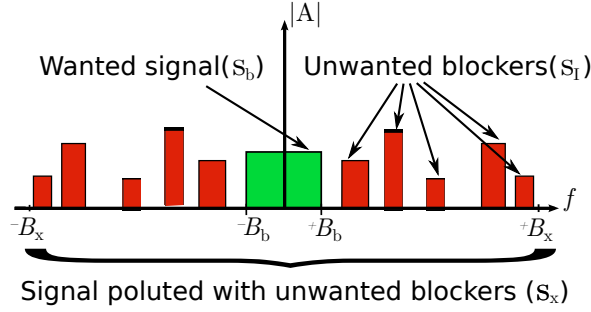
Figure C.1: Frequency spectrum of the received signal $\mathbf{s}_\mathrm{x}$. The signal consists of the wanted signal $\mathbf{s}_\mathrm{b}$ (green) and the unwanted blockers $\mathbf{s}_\mathrm{I}$ (red). The signal's frequency range is $(-B_\mathrm{x} < f \leq B_\mathrm{x})$.

where $\mathbf{s}_\mathrm{I}^{(i)}$ is the i-th blocker of power $P_\mathrm{I}^{(i)}$. In general, the blockers $\mathbf{s}_\mathrm{I}^{(i)}$ occupy non-overlapping continuous frequency ranges in positive and negative frequencies. Furthermore, we assume there is a certain unused frequency range between blockers. Hence, it can be stated that the blocking signal is sparse in the frequency domain. The received signal $\mathbf{s}_\mathrm{x} \in \mathbb{R}^{N \times 1}$ is a sum of the wanted signal $\mathbf{s}_\mathrm{b}$ and the blocking signal $\mathbf{s}_\mathrm{I}$: $\mathbf{s}_\mathrm{x} = \mathbf{s}_\mathrm{b} + \mathbf{s}_\mathrm{I}$ (Fig. C.1). The signal $\mathbf{s}_\mathrm{x}$ is bandlimited $(-B_\mathrm{x} \leq f \leq B_\mathrm{x})$, its Nyquist rate is $f_\mathrm{Nx} = 2B_\mathrm{x}$.

Due to the blocking signal $\mathbf{s}_\mathrm{I}$, the Nyquist rate f_Nx of the received signal $\mathbf{s}_\mathrm{x}$ is in many applications significantly higher than the Nyquist rate f_Nb of
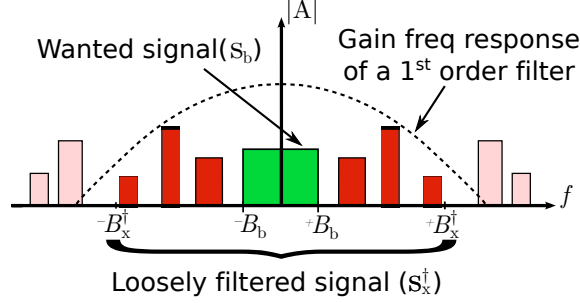
Figure C.2: Frequency spectrum of the loosely filtered signal $\mathbf{s}_\mathrm{x}^\dagger$ which consists of the wanted signal $\mathbf{s}_\mathrm{b}$ (green) and the loosely filtered interference signal $\mathbf{s}_\mathrm{I}^\dagger$ (red) which is still partly present in the signal. A part of the unwanted frequencies was removed (pale red).
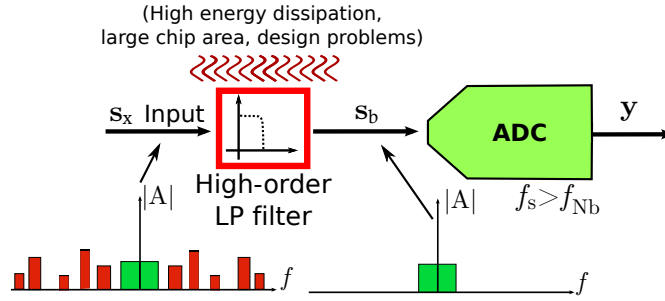
Figure C.3: Solution 1: High-order filtering enables lowered sampling frequency. Large filters utilize considerable chip area and cause high energy dissipation and integrated circuit design problems.

the wanted baseband signal $\mathbf{s}_\mathrm{b}$. To enable of sampling the signal with a low sampling frequency f_s ($f_\mathrm{Nb} < f_\mathrm{s} \ll f_\mathrm{Nx}$) the signal $\mathbf{s}_\mathrm{x}$ must be filtered with a high-order low-pass filter which removes the unwanted blockers (Fig. C.3). Unfortunately, high-order filters cause design and IC (Integrated Circuit) implementation problems due to high energy dissipation and chip area required to implement these filters [9, 10, 11].

Another possibility is to "loosely" filter a signal with a low-order filter (Fig. C.4). This approach reduces the mentioned problems caused by higher-order filters. Let us consider a bandlimited ($-B_\mathrm{x}^\dagger \leq f \leq B_\mathrm{x}^\dagger$) signal $\mathbf{s}_\mathrm{x}^\dagger$, which is created by applying a 1st-order filter on the received signal $\mathbf{s}_\mathrm{x}$. This partly removes high-frequency blockers (Fig. C.2). Nevertheless, there are

Figure C.4: Solution 2: Low-order filtering requires high sampling frequency. High sampling frequency causes high energy dissipation and is infeasible to implement in certain applications.

still considerable blocker signal content present in the filtered signal $\mathbf{s}_x^\dagger$. The Nyquist frequency of the signal $\mathbf{s}_x^\dagger$ is $f_{\mathrm{Nx}}^\dagger = 2B_x^\dagger$. The baseband $B_x^\dagger$ of the filtered signal depends on the powers of the blocker signals $P_{\mathrm{I}}^{(i)}$ and filter's cut off frequency f_c. The Nyquist rate $f_{\mathrm{Nx}}^\dagger$ of the filtered signal $s_x^\dagger$ is lower than the Nyquist rate f_{Nx} of the unfiltered, received signal s_x. Nevertheless, in many applications, it is still significantly higher than the Nyquist rate f_{Nb} of the wanted signal s_b:

$$f_{\mathrm{Nb}} \ll f_{\mathrm{Nx}}^\dagger \ll f_{\mathrm{Nx}} \tag{C.2}$$

Therefore, if a 1$^{\text{st}}$-order filter is used, a high signal sampling frequency must be applied on the signal (Fig. C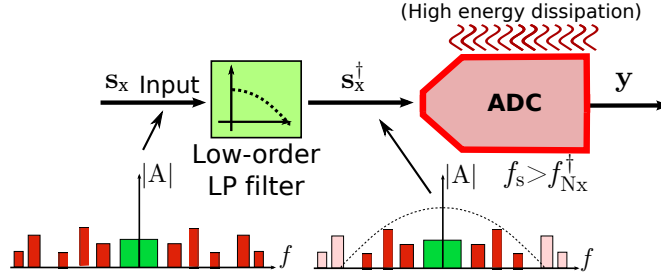.4). The high sampling frequency causes high energy dissipation [6, 7, 8] and may be infeasible to implement in certain applications [4, 37, 38].

   The authors' aim is to decrease the necessary sampling frequency in case the received signal is $\mathbf{s}_x^\dagger$ with bandwidth $(-B_x^\dagger \leq f \leq B_x^\dagger)$, while only a low-frequency part $(-B_b \leq f \leq B_b)$ of the signal $\mathbf{s}_x$ is needed to be correctly reconstructed. The rest of the received signal's frequency spectrum are unwanted blockers. The filtering problem is constituted by four parameters: baseband of the interfered signal $B_x^\dagger, B_b$, wanted signal baseband B_b, dictionary $\mathbf{\Phi}$, and a wanted average sampling frequency $f_s^\star$. Hence, we can introduce a filtering problem $\mathcal{P}(B_x^\dagger, B_b, \mathbf{\Psi}, f_s^\star)$. The solution presented in this paper is mostly dedicated to mobile systems, so it is assumed that there is a single analog-to-digital converter (ADC) present in a system. The authors present a frequency-selective compressed sensing method which allows for digital signal filtering and significant sampling frequency reduction under the described conditions. Although this paper presents a whole view on the presented signal filtering method, it focuses mostly on the signal acquisition part of the
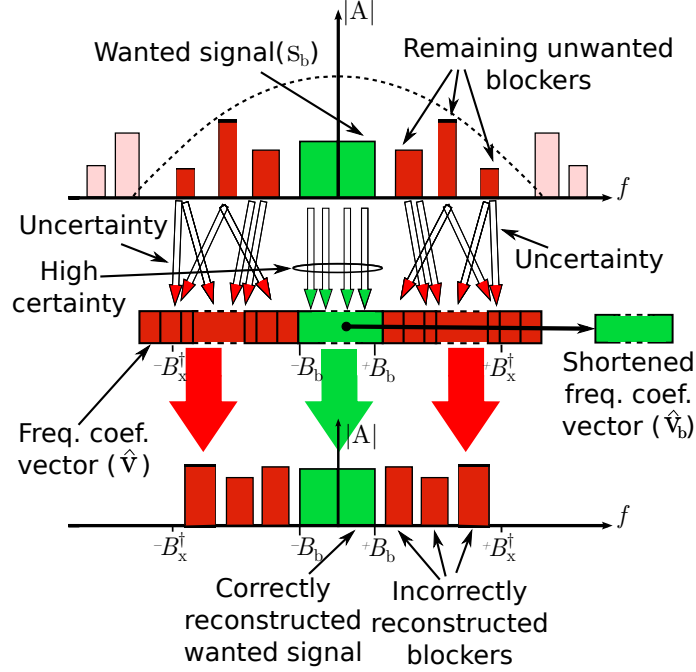
Figure C.5: Vectors with frequency coefficients in the frequency selective compressed sensing.

method.

C.3 Frequency-selective compressed sensing

C.3.1 Compressed sensing basics

Compressed sensing [15, 16, 17, 18, 19] is a process of acquiring a signal such that a vector of its observed samples is shorter than the original signal:

$$\mathbf{y} = \mathbf{\Phi}\mathbf{x} \tag{C.3}$$

where $\mathbf{x} \in \mathbb{C}^{N \times 1}$ is the original signal, $\mathbf{y} \in \mathbb{C}^{M \times 1}$ is the vector of observed samples, and $\mathbf{\Phi} \in \mathbb{C}^{M \times N}$, $M \ll N$, is a measurement matrix which reflects the process of signal acquisition. This paper narrows its scope to real signals, so $\mathbf{x} \in \mathbb{R}^{N \times 1}$, $\mathbf{y} \in \mathbb{R}^{M \times 1}$, $\mathbf{\Phi} \in \mathbb{R}^{M \times N}$.

The signal is compressible if it can be well-approximated by a sparse vector $\mathbf{v} \in \mathbb{C}^{L \times 1}$ in some dictionary $\mathbf{\Psi} \in \mathbb{C}^{N \times L}$:

$$\mathbf{x} \approx \mathbf{\Psi}\mathbf{v} \tag{C.4}$$

In other words, most of the coefficients in the vector $\mathbf{v}$ are small enough to be well approximated as zero. The vector of observed samples $\mathbf{y}$ is shorter than the original signal $\mathbf{x}$. Nevertheless, it is still possible to retrieve the original signal $\mathbf{x}$ if it is compressible. It is done using a reconstruction algorithm $\mathcal{R}$:

$$\mathcal{R}(\mathbf{y}, \mathbf{\Phi}, \mathbf{\Psi}) \rightsquigarrow \hat{\mathbf{x}} \approx \mathbf{x} \tag{C.5}$$

Significant work has been done in the area of compressed sensing reconstruction algorithms. There are two main classes of these algorithms: greedy algorithms [16, 22] and ℓ_1-norm relaxation-based optimization algorithms [16, 18, 23]. The latter algorithms are developments of a reconstruction algorithm, which is based on the following convex optimization problem:

$$\hat{\mathbf{v}} = \operatorname*{argmin}_{\mathbf{v}} \|\mathbf{v}\|_1 \quad \text{subj. to: } \|\mathbf{\Phi}\mathbf{\Psi}\mathbf{v} - \mathbf{y}\|_2 < \epsilon \tag{C.6}$$

After the above, the reconstructed signal $\hat{\mathbf{x}}$ can be computed as $\hat{\mathbf{x}} = \mathbf{\Psi}\hat{\mathbf{v}}$. Setting the constraint $\epsilon > 0$ makes the above optimization problem feasible if there is noise present in the oberved signal samples $\mathbf{y}$ [23]. The higher the noise level, the higher the ϵ needed to make the optimization problem feasible. As a tradeoff, the higher ϵ, the bigger the reconstruction error $\hat{e} = \|\hat{\mathbf{x}} - \mathbf{x}\|_2$ is.

As the dictionary $\mathbf{\Psi}$ in this paper the authors use a generalized Inverse Discrete Fourier Transform (IDFT) dictionary $\mathbf{\Psi}_\mathrm{I} \in \mathbb{C}^{N \times 2K}$ as the signal dictionary:

$$\mathbf{\Psi}_\mathrm{I} = \begin{bmatrix} \psi_{1,-K} & \cdots & \psi_{1,K} \\ \vdots & \ddots & \vdots \\ \psi_{N,-K} & \cdots & \psi_{N,K} \end{bmatrix} \tag{C.7}$$

where

$$\psi_{n,k} = \exp[j2\pi t_n f_k] \tag{C.8}$$

Frequencies of the columns of the matrix $\mathbf{\Psi}$ are:

$$f_k = k \cdot \gamma \quad k \in \pm\{1, \ldots, K\} \tag{C.9}$$

where γ is the frequency separation between the columns of the $\mathbf{\Psi}_\mathrm{I}$ dictionary, K is the number of positive frequencies reflected in the dictionary. Signal representation time steps t_n:

$$t_n = nT_\mathrm{r}, \quad T_\mathrm{r} = \frac{t_\mathrm{d}}{N} \tag{C.10}$$
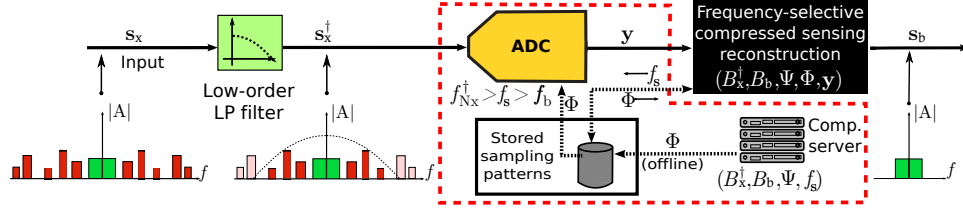
Figure C.6: The compressed sensing filtering system. The part of the system on which the paper is focused is embraced in red.

where T_r is the signal representation sampling period, t_d is the time period represented by the columns of the dictionary $\mathbf{\Psi}_I$.

C.3.2 Frequency-selective compressed sensing

In the canonical compressed sensing methodology, the signal reconstruction uses the whole reconstructed vector with the coefficients $\hat{\mathbf{v}}$:

$$\hat{\mathbf{x}} = \mathbf{\Psi}\hat{\mathbf{v}} \tag{C.11}$$

In the proposed, frequency-selective compressed sensing, only a low-frequency part of the frequency coefficients is in use during the signal reconstruction:

$$\hat{\mathbf{x}} = \mathbf{\Psi}_b\hat{\mathbf{v}}_b \tag{C.12}$$

where:

$$\hat{\mathbf{v}}_b = \hat{\mathbf{v}}(k), \quad k = \{-K_b, ..., K_b\} \tag{C.13}$$

It is because in a given filtering problem $\mathcal{P}(B_x^\dagger, B_b, \mathbf{\Psi}, f_s^\star)$ spectrum of the wanted signal is limited to B_b.

The number of elements $(2K_b)$ in the shortened freq. coeficient vector $\hat{\mathbf{v}}_b$ depends on the baseband B_b of the wanted signal $\mathbf{s}_b$:

$$K_b = \left\lceil \frac{B_b}{\gamma} \right\rceil \tag{C.14}$$

The shortened dictionary $\mathbf{\Psi}_b \subset \mathbf{\Psi}$ contains columns of the dictionary $\mathbf{\Psi}$ coresponding to the baseband frequency range of the wanted signal $\mathbf{s}_b$.

During the ℓ_1-optimization (C.6) the vector with reconstructed frequency coefficients $\hat{\mathbf{v}}$ represents the whole spectrum $(-B_x^\dagger \leq f \leq B_x^\dagger)$ of the received signal $\mathbf{s}_x$. Hence, the unwanted blockers are present in the reconstructed coefficients instead of being reflected in an increased feasibility region in (C.6)

(increased ϵ). Increasing the feasibility region would compromise the reconstruction quality, the proposed solution does not have this disadvantage. Only the frequency coefficients which correspond to the baseband signal $\mathbf{s}_\mathrm{b}$ must be reconstructed corectly, while corectness of the rest of the coefficients is unimportant. The above relaxes the requirements for the signal reconstruction, since these requirements concern only the wanted part of the spectrum. This idea is shown in Fig. C.5.

A sampling system which implements the idea of frequency-selective compressed sensing is shown in Fig. C.6. The sampling patterns are stored in the sampling system. It is explained in Section C.5 how these patterns are generated off-line. The sampling pattern is chosen according to the current wanted average sampling frequency $f_\mathrm{s}^\star$. The loosely filtered signal $\mathbf{s}_\mathrm{x}^\dagger$ is sampled by an ADC using the sampling pattern. Frequency-selective compressed sensing system reconstructs the wanted signal $\mathbf{s}_\mathrm{b}$.

C.3.3 Random sampling patterns

This paper focuses on generation and analysis of random sampling patterns for the frequency-selective compressed sensing problem. A sampling pattern $\mathbb{T}$ is a set with K_s fixed sampling time points:

$$\mathbb{T} = \{t_1, t_2, ..., t_{K_\mathrm{s}}\} \tag{C.15}$$

The set $\mathbb{T}$ is ordered:

$$t_1 < t_2 < \cdots < t_{K_\mathrm{s}} \tag{C.16}$$

The time length τ of the sampling pattern may be higher than the value of the last time point in the pattern: $\tau \geq t_{K_\mathrm{s}}$. The time length τ is equal to the time length t_d (10) of a signal on which the sampling pattern is applied.

Any sampling point $t_k \in \mathbb{T}$ is a multiple of the sampling grid period T_g:

$$t_k = mT_\mathrm{g}, \quad m \in \mathbb{N}^* \tag{C.17}$$

The sampling grid is a set:

$$\mathbb{G} = \{T_\mathrm{g},\, 2T_\mathrm{g},\, ...,\, K_\mathrm{g}T_\mathrm{g}\}, \quad K_\mathrm{g} = \left\lfloor \frac{\tau}{T_\mathrm{g}} \right\rfloor \tag{C.18}$$

where K_g is the number of sampling grid points in the sampling pattern. The sampling pattern is always a subset of the sampling grid $\mathbb{T} \subset \mathbb{G}$. The sampling grid period T_g defines the maximum resolution of the sampling process. The lower the sampling grid period is, the better the maximum resolution of
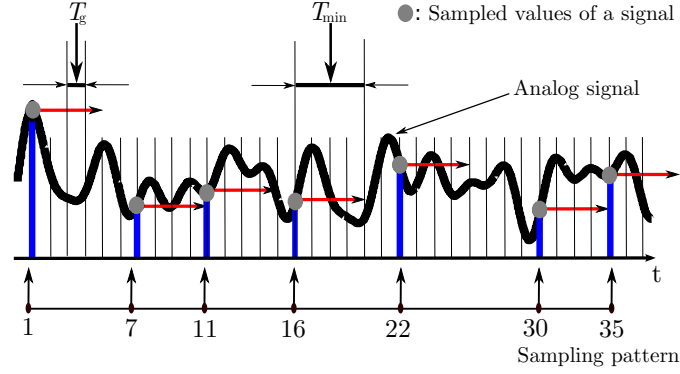
Figure C.7: The compressed sensing sampling pattern.

sampling. In practice, the minimum sampling grid period T_{g} depends on the performance of the ADC circuitry [5, 6, 7].

The sampling pattern $\mathbb{T}$ is applied to a signal $x(t)$ of a length $\tau = t_{\mathrm{d}}$:

$$\mathbf{y}_k = x(t_k), \quad t_k \in \mathbb{T} \tag{C.19}$$

where $\mathbf{y}_k$ is k-the entry in the observed vector $\mathbf{y}$.

C.3.4   Requeirements for random sampling patterns

Sampling patterns are generated either on-the-fly, or generated off-line by a sampling pattern generator and stored in a sampling system (Fig. C.6). In this paper the latter solution is discussed. There are certain requirements for the patterns generator. These requirements are presented below.

The average sampling frequency f_{s} of the random sampling pattern $\mathbb{T}$ of a timelength τ, depends on the number of sampling time points K_{s} in the pattern:

$$f_{\mathrm{s}} = \frac{K_{\mathrm{s}}}{\tau} \tag{C.20}$$

The sampling pattern generator must produce sampling patterns which have a given average sampling frequency $f_{\mathrm{s}}^{\star}$. If the average sampling frequency f_{s} is lower than the requested sampling frequency $f_{\mathrm{s}}^{\star}$, then the quality of signal reconstruction may be compromised. In the following we introduce a statistical error parameters which assess a system that randomly generates some number of sampling patterns which we must subsequently assess the quality of. Firstly, we introduce a statistical error parameter which indicates about how well

the assessed generator obeys the imposed requirement of average sampling
frequency $f_s^\star$:

$$e_f = \frac{1}{N_t} \sum_{n=1}^{N_t} \left| \frac{f_s^\star - f_s^{(n)}}{f_s^\star} \right| \tag{C.21}$$

where $f_s^{(n)}$ is the average sampling frequency of the n-th generated sampling
pattern. The e_f parameter should be as low as possible. The number of
analyzed patterns N_t depends on the desired confidence intervals of the e_f
parameter.

Due to ADC technological constraints there are requirements for minimum
distance between sampling moments. Violation of this requirement may cause
the sampling pattern to be impossible to implement on a given ADC. Every
sampling time point t_k must occur at least time t_{min} after the previous time
point (Fig. C.7):

$$t_{k+1} - t_k \leq t_{min} \tag{C.22}$$

Generating an adequate random sampling pattern is realizable, if $t_{min} < T_s^\star$,
where $T_s^\star = \frac{1}{(f_s^\star)}$ is the requested average sampling period.

The next statistical error parameter denotes the number of intervals be-
tween the sampling moments which do not fulfil the requirement of a minimum
interval ($C.22$). Let us define a set $\mathbb{D}$ of $K_d = K_s - 1$ intervals between the
sampling time points in a pattern $\mathbb{T}$:

$$\mathbb{D} = \{d_1, d_2, ..., d_K\}, \quad K = K_d \tag{C.23}$$

where:

$$d_k = t_{k+1} - t_k, \quad t_k \in \mathbb{T} \tag{C.24}$$

If all the intervals are equal ($d_1 = d_2 = ... = d_K = T_s$, $K = K_s$), then $\mathbb{T}$ is a
uniform sampling pattern with the sampling period equal to T_s. If the time
intervals are random, then $\mathbb{T}$ is a random sampling pattern. An example of a
random sampling pattern is shown in Fig. C.7. For a given sampling pattern
$\mathbb{T}$ let us create a subset $\mathbb{D}^- \subset \mathbb{D}$ with intervals between samples such that:
containing the admissible intervals (with respect to t_{min}) in $\mathbb{D}$:

$$\mathbb{D}^- = \{d_i^- \in \mathbb{D} : d_i^- < t_{min}\} \tag{C.25}$$

In words, intervals between the sampling points which are shorter than t_{min}
are stored in a subset $\mathbb{D}^-$. For a given sampling pattern $\mathbb{T}$ we can calculate
how many of the intervals between sampling points in this pattern violate the
imposed requirement in relation to the number of all the intervals:

$$e^- = \frac{|\mathbb{D}^-|}{|\mathbb{D}|} \tag{C.26}$$

We define the parameter e_{mean} to quantify how well the assessed pattern generator obeys the imposed requirements of $t_{\text{m}in}$. The error parameter is:

$$e_{\min} = \frac{1}{N_{\text{t}}} \sum_{n=1}^{N_{\text{t}}} e_n^- \tag{C.27}$$

where e_n^- is the parameter e^- of the n-th generated sampling pattern.

The last error parameter concerns the randomness in generation of sampling moments in the generated sampling patterns. It gives an information about the average number of different intervals between the sampling time points in a sampling pattern. Let us create a subset $\mathbb{D}^\star \subset \mathbb{D}$ which contains unique time differences from the set $\mathbb{D}$:

$$d_i^\star \in \mathbb{D}^\star \Leftrightarrow d_i^\star \in \mathbb{D} \wedge \nexists \, d_j^\star \in \mathbb{D}^\star : \; d_j^\star = d_i^\star \tag{C.28}$$

Now it is possible to calculate ratio $e^\star$ of the number of unique intervals between samples to the number of all the intervals in the sampling pattern and a statistical parameter e_{d} calculated based on N_{t} generated patterns:

$$e^\star = \frac{|\mathbb{D}^\star|}{|\mathbb{D}|} \qquad e_{\text{d}} = 1 - \frac{1}{N_{\text{t}}} \sum_{n=1}^{N_{\text{t}}} e_n^\star \tag{C.29}$$

where $e_n^\star$ is the ratio $e^\star$ calculated for n-th sampling pattern. The error parameter $e_{\text{d}} = 1$ means that assessed patterns generator produces only uniform sampling patterns.

C.3.5   Optimum sampling pattern

The sampling pattern is always a subset of its sampling grid: $\mathbb{T} \subset \mathbb{G}$. Hence, if no additional constraints are imposed on the sampling pattern, the number of possible different sampling patterns is:

$$N_{\text{p}} = \binom{K_{\text{g}}}{K_{\text{s}}} \tag{C.30}$$

where K_{s} is the number of sampling time points in a sampling pattern, K_{g} is the number of grid points in the grid.

Here a problem arises: how to generate sampling patterns which satisfy the given constraints: minimum distance between samples $t_{\min}$ and the average sampling frequency $f_{\text{s}}^\star$? Then how to choose the sampling pattern which corresponds to the best measurement matrix $\mathbf{\Phi}$ - such that the matrix $\mathbf{\Theta} = \mathbf{\Phi\Psi}$ guarantees the best possible reconstruction quality for the given filtering problem $\mathcal{P}(B_{\text{x}}^\dagger, B_{\text{b}}, \mathbf{\Psi}, f_{\text{s}})$?

C.4 Filtering restricted isometry property analysis

In [18] the authors introduce the concept of the Restricted Isometry Property (RIP). The RIP constant ζ_S measures how closely the columns of the matrix $\boldsymbol{\Theta} = \boldsymbol{\Phi\Psi}$, $\boldsymbol{\Theta} \in \mathbb{C}^{M \times 2K}$ behave like orthonormal vectors, for any subset of $S \leq 2K$ columns at a time. The RIP constant ζ_S is the smallest number which fulfills the inequality:

$$(1 - \zeta_S)||\mathbf{q}||_2^2 \leq ||\mathbf{Aq}||_2^2 \leq (1 + \zeta_S)||\mathbf{q}||_2^2 \tag{C.31}$$

for all the possible matrices $\mathbf{A}$, which consists of $S \leq 2K$ columns of the matrix $\boldsymbol{\Theta}$. The lower the ζ_S is, the higher the probability of successful reconstruction of S-sparse signals from an incomplete data set, in particular from a short observed vector $\mathbf{y}$.

Computing ζ_S constant is a problem of a combinatorial nature. For the predominant number of realistic frequency sparse signals, computation of the ζ_S defined as above, would require enormous computational power - it is an NP-hard problem. The computation algorithm needs to evaluate all the possible $\binom{2K}{S}$ combinations of the columns of the $\boldsymbol{\Theta}$ matrix (if $\boldsymbol{\Theta}$ is a IDFT, and only real signals are considered, the problem shrinks to $\binom{K}{S}$ combinations). Fig. 6 (blue plot) shows the number of combinations needed to evaluate for different sparsity (S) of the signals for 60-tones frequency dictionary. Black plot on Fig. 6 shows the number of combinations needed to evaluate for different size of the frequency dictionary, when it is assumed that sparsity is equal to half of the dictionary.

C.4.1 Atomic filtering-RIP analysis of combination of vectors

Let us consider a matrix $\boldsymbol{\Theta} = \boldsymbol{\Phi\Psi}$ where $\boldsymbol{\Phi}$ (C.3) is a given measurement matrix, $\boldsymbol{\Psi}$ is the IDFT dictionary matrix defined as in (C.7). Moreover, let us assume that support of the compressively sampled signal $\mathbf{s}_x$ corresponds to a subset $\mathbb{A}$ of S columns of the dictionary matrix $\boldsymbol{\Psi}$. Now, for a given matrix $\boldsymbol{\Theta}$, our aim is to quantify the possibility of correct reconstruction of i-th entry of the vector $\mathbf{v}$, using reconstruction as in (C.6). The i-th entry of the vector $\mathbf{v}$, corresponds to i-th column $\mathbf{a} = \boldsymbol{\Theta}_i$ and to one tone in the wanted signal $\mathbf{s}_b$. Hence, we can measure how well a corresponding frequency tone can be compressively filtered from the sampled signal when a given measurement matrix $\boldsymbol{\Phi}$ is used.

Let us create a matrix $\mathbf{A} \subset \boldsymbol{\Theta}$ which consists of S columns of the matrix $\boldsymbol{\Theta}$, corresponding to the subset $\mathbb{A}$. The authors propose a filtering-RIP analysis, which is a modified RIP analysis (C.31). The filtering-RIP constant $\hat{\zeta}_{\mathbf{a}}^{\mathbf{A}}$ is a
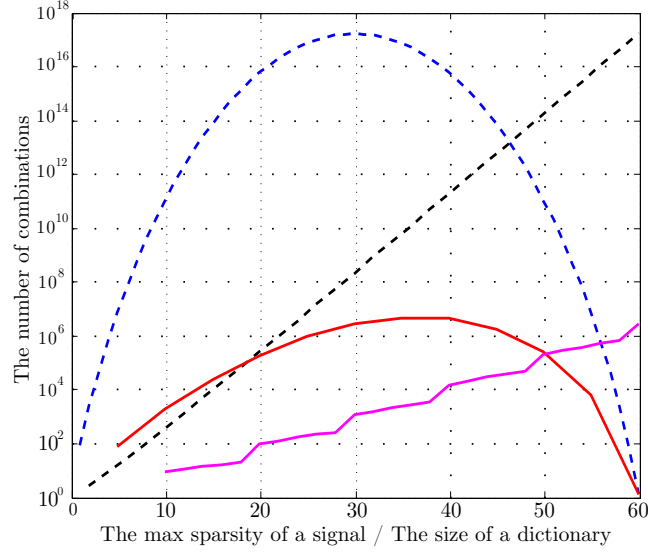
Figure C.8: Comparision between the number of combinations which must be performed to compute the canonical RIP parameter and the proposed filtering-RIP parameter. Blue plot: The number of combinations in canonical RIP for different sparsity, when the size of a dictionary (the number of tones) $K = 60$. Black plot: The number of combinations in canonical RIP for different size of a dictionary, when sparsity is equal to half of the size of a dictionary. Red plot: The number of combinations for interference scenarios (used in filtering-RIP) for different sparsity (different number of blockers). It is assumed that $K_I = 5$, the size of a dictionary $K = 60$. Violet plot: The number of combinations for interference scenarios (used in filtering-RIP) for different size of a dictionary. It is assumed that $K_I = 5$. Consider the logarithmic scale.

constant which satisfies the below inequality for the matrix $\mathbf{A}$ for all possible normalized vectors $\hat{\mathbf{q}}$:

$$(1 - \hat{\zeta}_{\mathbf{a}}^{\mathbf{A}})|\hat{\mathbf{q}}_i| \leq \|\mathbf{u}^{\odot}\|_2^2 \leq (1 + \hat{\zeta}_{\mathbf{a}}^{\mathbf{A}})|\hat{\mathbf{q}}_i|, \quad \mathbf{u} = \mathbf{A}\hat{\mathbf{q}} \tag{C.32}$$

The notations of filtering-RIP constant $\hat{\zeta}_{\mathbf{a}}^{\mathbf{A}}$ denotes that it corresponds to a vector $\mathbf{a}$ from the matrix $\mathbf{A}$. In (C.32) $\hat{\mathbf{q}}_i$ is i-th entry of the normalized vector $\hat{\mathbf{q}}$ which corresponds to the vector $\mathbf{a}$ (i is a position of the column $\mathbf{a}$ in the matrix $\mathbf{A}$). Length of the vector $\mathbf{u} = \mathbf{A}\hat{\mathbf{q}}$ in the direction pointed by the vector $\mathbf{a}$ is:

$$\|\mathbf{u}^{\odot}\|_2^2 = \|\mathbf{a}(\mathbf{a}^{\mathrm{T}}\mathbf{a}^{-1})\mathbf{a}^{\mathrm{T}}\mathbf{u}\|_2^2 \tag{C.33}$$
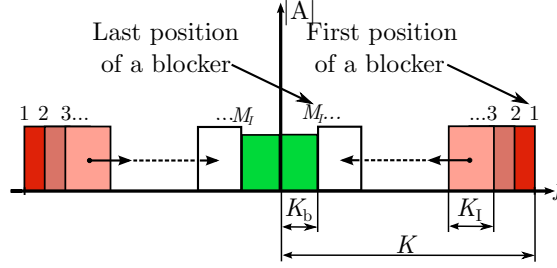
Figure C.9: The idea of creating possible interference scenarios (example for one blocker is shown). Since the blocker occupies continous frequency range in positive and negative frequencies, the scenario can be created by "sliding" the blocker down the spectrum.

Since it is impossible to compute the $\zeta_{\mathbf{a}}^{\mathbf{A}}$ for all the possible normalized vectors $\hat{\mathbf{q}}$, a Monte Carlo analysis is performed. Let us introduce a random normalized vector $\hat{\mathbf{q}} \in \mathbb{C}^{S \times 1}$

$$\hat{\mathbf{q}} = \frac{\mathbf{q}}{\|\mathbf{q}\|}, \quad \mathbf{q}(i) = x_i^n + j y_i^n, \quad i \in \{1, \ldots, S\} \tag{C.34}$$

where $x_i^n, y_i^n \in \mathcal{N}(0, 1)$. An atomic filtering-RIP parameter $\zeta_{\mathbf{a}}^{\mathbf{A}}$, computed for K_{q} random normalized vectors $\hat{\mathbf{q}}_k$ is:

$$\zeta_{\mathbf{a}}^{\mathbf{A}} = \max(\hat{\zeta}_{\mathbf{a}}^{\mathbf{A}}(k)) \tag{C.35}$$

where $\hat{\zeta}_{\mathbf{a}}^{\mathbf{A}}(k)$ is a $\hat{\zeta}_{\mathbf{a}}^{\mathbf{A}}$ (C.32) computed for the k-th vector $\hat{\mathbf{q}}_k$. The number of test vectors K_{q} depends on the desired confidence. The parameter $\zeta_{\mathbf{a}}^{\mathbf{A}}$ is atomic, since it corresponds to reconstruction of a single tone $\mathbf{a}$ for one possible subset $\mathbb{A}$ (and the corresponding matrix $\mathbf{A}$) of columns of the matrix $\mathbf{\Theta}$.

C.4.2 Scenarios of combinations

To enable the possibility of sub-Nyquist sampling, the received signal $\mathbf{s}_{\mathrm{x}}$ must be sparse in some domain. The more sparse is the signal $\mathbf{s}_{\mathrm{x}}$, the higher is a chance of a correct reconstruction. As stated in Sec. II, the given signal $\mathbf{s}_{\mathrm{x}}$ is sparse in the frequency domain. Sparsity of the signal $\mathbf{s}_{\mathrm{x}}$ depends on the number of blocking signals N_{I} (Sec. II) and the size of the spectrum occupied by these signals. Hence, there is a need to assign to a filtering problem $\mathcal{P}(B_{\mathrm{x}}^\dagger, B_{\mathrm{b}}, \mathbf{\Psi}, \mathbf{f}_{\mathrm{s}})$ a worst-case interference scenario $\mathcal{S}(N_{\mathrm{I}}^{\max}, K_{\mathrm{I}})$ with the maximum number $N_{\mathrm{I}}^{\max}$ of blocking signals $\mathbf{s}_{\mathrm{I}}^{(i)}$, and the maximum number K_{I} of positive frequency tones occupied by each i-th blocking signal $\mathbf{s}_{\mathrm{I}}^{(i)}$.

The total maximum number of positive frequency tones present in the spectrum of the blocking signal $\mathbf{s}_I$ is $\hat{K}_I = N_I^{\max} K_I$. The number of possible spectrum combinatons (M_I) in the canonical RIP analysis is:

$$M_I = \begin{pmatrix} K - K_b \\ \hat{K}_I \end{pmatrix} \tag{C.36}$$

where K (C.7) is the number of positive frequencies reflected in the used dictionary $\mathbf{\Psi} \in \mathcal{P}$, K_b (C.14) is the number of tones in half of the spectrum $0 \le f \le B_b$ of the wanted baseband signal $\mathbf{s}_b$.

Since all the blocking signals $\mathbf{s}_I^{(i)}$ occupy continous frequency range in positive and negative frequencies, the number of combinations needed to be tested is substantially reduced (Fig. C.8). Let us consider one blocking signal $\mathbf{s}_I^{(1)}$ which occupies K_I tones in the positive frequency spectrum. The number of possible combinations of support of the received signal $\mathbf{s}_x$, and hence the number of different matrices $\mathbf{A} \subset \mathbf{\Theta}$ (Sec. C.4.1) with columns of the matrix $\mathbf{\Theta}$ is:

$$M_I = K - K_I - K_b + 1 \tag{C.37}$$

All the spectrum combinations can be created by "sliding" the blocking signal down the spectrum (Fig. C.9). The number of combinations for $N_I^{\max}$ blockers is:

$$M_I =$$
$$= \underbrace{\sum_{i_{N-1}}^{K-K_0} \left(\sum_{i_{N-2}}^{i_{N-1}-K_0} \left(\cdots \sum_{i_2}^{i_3-K_0} \left(\sum_{i_1}^{i_2-K_0} (i_1 - K_i + 1) \right) \cdots \right) \right)}_{N_I^{\max}} \tag{C.38}$$

where $K_0 = K_b + K_I$, initial values of sum indices: $i_k^0 = kK_I$.

For a given worst case scenario $\mathcal{S}(N_I^{\max}, K_i)$ and a filtering problem $\mathcal{P}(B_x^{\dagger}, B_b, \mathbf{\Psi}, \mathbf{f}_s)$ it is possible to generate a set $\mathbb{A} = \{\mathbf{A}_1, \mathbf{A}_2, \ldots, \mathbf{A}_M\}$ with all the $M = M_I$ possible matrices $\mathbf{A}$ with $S = 2\hat{K}_I + K_b$ columns of the $\mathbf{\Theta}$ matrix. Hence, for a given measurement matrix $\mathbf{\Phi}$ such that, $\mathbf{\Theta} = \mathbf{\Phi}\mathbf{\Psi}$, it is possible to calculate a single-tone filtering-RIP parameter $\zeta_{\mathbf{a}}^{\mathbb{A}}$ for the column $\mathbf{a}$ of the matrix Θ and a given set $\mathbb{A}$:

$$\zeta_{\mathbf{a}}^{\mathbb{A}} = \max(\zeta_{\mathbf{a}}^m), \quad m = \{1, \ldots, M_I\} \tag{C.39}$$

where $\zeta_{\mathbf{a}}^m$ is an atomic filtering-RIP parameter $\zeta_{\mathbf{a}}^{\mathbf{A}}$ (C.35) computed for m-th matrix $\mathbf{A}_m$ from the set $\mathbb{M}$. The filtering-RIP parameter which asses a given
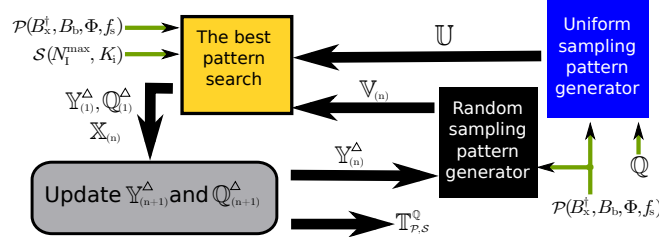
Figure C.10: The best sampling pattern search system.

matrix $\boldsymbol{\Phi}$ for the filtering problem $\mathcal{P}$ and the worst-case interference scenario $\mathcal{S}$ is:

$$\zeta_{\mathcal{P},\mathcal{S}}^{\boldsymbol{\Phi}} = \max(\zeta_{\mathbf{a}_{-K}}^{\mathbb{A}}, \ldots, \zeta_{\mathbf{a}_K}^{\mathbb{A}}), \quad K = K_{\mathrm{b}} \tag{C.40}$$

where $\zeta_{\mathbf{a}_k}^{\mathbb{A}}$ is single-tone filtering parameter (C.39) computed for k-th column $\mathbf{a} \in \Theta = \boldsymbol{\Phi}\boldsymbol{\Psi}$ which corresponds to a k-th tone in the wanted signal spectrum $(-B_{\mathrm{b}}) \leq f \leq B_{\mathrm{b}}$.

C.5 Best pattern search

The sampling patterns are prepared by the patterns search system presented in Fig. (C.10). The best pattern is a pattern which corresponds to a measurement matrix $\boldsymbol{\Phi}$ (C.3) such that matrix $\boldsymbol{\Theta} = \boldsymbol{\Phi}\boldsymbol{\Psi}$ has the best filtering-RIP parameters $\zeta_{\mathcal{P},\mathcal{S}}^{\boldsymbol{\Phi}}$ (C.40) for the given filtering problem $(\mathcal{P}(B_{\mathrm{x}}^{\dagger}, B_{\mathrm{b}}, \boldsymbol{\Psi}, \mathbf{f}_{\mathrm{s}}))$, a worst case scenario $\mathcal{S}(N_{\mathrm{I}}^{\max}, K_{\mathrm{i}})$, and a set $\mathbb{Q} = \{T_{\mathrm{g}}^{(1)}, T_{\mathrm{g}}^{(2)}, \ldots, T_{\mathrm{g}}^{(K_{\mathrm{Q}})}\}$ of K_{Q} acceptable sampling grid periods (C.17).

C.5.1 Grid analysis

Firstly, the set $\mathbb{Q}$ is ranked from the point of the given filtering problem. A set $\mathbb{U} = \{\mathbb{T}_{\mathrm{U}}^{(1)}, \mathbb{T}_{\mathrm{U}}^{(2)}, \ldots, \mathbb{T}_{\mathrm{U}}^{(K_{\mathrm{Q}})}\}$ of K_{Q} uniform sampling patterns is generated. The uniform sampling periods of the patterns in the set $\mathbb{U}$ are identical as the sampling grid periods in the set $\mathbb{Q}$. For all the generated uniform sampling patterns, filtering-RIP values $\zeta_{\mathcal{P},\mathcal{S}}^{\boldsymbol{\Phi}_{\mathbb{U}}^{(k)}}$ are computed for the given filtering problem $\mathcal{P}$ and the given worst case scenario $\mathcal{S}$. The values are stored in a set $\mathbb{Y} = \{\zeta_{\mathcal{P},\mathcal{S}}^{\boldsymbol{\Phi}_{\mathbb{U}}^{(1)}}, \zeta_{\mathcal{P},\mathcal{S}}^{\boldsymbol{\Phi}_{\mathbb{U}}^{(2)}}, \ldots, \zeta_{\mathcal{P},\mathcal{S}}^{\boldsymbol{\Phi}_{\mathbb{U}}^{(K)}}\}, K = K_{\mathrm{Q}}$, where $\boldsymbol{\Phi}_{\mathbb{U}}^{(k)}$ is a measurement matrix (C.3) which corresponds to a k-th uniform sampling pattern $\mathbb{T}_{\mathrm{U}}^{(k)} \in \mathbb{U}$. Let us introduce a set $\mathbb{Y}_{(1)}^{\triangle}$, which is a sorted set $\mathbb{Y}$. A set $\mathbb{Q}_{(1)}^{\triangle}$ is sorted accordingly
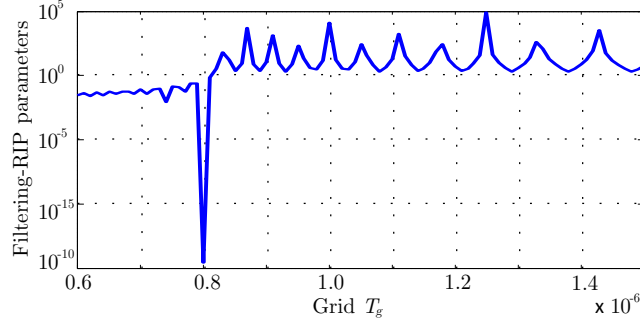
Figure C.11: Filtering-RIP parameters $\zeta_{\mathcal{P},\mathcal{S}}^{\mathbf{\Phi}_{\mathbb{U}}^{(k)}}$ for different sampling grids $\mathbb{T}_{\mathbb{U}}^{(k)} \in \mathbb{U}$. Consider the logarithmic scale.

to $\mathbb{Y}_{(1)}^{\triangle}$, such that $T_{\mathrm{g}}^{(k)} \in \mathbb{Q}_{(1)}^{\triangle}$ corresponds to $\zeta_{\mathcal{P},\mathcal{S}}^{\mathbf{\Phi}_{\mathbb{U}}^{(k)}} \in \mathbb{Y}_{(1)}^{\triangle}$. The sampling grid adjustment is further discussed in (C.5.1).

An example result of computing filtering-RIP parameters $\zeta_{\mathcal{P},\mathcal{S}}^{\mathbf{\Phi}_{\mathbb{U}}^{(k)}}$ for different grids $\mathbb{T}_{\mathbb{U}}^{(k)} \in \mathbb{U}$ is on Fig. C.11. The given filtering problem is $\mathcal{P}(B_{\mathrm{x}}^{\dagger}, B_{\mathrm{b}}, \mathbf{\Psi}, f_{\mathrm{s}})$, where $B_{\mathrm{b}} = 20\,\mathrm{kHz}$, $B_{\mathrm{x}}^{\dagger} = 100\,\mathrm{kHz}$, separation between dictionary $\mathbf{\Psi}$ columns $\gamma = 5\,\mathrm{kHz}$. The worst case scenario is $\mathcal{S} = \{1, 1\}$. I can be observed that the best filtering-RIP parameter is computed for grid value $\mathbb{T}_{\mathrm{g}} = 8\mu\mathrm{s}$.

C.5.2 Methodology

After grid ranking is done, the actual pattern search is started. A set $\mathbb{V}_{(n)} = \{\mathbb{T}_{(n)}^{(1)}, \mathbb{T}_{(n)}^{(2)}, \ldots, \mathbb{T}_{(n)}^{(K_{\mathrm{v}})}\}$ of K_{v} sampling patterns is generated by a random sampling patterns generator. The number K_{v} of generated sampling patterns depends on the desired confidence parameters. All the sampling patterns are generated with a sampling grid $T_{\mathrm{g}} = \mathbb{Q}_{(n)}^{\triangle}(1)$ The random sampling patterns generator is described in (C.5.3). A set $\mathbb{X}_{(n)} = \{\zeta_{\mathcal{P},\mathcal{S}}^{\mathbf{\Phi}_{(n)}^{(1)}}, \zeta_{\mathcal{P},\mathcal{S}}^{\mathbf{\Phi}_{(n)}^{(2)}}, \ldots, \zeta_{\mathcal{P},\mathcal{S}}^{\mathbf{\Phi}_{(n)}^{(K)}}\}$ of $K = K_{\mathrm{v}}$ filtering RIP-values $\zeta_{\mathcal{P},\mathcal{S}}^{\mathbf{\Phi}_{(n)}^{(k)}}$ is created, where $\mathbf{\Phi}_{(n)}^{(k)}$ is a measurement matrix which corresponds to a k-th sampling pattern $\mathbb{T}_{(n)}^{(k)} \in \mathbb{V}_{(n)}$. A sampling pattern $T_{(n)}^{\min} = T_{(n)}^{(k)} \in \mathbb{V}_{(n)}$ which corresponds to the lowest $\zeta_{\mathcal{P},\mathcal{S}}^{\mathbf{\Phi}_{(l)}^{(k)}} \in \mathbb{X}_{(n)}$ is stored in a set $\mathbb{L} = \{T_1^{\min}, T_2^{\min}, \ldots\}$. The corresponding lowest filtering RIP-value $\zeta_{\mathcal{P},\mathcal{S}}^{\mathbf{\Phi}_{(n)}^{\min}} \in \mathbb{X}_{(n)}$ is stored in a set $\mathbb{M} = \{\zeta_{\mathcal{P},\mathcal{S}}^{\mathbf{\Phi}_{(1)}^{\min}}, \zeta_{\mathcal{P},\mathcal{S}}^{\mathbf{\Phi}_{(2)}^{\min}}, \ldots\}$. The set $\mathbb{Y}_{(n+1)}^{\triangle}$

is updated such that:

$$\zeta_{\mathcal{P},\mathcal{S}}^{\mathbf{\Phi}_{\mathbb{U}}^{(k)}} \in \mathbb{Y}_{(n+1)}^{\triangle} \Leftrightarrow \zeta_{\mathcal{P},\mathcal{S}}^{\mathbf{\Phi}_{\mathbb{U}}^{(k)}} \in \mathbb{Y}_{(n)}^{\triangle} \wedge \zeta_{\mathcal{P},\mathcal{S}}^{\mathbf{\Phi}_{\mathbb{U}}^{(k)}} < \zeta_{\mathcal{P},\mathcal{S}}^{\mathbf{\Phi}_{(n)}^{\min}} \in \mathbb{X}_{(n)} \tag{C.41}$$

Furthermore, the currently filtering-RIP parameter which corresponds to the tested sampling grid period is removed from the set: $\mathbb{Y}_{(n+1)}^{\triangle} = \mathbb{Y}_{(n+1)}^{\triangle} \setminus \zeta_{\mathcal{P},\mathcal{S}}^{\mathbf{\Phi}_{\mathbb{U}}^{(1)}}$. The set $\mathbb{Q}_{(n+1)}^{\triangle}$ is updated accordingly. The above is repeated until $\mathbb{Y}_{(l+1)}^{\triangle} \neq \emptyset$. The best sampling pattern $\hat{T}_{\mathcal{P},\mathcal{S}}^{\mathbb{Q}}$ for the given filtering problem $\mathcal{P}$ and the worst-case scenario $\mathcal{S}$ with the acceptable set of sampling grids $\mathbb{Q}$ is a sampling pattern $\mathbb{T}_{(k)}^{\min}$ which corresponds to the lowest filtering-RIP value in the set $\mathbb{M}$.

C.5.3   Patterns generator

It was authors aim to develop a new algorithm which generates random sampling patterns. The patterns must be generated in a way that time intervals between adjacent sampling moments in the patterns must not be shorter than a given minimum time $t_{\min}$. Therefore, the quality attribute $e_{\min}$ (C.27) must be equal to 0. Furthermore, average sampling frequency f_s (C.20) in a given pattern time τ must be equal to the given expected sampling frequency $f_s^\star$. Therefore, the quality attribute e_f (C.21) must be equal to 0.

A new algorithm which generates a random sampling pattern is proposed. There are 5 input variables to the algorithm: time of the sampling pattern τ, sampling grid period T_g, average sampling frequency of a pattern $f_s^\star$, minimum time between sampling moments $t_{\min}$ and a standard deviation of internal random process σ.

Before the algorithm starts, the following precomputations must be done. The number of sampling moments K_s in a generated pattern, the number of grid points in the pattern K_g, and the number $N_{\min}$ of grid points in the minimum time $t_{\min}$ between samples are:

$$K_s = [\tau f_s^\star], \quad K_g = \left[\frac{\tau}{T_g}\right], \quad N_{\min} = \left\lceil \frac{t_{\min}}{T_g} \right\rceil \tag{C.42}$$

The proposed algorithm works as follows. It is assumed that the algorithm draws the sampling moments chronologically:

$$\forall k : t_{k-1} < t_k < t_{k+1}, \quad k \in \{1, \dots, K_s\} \tag{C.43}$$

All the computations are performed on integer numbers which represent the sampling grid periods. In the last step (C.55) the sampling grid periods are recalculated to the time values.

The first sampling point is calculated differently than the rest of the sampling points. Firstly, the average sampling period is calculated:

$$n_1^{\ddagger} = \left\lceil \frac{K_{\mathrm{g}}}{K_{\mathrm{s}}} \right\rceil \tag{C.44}$$

Than, the first sampling moment is drawn as:

$$n_1 = \lceil \xi_{\mathrm{u}} n_1^{\ddagger} \rceil \tag{C.45}$$

where $\xi_{\mathrm{u}} \in \mathcal{U}(0,1)$ is a uniformly-distributed random number. Algorithm of generation of the rest of sampling time points is as follows. For any k-th sampling point $(k > 1)$ the number of sampling points left is calculated:

$$n_k^{\mathrm{l}} = K_{\mathrm{s}} - k + 1 \tag{C.46}$$

The delimiters of a k-th sampling point, which are virtually first and last possible position of the k-th sampling point are calculated as:

$$n_k^{-} = N_{k-1} + N_{\mathrm{min}} \tag{C.47}$$
$$n_k^{+} = K_{\mathrm{g}} - N_{\mathrm{min}}(k-1) \tag{C.48}$$

The current average sampling period for the rest of sampling points is:

$$n_k^{\ddagger} = \left\lceil \frac{K_{\mathrm{g}} - N_{k-1}}{n_k^{\mathrm{l}}} \right\rceil \tag{C.49}$$

The expected position of the k-th sampling point is:

$$E[n_k] = n_{k-1} + n_k^{\ddagger} \tag{C.50}$$

It must be checked if the expected position is not higher than the delimiter n_k^{+} of the current sampling point:

$$E[n_k] = \begin{cases} E[n_k] & \text{for } E[n_k] \le n_k^{+} \\ n_k^{+} & \text{for } E[n_k] > n_k^{+} \end{cases} \tag{C.51}$$

In the proposed algorithm, a k-th sampling point N_k can differ from its exected position $E[n_k]$ by the distance n_k^{d}. This distance it is:

$$n_k^{d} = \min(|E[n_k] - n_k^{-}|, n_k^{+} - E[n_k]) \tag{C.52}$$

Finally, sampling moment n_{k} can be drawn as:

$$n_{\mathrm{k}} = [E[n_k] + \sigma n_k^{d} x_k^{\mathrm{n}}], \quad x_k^{\mathrm{n}} \in \mathcal{N}(0,1) \tag{C.53}$$

where σ is the internal variable of the proposed algorithm. The distribution of the random variable x_k^{n} is windowed such that $-3 \leq x_k^{\mathrm{n}} \leq 3$. In the last step of the k-th iteration of the algorithm it is checked if the drawn sampling moment n_k does not violate its delimiters n_k^- and n_k^+.

$$
n_k = \begin{cases} n_k^+ & \text{for } n_k > n_k^+ \\[2mm] n_k^- & \text{for } n_k < n_k^- \\[2mm] n_k & \text{otherwise} \end{cases} \tag{C.54}
$$

All K_{s} drawn sampling moments are recalculated from the number of sampling grid periods to the time values:

$$
\forall k : t_k = n_k T_{\mathrm{g}}, \quad k \in \{1, \ldots, K_{\mathrm{s}}\} \tag{C.55}
$$

The proposed algorihm is presented on the alg. 1. The above algorithm gu-

---

Algorithm 1 Random sampling pattern generator - pseudo code

1: **function** $[\mathbb{T}] = \mathrm{A1}(\boldsymbol{\tau}, \boldsymbol{T}_{\mathrm{g}}, \boldsymbol{f}_{\mathrm{s}}^{\star}, \boldsymbol{t}_{\min}, \boldsymbol{\sigma})$
2:     Compute K_{s}, K_{g}, $N_{\min}$ as in (C.42)
3:     Compute the average samp. period $n_1^{\ddagger}$ as in (C.44)
4:     Draw the first samp. moment n_1 according to (C.45)
5:     FOR $k = 2$ TO K_{s}
6:         Update the no. of samp. points left n_k^{l} as in (C.46)
7:         Compute the delimiters n_k^- and n_k^+ as in (C.47)
8:         Compute the average samp. period $n_k^{\ddagger}$ as in (C.49)
9:         Compute the expected position $E[n_k]$ as in (C.50)
10:         Check and correct $E[n_k]$ as in (C.51)
11:         Compute the distance n_k^d as in (C.52)
12:         Draw the samp. moment n_k according to (C.53)
13:         Check and correct n_k as in (C.54)
14:         Assign $\mathbb{T}(k) = n_k$
15:     END
16:     Recalculate the pattern as in (C.55)

---

rantess that the generated sampling pattern $\mathbb{T}$ has the errors $e_{\min} = 0$ and $e_{\mathrm{f}} = 0$ if the algorithm is realizable for a given set of parameters (τ, T_{g}, $f_{\mathrm{s}}^{\star}$, $t_{\min}$). Fig. $C.12$ compares the proposed algorithm with a well-known Additive Rad-
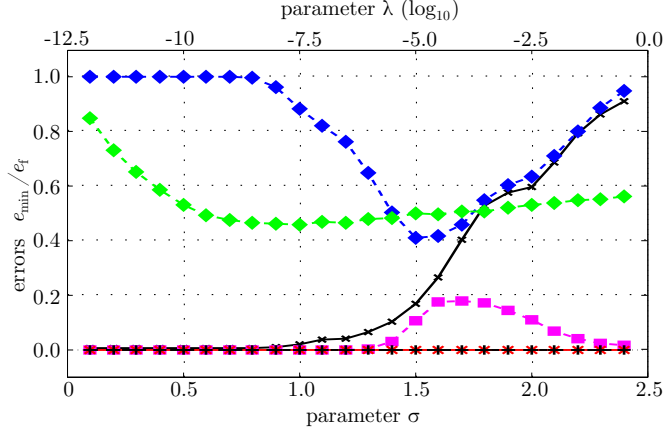
Figure C.12: Comparison between the proposed algorithm (A1) which generates random sampling patterns and Additive Random Sampling (ARS) algorithm for parameters $\tau = 200\mu s$, $T_{\mathrm{g}} = 4\mu s$, $f_{\mathrm{s}}^\star = 50$, $t_{\mathrm{min}} = 8\mu s$. The parameters $\lambda \in \{0.1, 0.2, \dots, 2.4\}$, $\sigma \in \{10^{-12.5}, 10^{-12.0}, \dots, 10^{-0.5}\}$

nom Sampling (ARS) [31, 32] in which every next point is drawn as:

$$t_k = \begin{cases} T_{\mathrm{s}}^\star + \sigma^2 x_k^{\mathrm{n}} & \text{for } k = 1 \\ t_{k-1} + T_{\mathrm{s}}^\star + \sigma^2 x_k^{\mathrm{n}} & \text{for } k \in \{2, \dots, K_{\mathrm{s}}\} \end{cases} \tag{C.56}$$

where $x_k^{\mathrm{n}} \in \mathcal{N}(0,1)$, the variance $\sigma^2 = \lambda T_{\mathrm{s}}$. It can be seen that the ARS violates the requirements of minimum distance between sampling moments and does not keep the requested average sampling frequency. For very low values of λ, for which the frequency and minium distance errors $(e_{\mathrm{f}}, e_{\mathrm{min}})$ improves, the ARS algorithm generates uniform smpling patterns $(e_{\mathrm{d}} = 1)$.

C.6 Numerical simulations

To demonstrate the proposed method in practice, an experiment was conducted. The parameters of the filtering problem $\mathcal{P}(B_{\mathrm{b}}, B_{\mathrm{x}}^\ddagger, \boldsymbol{\Psi}, f_{\mathrm{s}})$ are as follows. Spectrum where the wanted signal can be found is $-20\mathrm{kHz} \leq f \leq 20\mathrm{kHz}$, $(B_{\mathrm{b}} = 20\mathrm{kHz})$, there is 1 tone in the baseband signal. Frequency range of the interference signal is $B_{\mathrm{x}}^\ddagger = 100\mathrm{kHz}$. The frequency separation (C.9) between columns of the IDFT dictionary $\boldsymbol{\Psi}$ is $\gamma = 5\mathrm{kHz}$, the signal representation period (C.10) of the dictionary $\boldsymbol{\Psi}$ is $T_{\mathrm{r}} = 1\mu s$, the number of positive frequencies represented by the dictionary $\boldsymbol{\Psi}$ is $K = 20$. There are 10 average sam-
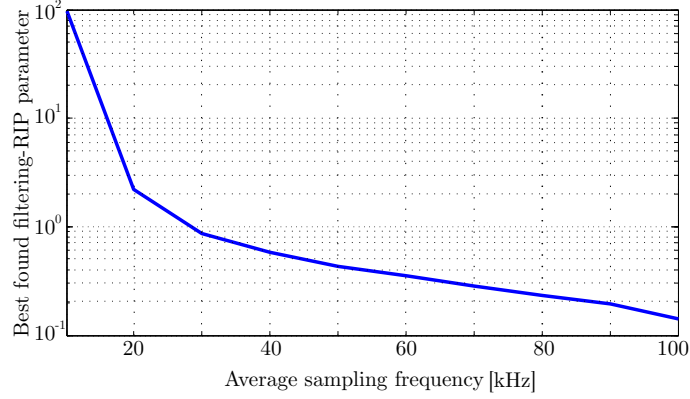
Figure C.13: The best filtering-RIP parameter found for different average sampling frequencies, for the filtering problem presented in the experiment.

pling frequencies tested: $f_s^{(1)} = 10\text{kHz}$, $f_s^{(2)} = 20\text{kHz}$, …, $f_s^{(10)} = 100\text{kHz}$. For simplicity, the worst-case interference scenario is $\mathcal{S}(N_I^{\max} = 1, K_I = 1)$.

The found filtering-RIP parameters $\zeta_{\mathcal{P},\mathcal{S}}^{\boldsymbol{\Phi}_{\mathbb{U}}^{(k)}}$ for different sampling grids $\mathbb{T}_{\mathbb{U}}^{(k)} \in \mathbb{U}$ are shown in Fig. C.11. It can be clearly seen that grid size $T_g = 8\mu s$ is significantly better than any other grid size. The best filtering sampling patterns for all the tested average sampling frequencies were found for this grid value. The filtering-RIP parameters (C.40) corresponding to the best patterns found for the average sampling frequencies are shown on Fig C.13.

Fig. C.14 shows reconstruction performance of the proposed method for average sampling frequencies $\{f_s^{(3)} = 30\text{kHz},\ f_s^{(4)} = 40\text{kHz},\ f_s^{(5)} = 50\text{kHz}.\ f_s^{(7)} = 70\text{kHz}\}$. The best found sampling patterns for the corresponding average sampling frequencies were used, while the spectrum containg the wanted signal was swept $B_b \in \{5\text{kHz}, 10\text{kHz}, \ldots, 95\text{kHz}\}$. The sampling patterns were searched for signal spectrum corresponding to $B_b = 20\text{kHz}$, so as expected, there is clearly a "cut-off point" of the reconstruction when the signal spectrum $B_b > 20\text{kHz}$. For the average sampling frequency $f_s^{(7)} = 70\text{kHz}$, all the sampled and reconstructed signals were reconstructed successfully for the $B_b \leq 20\text{kHz}$. It was experimentally verified that the average sampling frequency $f_s^{(7)} = 70\text{kHz}$ is the lowest frequency which guarantees perfect signal reconstruction for $B_b \leq 20\text{kHz}$.
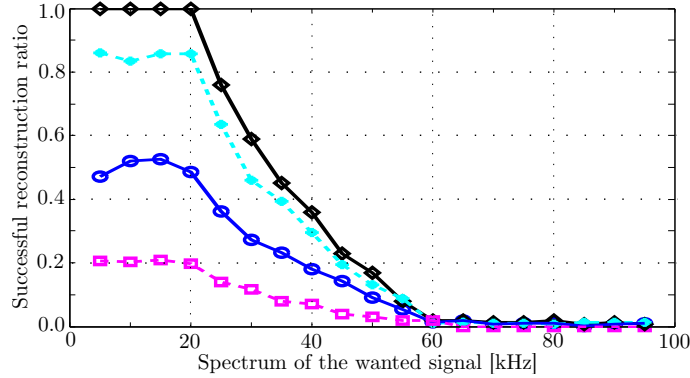
Figure C.14: The ratio of succesful signal reconstruction for different average sampling frequencies and different wanted signal spectrum B_b for sampling patterns adjusted to a given filtering problem. $f_s = 70$kHz: black $\diamond$, $f_s = 50$kHz: cyan $\circ$, $f_s = 40$kHz: blue $\circ$, $f_s = 30$kHz: purple $\square$

C.7   Conclusions

In this paper a new application of compressed sensing was presented. Compressed sensing is used to filter wanted signal from interferening signals without rising the sampling frequency to the Nyquist frequency of the interference-polluted signal. Filtering-RIP parameter, which assesses applicability of a sampling pattern for a given filtering problem, was introduced. This parameter is different from the canonical RIP parameter since it relates specifically to how well a wanted frequency range may be reconstructed. Furthermore, a method of filtering-RIP parameter estimation was proposed. In this method combinations needed to compute the filtering-RIP are created based on foreseen scenarios of filtering. This method significantly decreases the number of combinations which must be evaluated to compute the filtering-RIP. It makes the computation of filtering-RIP parameter practical in engineering applications.

Theory of sampling patterns was presented. A set of error parameters was proposed, to assess the random sampling patterns generator. It was explained why the sampling pattern has significant impact on the quality of reconstruction. A system for generating and choosing the best sampling pattern for a given filtering problem was introduced. A simple experiment was prepared to demonstrate the proposed method in practice. It was shown, that with compressed sensing, it is possible to move the filtering process from analog to the digital domain without increasing the sampling frequency to the Nyquist

frequency of the sampled signal. The above may increase area of applicability of compressed sensing.

Acknowledgment

[1] H. Nyquist, "Certain topics in telegraph transmission theory", *Trans. AIEE*, vol. 47, pp. 617-644, apr 1928

[2] R.G Lyons, "Understanding Digital Signal processing, 2nd edition, Prentice-Hall.", *Prentice Hall*, nov 2010, ISBN: 978-0-137-02731-5, Upper Saddle River, USA

[3] Nastaran Behjou, Ole Kiel Jensen, and **Torben Larsen**, "RF Sub-Sampling Receiver Architecture Based on Milieu Adapting Techniques", *IEEE Microwave Theory and Techniques Symposium*, 2012.

[4] J. Mitola, "The software radio architecture", *IEEE Commun. Mag.*, vol. 33(5), pp. 26–38, may 1995

[5] Analog Devices (2009). "A/D Converters. Analog Devices.",[Online] Available: `http://www.analog.com/en/analog-to-digital -converters/ad-converters/products/index.h tml`

[6] B. Le, T. W. Rondeau, J. H. Reed, W. Bostian, "Analog-to-Digital Converters. A review of the past, present, and future.", *IEEE Sig. Proc. Mag.*, vol. 22(6), nov 2005

[7] Besser, L. and Gilmore, R., "Practical RF Circuit Design for Modern Wireless Systems.", *Artech House*, oct 2003, ISBN 978-1-580-53521-2, Norwood, USA

[8] H. Baher, "Signal Processing and Integrated Circuits.", *Wiley-Blackwell*, apr 2012, ISBN: 978-0-470-71026-5, Hoboken, USA

[9] B. Razavi, "Architectures and Circuits for RF CMOS Receivers.", *Proc. of IEEE 1998 Custom Integrated Circuits Conference*, pp. 393-400, Santa Clara, USA, may 1998

[10] M. Pathak, S. K. Lim, "Fast Layout Generation of RF Embedded Passive Circuits Using Mathematical Programming", *IEEE Trans. Compon. Packag. Manuf. Technol.*, vol. 2(1), jan 2012

[11] S. H. Yeung, W. S. Chan, K. T. Ng, K. F. Man, "Computational Optimization Algorithms for Antennas and RF/Microwave Circuit Designs: An Overview", *IEEE Trans. Ind. Inf.*, vol. 8(2), may 2012

[12] M. Ben-Romdhane, C. Rebai, K. Grati, A. Ghazel, G. Hechmi, P. Desgreys and P. Loumeau, "Non-Uniform Sampled Signal Reconstruction for Multistandard WiMax/WiFi Receiver", *IEEE International Conference on Signal Processing and Communication*, pp. 181-184, Dubai, nov 2007

[13] M. Ben-Romdhane, C. Rebai, P. Desgreys, A. Ghazeli, P. Loumeau, "Pseudorandom Clock Signal Generation for Data Conversion in a Multi-standard Receiver", *Proc. IEEE Int. Conference on Design and Technology of Integrated Systems in Nanoscale Era*, pp. 1-4, Tozeur, Tunisia, mar 2008

[14] M. Ben-Romdhane, C. Rebai, P. Desgreys, A. Ghazeli, P. Loumeau, "Flexible Baseband Analog Front-end for NUS based Multistandard Receiver", *Proc. Joint IEEE North-East Workshop on Circuits and Systems and TAISA Conference*, Toulouse, France, pp. 1–4, jun 2009

[15] E.J. Candès and M. B. Wakin, "An Introduction To Compressive Sampling", *IEEE Signal Process. Mag.*, vol. 25(2), pp. 21–30, mar. 2008

[16] M. Elad, *Sparse and Redundant Representations. From Theory to Applications in Signal and Image Processing.* Springer, aug 2010, ISBN 978-1-441-97011-4, Berlin, Germany

[17] R.G. Baraniuk, "Compressive Sampling", *IEEE Signal Process. Mag.*, vol. 24(4), pp. 118–120,124, jul 2007

[18] E.J. Candès and T. Tao, "Decoding by Linear Programming", *IEEE Trans. Inf. Theory*, vol. 51(12), pp. 4203–4215, nov 2005

[19] D.L. Donoho, "Compressed Sensing", *IEEE Trans. Inf. Theory*, vol. 52(4), pp. 1289–1306, apr 2006

[20] R.G. Baraniuk, M. Davenport, R. Devore, M. Wakin, "A Simple Proof of the Restricted Isometry Property for Random Matrices", *Constructive Approximation*, vol. 28(3), pp. 253–236, dec 2008

[21] E.J. Candès, J. Romberg and T. Tao, "Robust Uncertainty Principles: Exact Signal Reconstruction From Highly Incomplete Frequency Information", *IEEE Trans. Inf. Theory*, vol. 52(2), pp. 489–509, feb. 2006

[22] J.A. Tropp and A.C. Gilbert, "Signal Recovery From Random Measurements Via Orthogonal Matching Pursuit", *IEEE Trans. Inf. Theory*, vol. 53(12), pp. 4655–4666, dec. 2007

[23] J.A. Tropp, "Just Relax: Convex Programming Methods for Identifying Sparse Signals in Noise", *IEEE Trans. Inf. Theory*, vol. 52(3), pp. 1030–1051, mar. 2006

[24] S. Kirolos, J. Laska, M. Wakin, M. Duarte, D. Baron, T. Ragheb, Y. Massoud, R. Baraniuk, "Analog-to-Information Conversion via Random Demodulation", *Proc. IEEE Dallas/CAS Workshop on Design Applications Integration and Software (DCAS)*, pp. 71–74, Dallas, USA, 2006

[25] J. Tropp, J. Laska, M. Duarte, J. Romberg, and R. Baraniuk, "Beyond Nyquist: Efficient Sampling of Sparse Bandlimited Signals", *IEEE Trans. Inf. Theory*, vol. 56(1), pp. 520–540, jan 2010

[26] J. Laska, S. Kirolos, Y. Massoud, R. Baraniuk, A. Gilbert, M. Iwen and M. Strauss, "Random Sampling for Analog-to-Information Conversion of Wideband Signals", *Proc. IEEE Dallas Circuits and Systems Workshop (DCAS)*, pp. 119–122, Dallas, USA, jul 2006

[27] M. Mishali, Y. C. Eldar, "From Theory to Practice: Sub-Nyquist Sampling of Sparse Wideband Analog Signals", *IEEE J. Sel. Topics Signal Process.*, vol. 4(2), pp. 375-391, apr. 2010

[28] M. Mishali, Y. C. Eldar, A. Elron, "Xampling: Signal Acquisition and Processing in Union of Subspaces", *IEEE Trans. Sig. Proc.*, vol. 59(16), pp. 4719-4734, oct. 2011

[29] P. Feng, and Y. Bresler, "Spectrum-Blind Minimum-Rate Sampling and Reconstruction of Multiband Signals", *Proc. 1996 IEEE Intl. Conf. Acoustics, Speech, and Signal Processing (ICASSP)*, pp. 1688-1691, Atlanta, USA, may 1996

[30] H. S. Shapiro, R. A. Silverman, "Alias free sampling of Random Noise", *IEEE Trans. Info. Theory*, vol. 16, pp. 147–152, june 1960

[31] J.J. Wojtiuk, "Randomized Sampling for Radio Design", *PhD Thesis*, University of Southern Australia, 2000

[32] I. Bilinskis, A. Mikelsons, "Randomized Signal Processing.", *Prentice Hall*, aug 1992, ISBN: 978-0-137-51074-0, Cambridge, UK

[33] F. Papenfuß, Y.Artyukh, E. Boole, D. Timmermann, "Nonuniform Sampling Driver Design For Optimal ADC Utilization", *Proc. Internal Symposium on Circuits and Systems, 2003 (ISCAS'03)*, vol. 4, pp. 516–519, Bangkok, Thailand, may 2003

[34] A. C. Gilbert, M. J. Strauss, and J. A. Tropp, "A Tutorial on Fast Fourier Sampling", *IEEE Signal Process. Mag.*, vol. 25(2), pp. 57–66, mar 2008

[35] Y. P. Lin, and P.P. Vaidyanathan, "Periodically Nonuniform Sampling of Bandpass Signals", *IEEE Trans. Circuits Syst. II*, vol. 45(3), pp. 340-351, mar. 1998

[36] I. Homjakovs, M. Greitans, R. Shavelis, "Real-Time Acquisitions of Wideband Signals Data Using Non-Uniform Sampling", *Proc. IEEE Eurocon 2009*, pp. 1158-1163, Saint-Petersburg, may. 2009

[37] K. Yang, "Interference management in LTE wireless networks [Industry Perspectives]", *IEEE Wireless Commun. Mag.*, vol. 19(3), pp. 8-9, june 2012

[38] G. Boudreau, J. Panicker, R. Chang, N. Wang, S. Vrzic, "Interference Coordination and Cancellation for 4G Networks", *IEEE Commun. Mag.*, vol. 47(4), pp. 74-81, apr 2009

[39] M. Huang, W. Xu, "Macro-femto inter-cell interference mitigation for 3GPP LTE-A downlink", *Proc. 2012 IEEE Wireless Communications and Networking Conference Workshops (WCNCW)*, pp. 75–80, Paris, France, apr 2012

[40] P. Vandewalle, J. Kovacevic, and M. Vetterli, "Reproducible Research in Signal Processing [What, why and how]", *IEEE Signal Process. Mag.*, vol. 26(3), pp. 37–47, may 2009